Dissertation

submitted to the
Combined Faculties for the Natural Sciences and for Mathematics
of the Ruperto-Carola University of Heidelberg, Germany

for the degree of
Doctor of Natural Sciences

presented by
Mathias Haag, Dipl.-Ing. (FH)

Born: 25 May 1981 in Darmstadt
Oral examination: 17 December 2010

Development of Mass Spectrometric Methods for the Quantification of Membrane Lipids

–

Studies on Mitochondria, T Cells, Golgi Membranes and COPI Vesicles

Referees: Prof. Dr. Felix Wieland

PD. Dr. Britta Brügger

List of publications

Christof Osman, Mathias Haag, Felix T. Wieland, Britta Brügger and Thomas Langer
“A mitochondrial phosphatase required for cardiolipin biosynthesis: the PGP phosphatase Gep4“
EMBO J. 2010. Jun 16; 29(12); 1976-1987.

Christof Osman, Mathias Haag, Christoph Potting, Jonathan Rodenfels, Phat Vinh Dip, Felix T. Wieland, Britta Brügger, Benedikt Westermann and Thomas Langer
“The genetic interactome of prohibitins: coordinated control of cardiolipin and phosphatidylethanolamine by conserved regulators in mitochondria”
J. Cell Biol. 2009. Feb 23; 184(4); 583-596.

Table of contents

Abbreviations

µCi	Microcurie
AP-1	Activator protein 1
CDP	Cytidine diphosphate
CE	Collision energy
CHO	Chinese hamster ovary
CL	Cardiolipin
COP	Coat protein
cpm	counts per minute
Da	Dalton
DAG	Diacylglycerol
ER	Endoplasmatic reticulum
ESI	Electrospray ionization
eV	Electron volt
FA	Fatty acid
GEP/Gep	Genetic interactor of prohibitin
GTPγS	Guanosin-5'[γ-thio]-triphosphat
h	hour(s)
HeLa	Henrietta Lacks
HPLC	High performance liquid chromatography
IFNγ	Interferon gamma
IL-2	Interleukin-2
IP_3	Inositol triphosphate
IQ	Ilimaquinone
LC	Liquid chromatography
LPA	Lysophosphatidic acid
LPC	Lysophosphatidylcholine
LPE	Lysophosphatidylethanolamine
m/z	mass-to-charge ratio
MAG	Monoacylglycerol
MAM	Mitochondria-associated membrane
mCi	Millicurie
min	minute(s)
MLCL	Monolysocardiolipin
MPIS	Multiple precursor ion scanning
MS/MS	Tandem mass spectrometry
nCi	Nanocurie

NFAT	Nuclear factor of activated T cells
NF-κB	Nuclear factor kappa-light-chain-enhancer of activated B cells
NL	Neutral loss
NRK	Normal rat kidney
PC	Phosphatidylcholine
PE	Phosphatidylethanolamine
PG	Phosphatidylglycerol
PGP	Phosphatidylglycerolphosphate
Phb	Prohibitin
PI	Phosphatidylinositol
PIP	Phosphatidylinositolphosphate
PIP_2	Phosphatidylinositoldiphosphate
PIPs	Phosphoinositides (PIP and PIP_2)
PKC(θ)	Protein kinase C (theta)
PLC(γ1)	Phospholipase C (gamma 1)
PLD	Phospholipase D
pl-PE	Plasmalogen phosphatidylethanolamine
PM	Plasma membrane
PS	Phosphatidylserine
Rf	Response factor (factor to correct for mass spectrometric response differences between internal standards and endogenous lipids used as reference standards)
RLC	Rat liver cytosol
rpm	Revolutions per minute
RT	Room temperature
sec	second(s)
SM	Sphingomyelin
TAG	Triacylglycerol
Tcon	conventional T cell
TCR	T cell receptor
TGN	trans-Golgi network
Th1	T-helper type 1
TLC	Thin layer chromatography
TOF-MS	Time-of-flight mass spectrometry
Treg	regulatory T cell
wt	wild-type

Abstract

Biological membranes contain more than thousand different lipid classes and lipid species that are far from being fully characterized. In order to understand molecular processes that are connected to membrane lipids a continuous development of analytical methods is required. In this thesis, nano-electrospray ionization tandem mass spectrometry (nano-ESI-MS/MS) was employed to establish methods for the quantification of cardiolipin (CL), diacylglycerol (DAG) and the phosphoinositides PIP and PIP_2. The methods were applied for the analysis of mitochondria, Golgi membranes and T cells in order to address scientific questions:

I. The quantitative analysis of CL in mitochondria, isolated from yeast mutants, showed that GEP genes (genetic interactors of prohibitins) are involved in the regulation of mitochondrial phospholipids CL and phosphatidylethanolamine. Strikingly, the mass spectrometric identification of the lipid intermediate phosphatidylglycerolphosphate (PGP) in mitochondria from ∆gep4 mutants supported the identification of Gep4 as a novel PGP phosphatase required for CL biosynthesis.

II. The quantitative analysis of DAG revealed that ilimaquinone (IQ)-induced vesiculation of the Golgi complex significantly affects the level of DAG. This result is consistent with previous observations that lipid-modifying enzymes, such as phospholipase D and PA phosphatase, are activated and suggests that membrane lipids play a critical role during the process of IQ-mediated Golgi vesiculation.

III. The quantitative analysis of PIP, PIP_2 and DAG in conventional T cells showed that T cell receptor (TCR)-induced stimulation significantly affects the level of signaling lipids. This result was an important readout to address the question whether regulatory T cells interfere with proximal lipid signaling events in conventional T cells.

Furthermore, a lipidome analysis of Golgi membranes and COPI vesicles was performed. The generated data confirmed previous findings that sphingomyelin and cholesterol are segregated during the formation of COPI vesicles. Moreover, the lipid analysis revealed that COPI vesicles display a lipid composition similar to the endoplasmatic reticulum, with elevated levels of phosphatidylcholine and phosphatidylinositol. The characteristic lipid composition supports the scenario that COPI vesicle formation occurs at liquid-disordered domains in the Golgi complex.

Zusammenfassung

Biologische Membranen bestehen aus mehr als tausend verschiedenen Lipidklassen und Lipidspezies, welche bisher nur unvollständig charakterisiert sind. Mit dem Ziel molekulare Prozesse, an denen Membranlipide beteiligt sind, zu verstehen, bedarf es einer kontinuierlichen Weiterentwicklung analytischer Methoden. In dieser Arbeit wurde Nano-Elektrospray-Ionisations-Tandem-Massenspektrometrie (Nano-ESI-MS/MS) verwendet, um Methoden für die Quantifizierung von Cardiolipin (CL), Diacylglycerol (DAG) und den Phosphoinositiden PIP und PIP_2 zu etablieren. Mit dem Ziel wissenschaftliche Fragestellungen zu adressieren, wurden die Methoden für die Analyse von Mitochondrien, Golgi-Membranen und T-Zellen angewendet:

I. Die Quantifizierung von CL in Mitochondrien, welche aus Hefemutanten isoliert wurden, zeigte, dass GEP Gene (Genetische Interaktoren von Prohibitinen) an der Regulation der mitochondrialen Phospholipide CL und Phosphatidylethanolamin beteiligt sind. Weiterhin unterstützte die massenspektrometrische Identifizierung des Lipidintermediates Phosphatidylglycerolphosphat (PGP) in Mitochondrien von ∆gep4 Mutanten die Identifizierung von Gep4 als neuartige PGP-Phosphatase welche für die CL-Biosynthese benötigt wird.

II. Die Quantifizierung von DAG zeigte, dass die Ilimaquinone (IQ)-induzierte Vesikulierung des Golgi-Komplexes einen signifikanten Einfluss auf DAG-Level hat. Dieser Effekt bestätigte, dass Lipid-modifizierende Enzyme, wie Phospholipase D und PA-Phosphatase, aktiviert werden und lässt darauf schließen, dass Membranlipide eine entscheidende Rolle während der IQ-vermittelten Golgi-Vesikulierung spielen.

III. Die quantitative Analyse von PIP, PIP_2 und DAG in konventionellen T-Zellen, zeigte, dass die T-Zell-Rezeptor (TZR)-induzierte Stimulierung einen signifikanten Einfluss auf die Mengen dieser Signallipide hat. Dieses Resultat war von Bedeutung für die weitere Fragestellung, ob regulatorische T-Zellen die proximale Lipid-Signalweiterleitung in konventionellen T-Zellen beeinflussen.

Weiterhin wurde eine Lipidome-Analyse von Golgi-Membranen und COPI-Vesikeln durchgeführt. Die erhobenen Daten bestätigten, dass Sphingomyelin und Cholesterin während der COPI-Vesikelbildung segregiert werden. Weiterhin zeigten die Lipidanalysen, dass COPI-Vesikel eine ähnliche Lipidzusammensetzung wie das Endoplasmatische Retikulum aufweisen, mit erhöhtem Gehalt an Phosphatidylcholin und Phosphatidylinositol. Die charakteristische Lipidzusammensetzung lässt darauf schließen, dass die Bildung von COPI-Vesikeln an „liquid-disordered“ Domänen innerhalb des Golgi-Komplexes stattfindet.

List of figures

List of tables

1 Introduction

1.1 Biological membranes

Biological membranes are organized assemblies of lipids, proteins and carbohydrates that are required for barrier function, compartmentalization, transport and signaling processes in living cells. The plasma membrane (PM) and intracellular compartments such as the endoplasmatic reticulum (ER), the Golgi complex and mitochondria are characterized by distinct lipid compositions that reflect the various tasks that have to be fulfilled by different biological membranes (van Meer et al., 2008).

The variety of lipids in cellular and organellar membranes is exceedingly complex with more than thousand different lipid classes and species (van Meer, 2005). According to a comprehensive classification system, lipids can be separated in eight different groups: fatty acids, glycerophospholipids, glycerolipids, sphingolipids, prenol lipids, saccharolipids, polyketides and sterols (Fahy et al., 2005). Of particular interest for the present work are glycerophospholipids, glycerolipids, sphingolipids and sterols that are introduced here with respect to their structure, synthesis and function.

1.2 Structure, synthesis and function of membrane lipids

1.2.1 Glycerophospholipids

Glycerophospholipids consist of a glycerol moiety that is linked to a phosphate containing headgroup in sn-3 position and two fatty acids bound to the sn-1 and sn-2 position, respectively. The sn-1 position often contains saturated fatty acids, whereas unsaturated fatty acids are commonly attached to the sn-2 position. Phosphatidic acid (PA) (Figure 1), the simplest glycerophospholipid containing only a glycerolphosphate and two fatty acids, is an important signaling molecule and a key intermediate in the synthesis of other lipid classes (Athenstaedt and Daum, 1999). The phosphate group of PA can be further modified to generate other glycerophospholipids such as phosphatidylcholine (PC).

PC (Figure 1), the most abundant glycerophospholipid in biological membranes, is synthesized mainly in the ER by the bifunctional enzyme DAG-choline/ethanolamine phosphotransferase (CEPT) via the Kennedy or CDP-choline pathway (Gibellini and Smith, 2010). In a first step, choline is phosphorylated to phosphocholine that is further converted to CDP-choline. CEPT catalyzes the reaction of CDP-choline and DAG to generate PC. The Golgi-located enzyme DAG-choline phosphotransferase (CPT) can also contribute to the cellular production of PC via the Kennedy pathway (Henneberry et al.,

2002; Fagone and Jackowski, 2009). Alternatively, PC can be synthesized by sequential methylation of phosphatidylethanolamine (PE), catalyzed by the N-methyltransferases PEMT1 in the ER and PEMT2 in mitochondria-associated membranes (MAMs) (Cui et al., 1993; Vance et al., 1997). MAMs represent membrane-connecting structures between ER and mitochondria that are involved in the biosynthesis and transport of lipids between both organelles (Hayashi et al., 2009). PC has a cylindrical shape and therefore spontaneously organizes into bilayers being an ideal structural component of membranes. In addition to its function as a membrane building block, PC has been linked to biological processes such as phospholipase-mediated signaling (Jackowski et al., 1997; Billah and Anthes, 1990).

The aminophospholipid PE (Figure 1) comprises an abundant lipid of biological membranes that is synthesized via the Kennedy pathway in the ER by CEPT (Gibellini and Smith, 2010) or by a PE-specific DAG-ethanolamine phosphotransferase (EPT) (Horibata and Hirabayashi, 2007). Alternatively, the enzymatic action of a PS-decarboxylase (Psd) can also contribute to the production of PE. In yeast, two types of decarboxylases have been identified, Psd1 and Psd2, which are localized to the inner mitochondrial membrane and the Golgi/vacuolar membrane, respectively (Voelker, 1997). Only one mitochondria-located PS decarboxylase (Psd1) has been identified in mammals (Vance, 2008). Although it seems that PE is quite similar to PC, regarding its function as a structural membrane lipid, there are some significant differences in the biophysical properties of these lipids. PE has a smaller headgroup than PC, which gives the lipid a cone shape. This property allows PE, similar to CL, the formation of non-bilayer structures in biological membranes (see chapter 1.2.1.1).

The aminophospholipid phosphatidylserine (PS) (Figure 1) is synthesized by the reaction of serine with CDP-DAG, that is catalyzed in yeast, but not in mammals, by the PS synthase Cho1p in MAMs (Kohlwein et al., 1988; Vance and Steenbergen, 2005). In mammals, PS synthesis is catalyzed by two different base exchange enzymes, PS-synthase 1 (Pss1) and PS-synthase 2 (Pss2) that exchange the choline and ethanolamine headgroups of PC and PE, respectively, for serine (Vance and Steenbergen, 2005). Both PS synthases are localized to MAMs (Stone and Vance, 2000). PS is found, together with PE, mainly in the inner leaflet of the PM where it can interact with proteins due to its negatively charged headgroup. For instance, the cytoskeletal protein spectrin binds to PS in erythrocytes and thus being involved in maintaining membrane integrity and mechanical stability (An et al., 2004). The loss of PS asymmetry at the PM is an indicator of apoptosis since PS is exposed to the outer leaflet in apoptotic cells as a result of decreased

aminophospholipid translocase activity and increased scramblase activity. The exposure of PS is an important signal for the recognition and removal of apoptotic cells by phagocytes (Fadok et al., 1998). Furthermore, PS has been associated with signaling processes acting as a cofactor for the activation of protein kinase C (PKC) together with DAG and Ca^{2+} (Newton, 1995).

Phosphatidylglycerol (PG) (Figure 1) is a minor lipid in mammalian membranes but it is known as the main constituent of bacterial bilayers where it supports membrane stability (Zhao et al., 2008). PG is an important lipid intermediate in the biosynthesis of mitochondrial CL (see chapter 1.2.1.1).

Phosphatidylinositol (PI) (Figure 1) is a glycerophospholipid consisting of a PA backbone that is linked via the phosphate group to *myo*-D-inositol (hexahydroxycyclohexane). The final step of PI synthesis, catalyzed by PI synthase, is the condensation of inositol and CDP-DAG (Antonsson, 1997). Most of *de novo* PI synthesis takes place at the ER, however, other intracellular sites of PI production have been assigned to the plasma membrane, the Golgi apparatus, the nucleus and to secretory vesicles (Monaco et al., 2006). The fatty acid composition of PI in animal tissues is rather distinctive, since it contains mainly C18:0 and C20:4 fatty acids attached to the sn-1 and sn-2 position, respectively. Polyunsaturated PI is intracellular enriched at the ER, where it contributes to a loose packed and flexible ER-membrane, thus facilitating the insertion of newly synthesized lipids and proteins (van Meer et al., 2008). Furthermore, PI is the precursor of the phosphoinositides PIP, PIP_2 and PIP_3, which play fundamental roles in a variety of cellular processes (see chapter 1.2.1.2).

Ether lipids, such as plasmalogen phosphatidylethanolamine (pl-PE) (Figure 1), comprise a class of glycerophospholipids that are produced by sequential action of several enzymes (Nagan and Zoeller, 2001). The first step of ether lipid synthesis is catalyzed by dihydroxyacetonphosphate-acyltransferase (DHAPAT) that produces acyl-DHAP in peroxisomes. In a second step, the ether bond is introduced by alkyl-DHAP synthase to form alkyl-DHAP. Depending on the specificity of the following enzymes, ether lipids with either an ether (O-alkyl) or a vinyl ether (O-alkenyl = plasmalogens) bond in the sn-1 position of glycerol can be generated. The majority of the O-alkyl moieties generally occur as plasmanylcholines (PC-O), whereas the O-alkenyl group is mainly associated with plasmalogen phosphatidylethanolamines. A prominent member of ether lipids is the platelet-activation-factor (PAF), a plasmanylcholine with an acetate group in the sn-2 position and a C16 fatty acid in the sn-1 position. PAF is a potent activator and mediator

of many leukocyte functions, including platelet aggregation and inflammation (Hanahan, 1986). Furthermore, ether lipids have been linked to signaling processes (Smets et al., 1999), antioxidative functions (Brosche and Platt, 1998) and membrane trafficking (Thai et al., 2001).

Lysophospholipids are generated from their diacyl-precursors by specific action of the phospholipases A1 and A2 (Newkirk and Waite, 1973). Lysophosphatidylcholine (LPC) (Figure 1) for example is involved in signaling processes (Tan et al., 2009) and acts as an intermediate in the fatty acid remodeling of other glycerophospholipids such as cardiolipin (Xu et al., 2003). The inverted cone shape of lysophospholipids enables the induction of membrane curvature (Fuller and Rand, 2001), thereby supporting membrane fusion and fission events. Consistently, lysophospholipids have been associated with Golgi membrane dynamics and vesicular trafficking (Bankaitis, 2009; Drecktrah et al., 2003).

1.2.1.1 Cardiolipin (CL)

CL is a dimeric glycerophospholipid (Figure 1) that is found in bacteria and mitochondrial membranes of eukaryotic cells. CL is mainly located in the inner mitochondrial membrane and to a minor extend also present in the outer mitochondrial membrane (Daum and Vance, 1997; Gebert et al., 2009; Schlame, 2008). In yeast cells, mitochondrial CL is a rather low abundant class of lipids, accounting to ~1 mol% of the lipidome (Ejsing et al., 2009). CL can be enriched to ~15 mol% in isolated mitochondrial fractions (Daum and Vance, 1997).

The synthesis of CL in yeast mitochondria requires that PA is transferred from the outer to the inner membrane, where it is activated by the CDP-diacylglycerol synthase Cds1 to CDP-DAG (Kuchler et al., 1986). CDP-DAG, together with glycerol-3-phosphate, is converted to phosphatidylglycerolphosphate (PGP) (Figure 1) by the PGP synthase Pgs1 (Chang et al., 1998a). The low abundant lipid intermediate PGP is rapidly dephosphorylated to PG by the recently identified PGP phosphatase Gep4 (Osman et al., 2010). In the final step, a pool of “premature” CL species is synthesized by the cardiolipin synthase Crd1 through condensation of PG with CDP-DAG. “Premature” CL, characterized by a high degree of saturated fatty acids, undergoes acyl chain remodeling to produce a “mature” pool of CL species that contain fatty acids with a higher degree of unsaturation. This process is initiated by the CL-specific phospholipase Cld1 (Beranek et al., 2009), which generates monolysocardiolipin (MLCL). The transacylase taffazin (Taz1) incorporates unsaturated fatty acids onto MLCL to generate “mature” CL (Gu et al., 2004).

In most cases, “mature” CL species contain only two types of fatty acids which results in a high degree of structural uniformity and molecular symmetry of CL species (Schlame et al., 2005). The physiological importance of symmetric CL species is supported by the fact that Barth syndrome patients (BTHS) contain CL species with an aberrant fatty acid distribution (Valianpour et al., 2002; Valianpour et al., 2005). Aberrant CL species of BTHS affect the stability of respiratory chain supercomplexes in mitochondrial membranes (McKenzie et al., 2006), accordingly, syndromes of BTHS, such as cardiomyopathy, neutropenia and muscle weakness, can be ascribed to an impaired energy production in mitochondria.

CL is structurally related to PE since both molecules are able to form non-bilayer, hexagonal phases in membranes (Verkleij et al., 1984; Cullis and de Kruijff, 1978; Vasilenko et al., 1982). Hexagonal phase structures are discussed to be required for the formation of membrane contact sites during fusion and fission processes and in transmembrane movement of proteins (Cullis and de Kruijff, 1979; van den Brink-van der Laan et al., 2004; Schlame et al., 2000). Consistently, PE- and CL-rich domains have been discovered in bacterial membranes where they might serve as platforms for fusion and fission events (Matsumoto et al., 2006). Furthermore, CL has been linked to a variety of mitochondrial and cellular processes such as energy production (Pfeiffer et al., 2003), apoptosis (McMillin and Dowhan, 2002; Ostrander et al., 2001) and diseases like diabetes (Han et al., 2007) and cancer (Kiebish et al., 2008).

1.2.1.2 Phosphoinositides (PIPs)

PIPs are low abundant lipid classes in biological membranes accounting to ~0.1-1 mol% (PIP and PIP_2) (Figure 1) and <0.0002 mol% (PIP_3) (Mallo et al., 2008). For the biosynthesis of PIPs, the precursor PI needs to be transported from the ER to different organelles, where PIPs are metabolically generated and interconverted by the enzymatic action of several kinases and phosphatases (Downes et al., 2005; Sasaki et al., 2009; Tolias and Cantley, 1999; Blero et al., 2007). Dependent on the side and extend of phosphorylation, seven distinct phosphoinositide classes are known in nature: PI(3)P, PI(4)P, PI(5)P, PI(3,4)P_2, PI(3,5)P_2, PI(4,5)P_2 and PI(3,4,5)P_3, whereas PI(4)P and PI(4,5)P_2 reflect the most abundant forms. Different phosphoinositide classes can be regarded as organelle markers since they are predominantly synthesized and located at different membranes such as PI(3)P at early endosomes, PI(4)P at the Golgi complex and PI(4,5)P_2 and PI(3,4,5)P_2 at the plasma membrane (Di Paolo and De Camilli, 2006).

The phosphorylated headgroup of PIPs can bind to effector proteins and thereby trigger signaling and activation processes. Several domains have been described to specifically interact with different types of PIPs. These domains include pleckstrin homology (PH), phagocyte oxidase (PX), epsin N-terminal homology (ENTH), C2 and FYVE zinc finger domains (Downes et al., 2005; Di Paolo and De Camilli, 2006). For example, at the trans-Golgi network (TGN), PI(4)P binds to a variety of proteins such as epsinR, AP-1, FAPP1, FAPP2, OSPB and to CERT indicating important functional roles of PIPs in vesicular transport (De Matteis et al., 2005). Plasma membrane-located PI(4,5)P_2 is involved in a plethora of processes such as endo- and exocytosis, plasma membrane cytoskeleton interactions and signal transduction (Di Paolo and De Camilli, 2006). TCR-induced signaling in activated T cells (Smith-Garvin et al., 2009) comprises, among other things, the activation of phospholipase PLCγ1 that specifically cleaves plasma membrane anchored PI(4,5)P_2, thereby generating the second messenger molecules IP_3 and DAG. DAG activates two major pathways involving Ras and PKCθ (Carrasco and Merida, 2004). The water soluble IP_3 stimulates Ca^{2+}-permeable ion channel receptors in the ER, leading to Ca^{2+}-release into the cytoplasm.

1.2.2 Glycerolipids

The family of glycerolipids comprises mainly monoacylglycerols (MAGs), diacylglycerols (DAGs) and triacylglycerols (TAGs). Whereas the main function of TAGs is to store energy in lipid droplets, MAGs and DAGs are involved in more dynamic cellular processes such as lipid synthesis and signaling (Askari et al., 1991; Toker, 2005).

1.2.2.1 Diacylglycerol (DAG)

DAG (Figure 1) is a low abundant glycerolipid with two fatty acids attached to the sn-1 and sn-2 position. The sn-3 position remains in its unmodified, hydroxylated form. *De novo* formation of DAG includes the synthesis of lysophosphatidic acid (LPA) that is acylated to PA by LPA acyltransferase (Carrasco and Merida, 2007). PA is then hydrolyzed by a PA phosphatase (PAP) (Kocsis and Weselake, 1996) to finally produce DAG. In addition to *de novo* synthesis, three alternative pathways can generate DAG through the action of the sphingomyelin synthase and the phospholipases PLD and PLC. The latter mechanisms of DAG production results in temporally and spatially increased DAG levels that are rather required for signaling events than for metabolic purposes (see chapter 1.2.1.2).

Besides function as lipid intermediate and effector molecule, DAG possesses important biophysical properties that can significantly influence the behavior of membranes (Goni and Alonso, 1999). Due to its small headgroup, DAG resembles a cone-shaped lipid that induces negative curvature in membranes. This property links DAG to processes like vesicle formation at the Golgi complex (Fernandez-Ulibarri et al., 2007; Kearns et al., 1997; Litvak et al., 2005; Asp et al., 2009) and ilimaquinone-induced vesiculation of the Golgi complex (Sonoda et al., 2007).

1.2.3 Sphingolipids

The basic building block of sphingolipids is a sphingoid base. The most common base in mammals is sphingosine (1,3-dihydroxy-2-amino-4-octadecene), with a *trans*-double bond between C_4 and C_5 (Karlsson, 1970; Barenholz and Thompson, 1999). Different kind of fatty acids (mainly C16-C24) can be linked via an amid bond to sphingosine to produce ceramide (Figure 1). In eukaryotic cells, ceramide is produced at the ER by the ceramide synthase (Wang and Merrill, Jr., 2000), which catalyzes the N-acylation of the sphingoid base. *De novo* synthesized ceramide is transported via a non-vesicular pathway by the ceramide transport protein CERT (Hanada et al., 2009; Hanada et al., 2007; Hanada, 2010) to the Golgi where it is further processed to sphingomyelin (SM) (Figure 1). Alternatively, ceramide can be produced through the catabolism of SM by the action of sphingomyelinases (Goni and Alonso, 2002). Like DAG, ceramide is a cone-shaped molecule with a relatively compact headgroup. These properties contribute to curvature stress that promotes hexagonal phase formation and membrane trafficking through vesiculation and fusion (van Blitterswijk et al., 2003). Furthermore, ceramide can induce lipid flip-flop in biological membranes (Contreras et al., 2009) and act as a second messenger that activates apoptotic processes (Haimovitz-Friedman et al., 1997).

The synthesis of SM is mediated by the SM synthase (SMS) that transfers the phospho-choline moiety from PC onto the primary hydroxyl group of ceramide, thus generating SM and DAG (Ullman and Radin, 1974; Voelker and Kennedy, 1982). Two SM synthases SMS1 and SMS2 are encoded in the mammalian genome catalyzing the SM production as Golgi- and PM-associated enzymes (Sadeghlar et al., 2000; Tafesse et al., 2007). Molecular differences between glycerophospholipids and sphingolipids become apparent, when comparing PC and SM. Although showing a high degree of structural similarity, the presence of the hydroxyl- and amide-moiety in SM results in unique biophysical properties that are responsible for a high degree of acyl chain ordering and furthermore for the formation of intra- and intermolecular hydrogen bonding (Ernst et al., 2010; Mombelli et

al., 2003). SM has a high affinity for cholesterol (Veiga et al., 2001), therefore contributing to the formation of densely packed, liquid-ordered microdomains (Ramstedt and Slotte, 2006).

1.2.4 Sterol lipids

The most prominent sterol is cholesterol (Figure 1). The biosynthesis of cholesterol, rewarded with the Nobel Prize in medicine in 1964, is a highly complex series of more than thirteen enzymatic reactions (Bloch, 1965). Besides being an important precursor of hormone synthesis, one of the main functions of cholesterol is to modulate the fluidity of membranes. The structural properties of cholesterol enables both, the induction of local order in a fluid phase and the fluidization of lipids in gel phase (Ernst et al., 2010). The ability of cholesterol to modulate membrane fluidity can be attributed to its interaction potential with neighboring phospholipids and SM (Ramstedt and Slotte, 1999; Halling et al., 2008; Ohvo-Rekila et al., 2002).

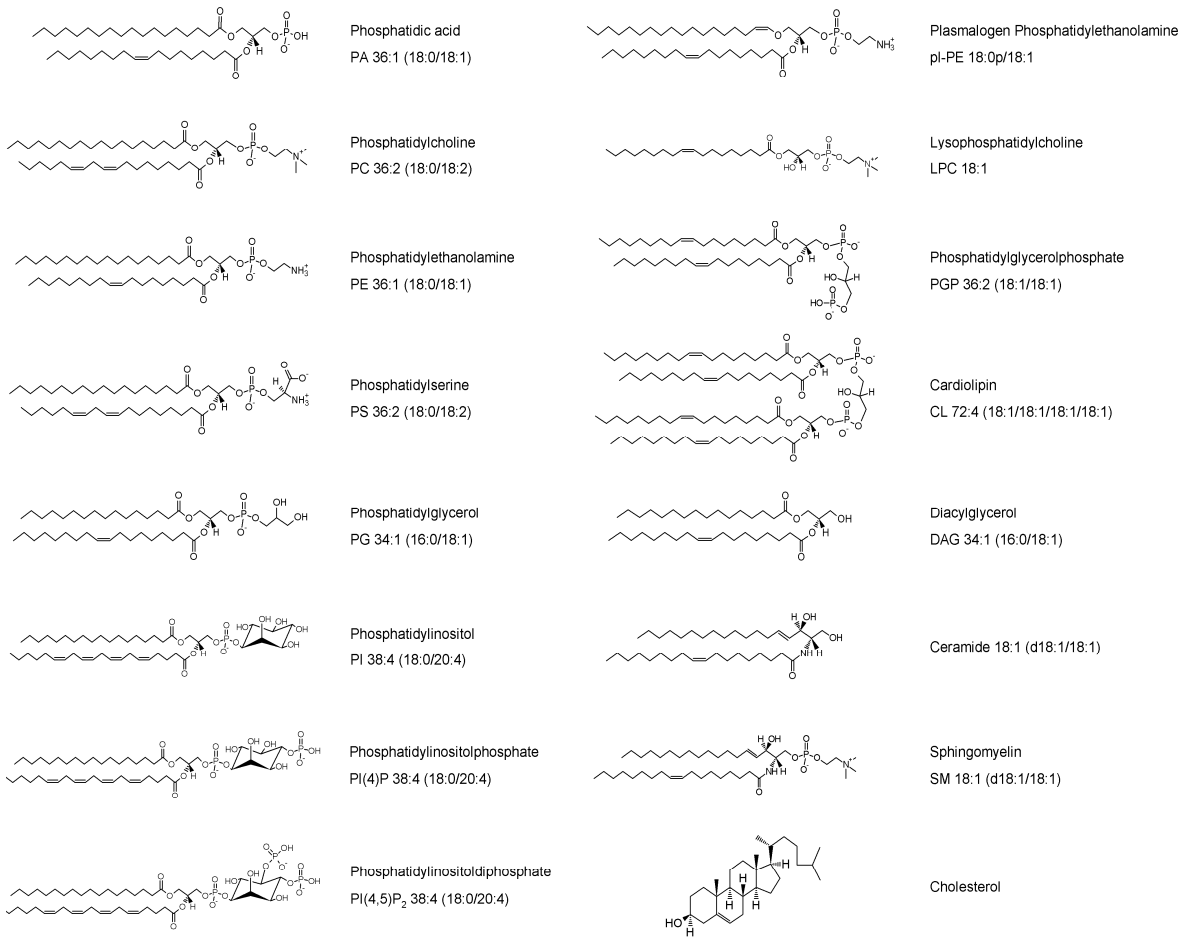

Figure 1: Chemical structures of lipid classes. The fatty acid composition of a given lipid class is indicated by the sum of C atoms and sum of double bonds (Σ C atoms: Σ double bonds).

1.3 Heterogeneity of lipid membranes

A remarkable feature of living cells is that they establish and maintain distinct lipid compositions of different membranes such as the PM, the ER, the Golgi complex and mitochondria (van Meer, 1989; van Meer et al., 2008). This phenomenon is quite distinct along the secretory pathway where a lipid gradient exists between the ER and the PM (Schneiter et al., 1999; Fleischer et al., 1974; Zambrano et al., 1975). The PM reflects a liquid-ordered membrane with high levels of cholesterol, saturated glycerophospholipids and sphingolipids thus promoting bilayer rigidity and impermeability (van Meer et al., 2008; Holthuis and Levine, 2005). In contrast, the ER contains low amounts of sphingolipids and cholesterol but is highly enriched in unsaturated glycerophospholipids resulting in a flexible membrane that facilitates the incorporation of newly synthesized lipids and proteins (van Meer et al., 2008; Holthuis and Levine, 2005). The lipid composition of the Golgi complex, as a lipid-based sorting station, resembles an intermediate state between ER and PM (van Meer, 1998).

Another level of complexity within membranes arises from the fact that lipids are differently orientated within the bilayer (bilayer asymmetry) (Devaux and Morris, 2004; Op den Kamp, 1979). Whereas lipids of the ER membrane are relatively symmetric distributed within the bilayer, lipids of the PM are asymmetrically distributed between the two leaflets of the membrane with PC, SM and glycosphingolipids (GSLs) preferentially located on the luminal side of the leaflet and the aminophospholipids PS and PE concentrated in the cytosolic leaflet (Holthuis and Levine, 2005; Sprong et al., 2001).

Lipid heterogeneity also occurs laterally within a bilayer (Devaux and Morris, 2004). Lateral heterogeneity exists in polarized epithelial cells where GSLs and PCs are differentially localized to apical and basolateral domains, respectively (Simons and van, 1988; van Meer and Simons, 1988; van Meer et al., 1987). Lipid rafts (Lingwood and Simons, 2010; Lingwood et al., 2009) can also be regarded as laterally segregated SM- and cholesterol-enriched platforms. Segregation of cholesterol and SM during vesicle formation at the Golgi complex (Brugger et al., 2000; Klemm et al., 2009) and the enrichment of raft lipids in viral membranes (Brugger et al., 2006) are indications that membrane budding events might be restricted to laterally segregated membrane domains.

1.4 Lipid transport mechanisms

The intracellular transport of lipids can be achieved in several ways such as lateral movement, transbilayer movement, monomeric exchange and vesicular transport (Sprong et al., 2001; Holthuis and Levine, 2005).

Lateral movement is a rapid process where lipids diffuse in the lateral plane of a bilayer with diffusion coefficients that are 10-100-fold higher than those of membrane proteins (Holthuis and Levine, 2005). A typical phospholipid can diffuse laterally in a bilayer at a rate of several µm/sec, thus one lipid molecule can travel from one end of a cell to the other end within a few seconds.

Transbilayer movement (flip-flop) is the exchange of lipids between the two leaflets of a bilayer. Lipids can traverse bilayers either in a non-catalyzed fashion or catalyzed by enzymes or external agents (Contreras et al., 2010). The non-catalyzed flip-flop is rapid (seconds to minutes) for lipids with a small headgroup such as LPC, DAG and ceramide (Holthuis and Levine, 2005). In contrast, for lipids with large headgroups (PC and SM) non-catalyzed flip-flop can take up to hours or days (Holthuis and Levine, 2005). Several enzymes such as flippases, floppases and scramblases greatly enhance the catalyzed flip-flop of lipids within a bilayer. For example, the asymmetric distribution of PE and PS at the plasma membrane is generated and maintained by the flippase “aminophospholipid translocase” (Devaux et al., 1990).

Monomeric exchange is a relevant mode of lipid transport for mitochondria and peroxisomes, organelles that are not connected to vesicular transport pathways. This transfer can be mediated in a non-catalyzed fashion through the cytosol or at increased rates at membrane contact sites (Levine and Loewen, 2006). Additionally, the presence of lipid transfer proteins (LTPs) can markedly accelerate the exchange of lipids through the cytosol and at membrane contact sites (Lev, 2010).

Vesicular transport of lipids is achieved by selective inclusion or exclusion of certain lipid classes during the formation of transport carriers. The Golgi apparatus and vesicles derived thereof play important roles in vesicle-mediated transport and sorting of lipids (Nickel et al., 1998a; Brugger et al., 2000; Ikonen and Simons, 1998; Klemm et al., 2009). For COPI vesicles, it was shown that they contain less cholesterol and SM compared to the donor Golgi membrane (Brugger et al., 2000) demonstrating a direct role of COPI vesicles in maintaining the lipid gradient along the secretory pathway. A similar role of lipid

transport and sorting can be ascribed to TGN-derived secretory vesicles that were found to be specifically enriched in SM and cholesterol (Klemm et al., 2009).

1.5 Nano-ESI-MS/MS for lipid quantification

To study molecular processes that are linked to changes in cellular and intracellular lipid levels, sensitive methods for the comprehensive quantification of membrane lipids are required. Conventional approaches for lipid analysis employ TLC (Skipski et al., 1964), HPLC (Hax and van Kessel, 1977) and gas chromatography mass spectrometry (GC-MS) (Figure 2). Nevertheless, these methods are time and sample consuming and, furthermore, show limitations in the resolution of lipid classes and lipid species.

The combination of electrospray ionization (ESI) with (tandem) mass spectrometry was an important progress in the field of structural and quantitative lipid analysis (Han and Gross, 1994; Kerwin et al., 1994). However, ESI alone requires relatively high amounts of starting material since lipid extracts are infused at flow rates in the µl/min-range. The replacement of the ESI source by a nano-ESI source was an imperative step forward in terms of sample consumption, thus allowing the sensitive analysis of lipid extracts at flow rates in the nl/min-range (Brugger et al., 1997). Furthermore, nano-ESI in combination with lipid class specific precursor and neutral loss scans on a triple quadrupole mass spectrometer (Figure 2) enabled the parallel identification and quantification of lipid classes (e.g. PC) and lipid species (e.g. PC 34:2) directly from crude lipid mixtures (Brugger et al., 1997). Consequently, the concept of shotgun-lipidomics arose (Han and Gross, 2005).

The invention of hybrid tandem mass spectrometers (Figure 2) such as quadrupole time-of-flight and linear ion trap-Orbitrap instruments, combined with automated nano-ESI infusion devices, facilitates high throughput lipidomics analysis by multiple precursor ion scanning (MPIS) (Stahlman et al., 2009; Ekroos et al., 2002; Ejsing et al., 2006), data dependent acquisition (DDA) (Schwudke et al., 2006; Schwudke et al., 2007b) and top-down lipidomics screen (Schwudke et al., 2007a). Such analytical approaches allow lipid analysis down to the molecular species level (e.g. PC 16:0/18:2 or PC 16:1/18:1).

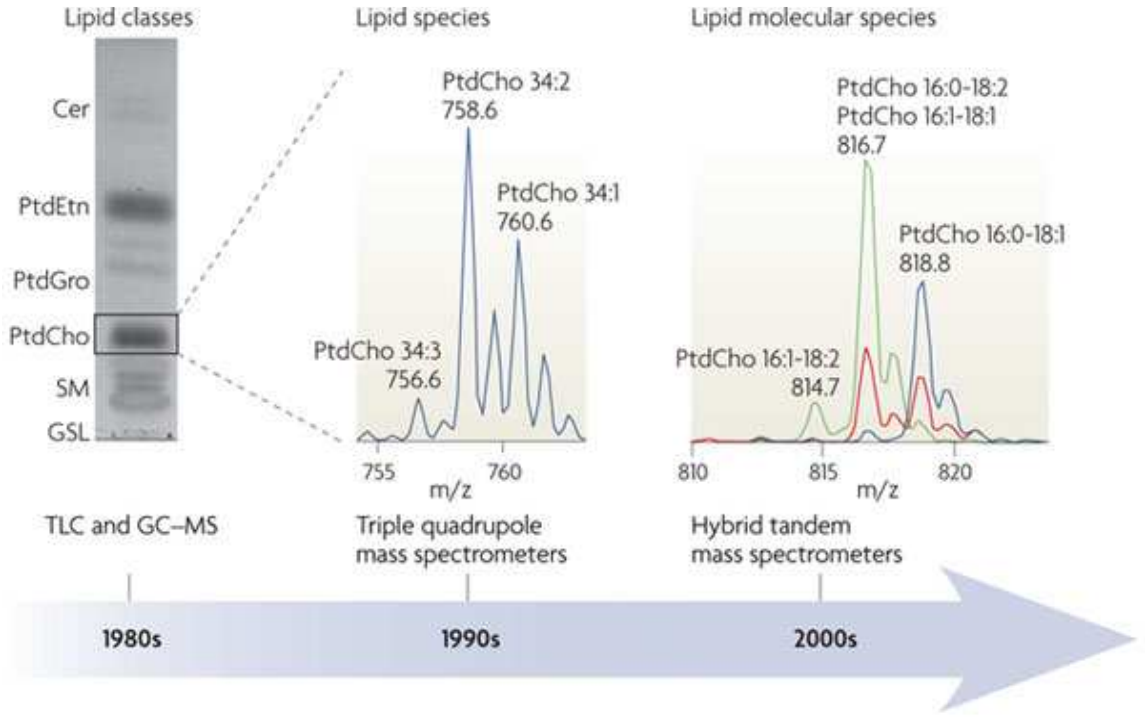

Figure 2: The development of quantitative lipid analysis. Taken from Shevchenko and Simons 2010.

1.5.1 Nano-ESI-MS/MS for quantification of CL, DAG and PIPs

The analysis of CL was conventionally performed by HPLC (Schlame and Otten, 1991) and has been continuously replaced by quantitative MS techniques. LC-ESI-MS/MS facilitates CL quantification by monitoring on singly charged (Sparagna et al., 2005) or doubly charged ions (Valianpour et al., 2002; Garrett et al., 2007). Han and Gross went a step further and demonstrated the quantification of doubly charged CLs by direct infusion ESI-MS/MS employing two-dimensional MS analysis (Han et al., 2006). CL quantification by nano-ESI-MS/MS was recently demonstrated by Ejsing *et al,* who quantified doubly charged CLs by multiple precursor ion scanning (MPIS) (Ozcan et al., 2007) and linear ion Trap-Orbitrap mass spectrometry (Ejsing et al., 2009).

DAG has traditionally been analyzed by the DAG kinase assay (Bielawska et al., 2001) or by GC-MS after chemical derivatization (Falardeau et al., 1993; Hubbard et al., 1996). ESI-MS/MS can be used for DAG quantification after LC separation (Callender et al., 2007) or by direct infusion after derivatization (Li et al., 2007b). Quantification of positively charged DAG ammonium adducts by nano-ESI-MS/MS was recently demonstrated by neutral loss scanning (Murphy et al., 2007) and MPIS (Stahlman et al., 2009). Ejsing *et al* reported the quantification of negatively charged DAG by MPIS (Ejsing et al., 2009).

Due to their extreme low abundance, PIPs are traditionally analyzed by metabolic labeling with *myo*-[^{3}H]-inositol followed by TLC- or LC-analysis (Hama et al., 2004; Bird, 1994; Cooke, 2009; Mallo et al., 2008). ESI-MS/MS has been applied for the identification (Milne et al., 2005) and structural elucidation of PIPs (Hsu and Turk, 2000). Quantification of PIPs can be achieved by ESI-MS/MS after LC separation (Pettitt et al., 2006) or by direct infusion of lipid extracts (Wenk et al., 2003). However, there is currently no method available that facilitates the quantification of PIPs by nano-ESI-MS/MS.

1.6 Aims of the thesis

In the first project (collaboration with Prof. Dr. Thomas Langer and Dr. Christof Osman, Institute for Genetics, University of Cologne), we planned to investigate how mitochondrial phospholipids are affected in the absence of GEP genes (genetic interactors of prohibitins). GEP genes comprise a set of genes that were identified in a genome wide screen to genetically interact with prohibitins in yeast mitochondria (Osman, 2009; Osman et al., 2009). Initial experiments indicated a critical connection between GEP genes and mitochondrial lipid composition. We therefore aimed at a quantitative analysis of the phospholipids PE and CL in mitochondria derived from yeast cells lacking GEP genes. To this end, a method for CL quantification by nano-ESI-MS/MS was established.

Another goal (collaboration with Prof. Dr. Vivek Malhotra and Dr. Josse van Galen, Center for Genomic Regulation, Barcelona, Spain) was to determine if the marine sponge metabolite ilimaquinone (IQ) affects lipid levels in Golgi membranes. IQ is known to induce reversible vesiculation of the Golgi complex (Takizawa et al., 1993). The molecular mechanism of this process is still unknown. Previous data indicated that lipids such as DAG are required for IQ-induced Golgi fragmentation (Sonoda et al., 2007), however this has never been confirmed by quantitative lipid analysis. In order to determine the effect of IQ on Golgi membranes, a method for DAG quantification by nano-ESI-MS/MS was established.

A further task was to elucidate whether proximal lipid signaling in primary human T cells (Tcons) is affected by regulatory T cells (Tregs) (collaboration with Prof. Dr. Peter H. Krammer and Angelika Schmidt, DKFZ, Heidelberg). *In vitro* experiments revealed fast kinetics of Tcon suppression in the presence of Tregs (Oberle et al., 2007). The exact mechanism of suppression, however, is still unknown. In order to analyze signaling lipids in Tcons we planned to set up an approach that facilitates the simultaneous quantification of PIP, PIP_2 and DAG by nano-ESI-MS/MS.

In the final part of this thesis, the question to what extend COPI vesicles are involved in intracellular lipid sorting was addressed. Previous experiments showed that SM and cholesterol are segregated during the formation of COPI vesicles at the Golgi complex (Brugger et al., 2000). An extended lipid analysis of COPI vesicles was planned in order to reveal if other lipid classes or species are selectively enriched or reduced in COPI vesicles.

2 Results

2.1 Method development

2.1.1 Quantification of CL

CL is a dimeric glycerophospholipid that is found in bacteria and mitochondrial membranes of eukaryotic cells. Mitochondrial CL is required to maintain cellular functions such as energy production by stabilizing and activating respiratory chain complexes III and IV (Pfeiffer et al., 2003). Furthermore, CL has been associated with apoptosis (McMillin and Dowhan, 2002) and diseases such as Barth syndrome (Hauff and Hatch, 2006). To study cellular mechanisms that are linked to mitochondrial CL, sensitive methods for the quantification of CL molecular species are required. In order to develop a method for CL quantification by nano-ESI-MS/MS, the mass spectrometric ionization and fragmentation behavior of two commercially available CL species was characterized.

2.1.1.1 Mass spectrometric characterization of CL molecular species

CL 56:0 with the fatty acid composition 14:0/14:0/14:0/14:0 is not detectable in yeast mitochondria (Schlame et al., 1993) and was therefore used as an internal standard for the quantification of endogenous CL species. Furthermore, CL 72:4 with a typical "endogenous-like" fatty acid composition 18:1/18:1/18:1/18:1 was used as reference standard to analyze the behavior of endogenous CL species from yeast (Schlame et al., 1993). Due to two phosphate groups, CL can occur either as singly $[M-H]^-$ (Sparagna et al., 2005) or doubly charged $[M-2H]^{2-}$ molecule (Valianpour et al., 2002; Han et al., 2006; Garrett et al., 2007). Although the quantification of doubly charged CLs from crude lipid mixtures was previously demonstrated (Han et al., 2006) we aimed at conditions that facilitate the analysis of singly charged CL ions in order to avoid interference with other phospholipids such as PE, PA and PG that appear in the same mass range as doubly charged CL ions.

To check the ionization behavior of CLs on the mass spectrometric system used in this study an equimolar mixture of the two CL species was prepared and analyzed by TOF-MS. Analyzing both CL species in pure methanol, doubly charged CL-ions $[M-2H]^{2-}$ at m/z 619.42 (CL 56:0) and at m/z 727.51 (CL 72:4) were the sole signals in the spectra (Figure 3 A). Notably, after adjusting the solvent system to 5 mM ammonium acetate and 0.05% piperidine, singly charged ions at m/z 1239.83 (CL 56:0) and at m/z 1456.01 (CL 72:4) became the prevailing signals (Figure 3 B). The abundance of singly charged ions was ~70-80% compared to ~20-30% residual doubly charged ions that were still

detectable (Figure 3 B). Irrespective of the charge state, CL 56:0 and CL 72:4 showed significant differences in their response behavior indicated by response factors (Rfs) (peak intensity ratio CL 56:0 / CL 72:4) of ~1.33 (doubly charged ions) and ~1.66 (singly charged ions).

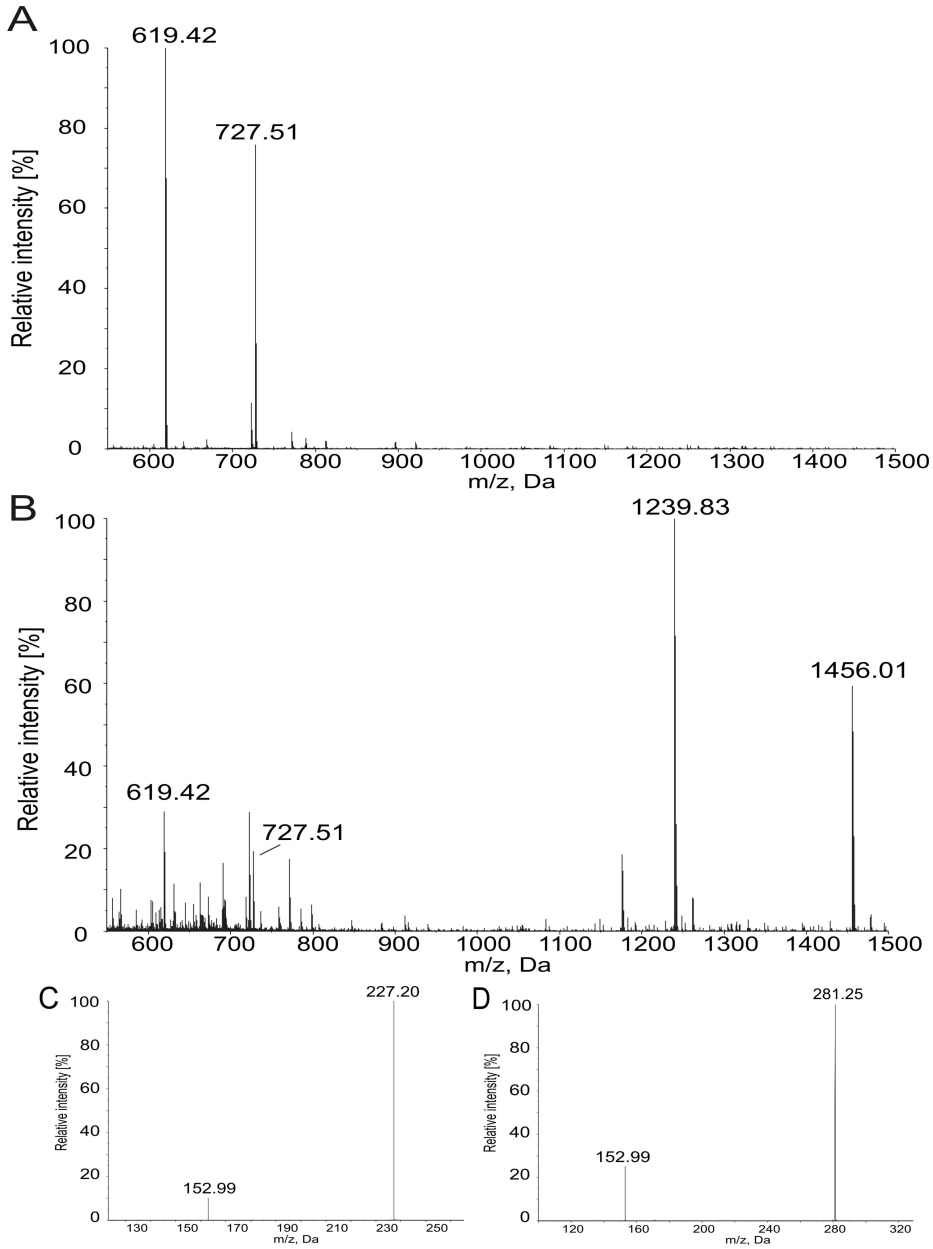

Figure 3: Ionization and fragmentation of CL 56:0 and CL 72:4. (A) TOF-MS spectrum of negatively, doubly charged CL 56:0 (m/z 619.42) and CL 72:4 (m/z 727.51) resulting from the infusion in methanol. (B) TOF-MS spectrum of negatively, singly charged CL 56:0 (m/z 1239.83) and CL 72:4 (m/z 1456.01) resulting from the infusion in 5 mM ammonium acetate and 0.05% piperidine in methanol. (C and D) Product ion spectra of CL 56:0 (C) and CL 72:4 (D). The glycerolphosphate-H_2O fragments (m/z 152.9) and the fatty acid fragments 14:0 (m/z 227.2) and 18:1 (m/z 281.25) are displayed.

Collision-induced dissociation (product ion mode) of singly charged CL ions confirmed the identity of the molecular species (Hsu et al., 2005) by the presence of the glycerol-phosphate-H_2O fragment (m/z 152.99) and the fatty acid derived ions at m/z 227.2 (FA 14:0 of CL 56:0) (Figure 3 C) and at m/z 281.25 (FA 18:1 of CL 72:4), respectively (Figure 3 D).

We next wanted to determine the limits of quantification for singly charged CL ions in the TOF-MS mode and the product ion mode. To this end, quantification of “endogenous-like” CL 72:4 was achieved by the internal standard CL 56:0 whereas the peak intensities of the monoisotopic ions (m/z 1239.83 and m/z 1456.01) were used for quantification in the TOF-MS mode. The fatty acid ions (m/z 227.2 and m/z 281.25) were taken for quantification in the product ion mode. In order to determine optimal dissociation conditions for product ion experiments, the dependency of the applied collision energy (CE) on the fatty acid signal intensities was investigated (Figure 4). CE ramping experiments revealed that a CE of -85 eV results in most intense signals of the fatty acid derived ions. Notably, the signal derived from CL 56:0 (m/z 227.2) gave higher ion counts compared to the signal from CL 72:4 (m/z 281.25) at any applied collision energy. This effect can be explained in a way that the smaller molecular size of CL 56:0 results in a more efficient dissociation compared to CL 72:4. For compensation of this discrepancy, a Rf (peak area fatty acid 14:0 / peak area fatty acid 18:1) of 1.5 ± 0.1 (n=4) was determined.

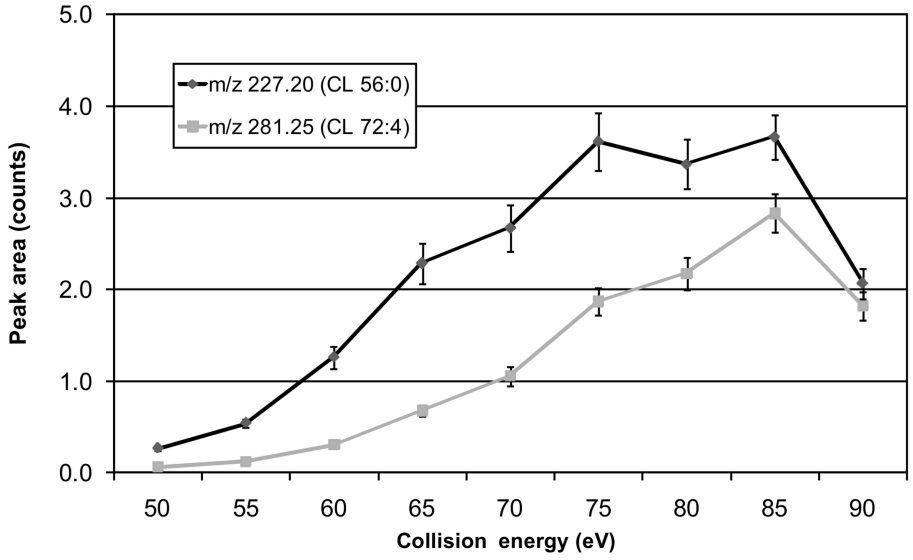

Figure 4: Fragmentation efficiency of CL 56:0 and CL 72:4 at different CEs. Fatty acid peak area intensities at different collision energies are displayed for CL 56:0 and CL 72:4. Data represent mean ± average deviation of three independent experiments.

The limits of quantification for TOF-MS and the product ion mode were investigated by analyzing a dilution series of CL 72:4 quantified by fixed amounts of CL 56:0. Differences in signal intensities between both CL species were corrected by applying Rfs of 1.66 (TOF-MS mode) and 1.5 (product ion mode). As show in Figure 5, no significant differences between both analytical approaches were observed when CL 72:4 was quantified at concentration levels from 10 nM to >100 nM. Within this range, CL 72:4 could be linearly quantified in both modes. However, when the concentration of CL 72:4 reached levels <10 nM, quantification in the TOF-MS mode was not possible anymore. Due to noise peaks, very low amounts of CL 72:4 were not distinguishable from background peaks, leading to apparent higher amounts. Noticeably, in the product ion mode, CL 72:4 could be linearly quantified down to concentration levels of ~1 nM, indicating an extended dynamic range towards lower concentrations.

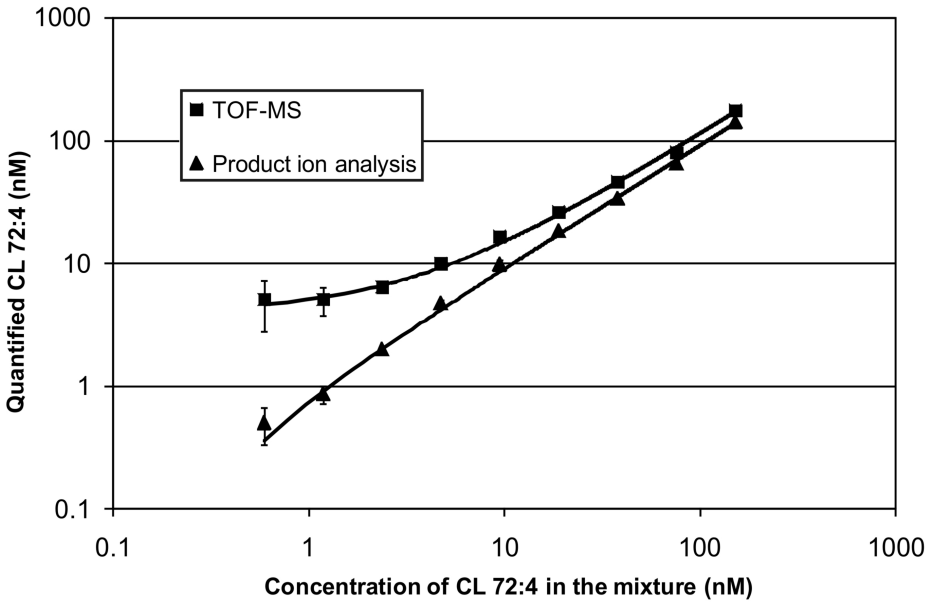

Figure 5: Limit of CL quantification. CL 72:4 was titrated over the indicated concentration range and quantified by fixed amounts of the internal standard CL 56:0. Mass spectrometric analysis was performed by TOF-MS and in the product ion mode. Data represent mean ± average deviation of three independent experiments.

2.1.1.2 CL quantification in the presence of mitochondrial lipid extracts

In order to ensure robust and accurate quantification of endogenous CL species in mitochondrial lipid extracts, the influence of mitochondrial lipid background on the quantification of CL 72:4 was tested. For this purpose, mitochondria were isolated from Δcrd1 yeast mutants that cannot synthesize CL due to the absence of the cardiolipin

synthase Crd1 (Chang et al., 1998b; Jiang et al., 1997). A dilution series of CL 72:4 was prepared and spiked together with a fixed proportion of CL 56:0 (50 pmol) into constant amounts of ∆crd1 mitochondria (~1 nmol phospholipids). After lipid extraction, CL 72:4 was quantified in the product ion mode by the internal standard CL 56:0. As depicted in Figure 6, quantification of CL 72:4 was linear over a broad range of analyzed CL amounts clearly indicating that the lipid background of mitochondrial preparations did not influence the quantification of singly charged CL in the product ion mode.

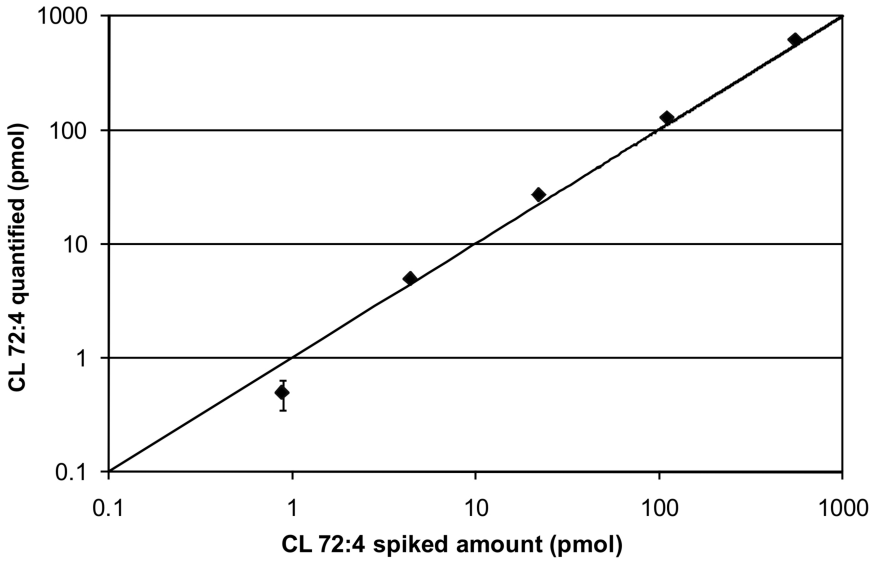

Figure 6: CL quantification in the presence of mitochondrial lipid extracts. Different amounts of CL 72:4 were spiked into mitochondrial fractions derived from ∆crd1 yeast cells. After spiking a fixed amount of the internal standard CL 56:0, lipids were extracted and CL 72:4 was quantified in the product ion mode. Data represent mean ± average deviation of two independent experiments.

2.1.1.3 Identification and quantification of CL in yeast mitochondria

In order to demonstrate that endogenous CL species can be identified and quantified by product ion analysis of singly charged CL ions, mitochondrial fractions were isolated from wt and taffazin knock out yeast cells (∆taz1) and lipid extracts were investigated with respect to CL. Taz1 has been described as a putative transacylase involved in fatty acid remodeling of CL (Xu et al., 2006; Malhotra et al., 2009; Xu et al., 2003). In particular, taffazin is responsible for the attachment of unsaturated fatty acids onto monolyso-cardiolipin (MLCL) in order to generate a “mature” CL pool with a high degree of unsaturated, symmetric CL species (Schlame et al., 2005). In the absence of taffazin, mitochondria exhibit an aberrant CL species profile with a higher degree of saturated species as compared to the wt profile (Gu et al., 2004; Li et al., 2007a).

For quantification of mitochondrial CL, product ion analysis of putative, endogenous CL species was performed (Table 1). The list covers 45 different CL species with all possible combinations of the fatty acids 16:0, 16:1, 16:2, 18:0, 18:1 and 18:2 which were previously identified in yeast cells (Schneiter et al., 1999) and yeast mitochondrial fractions (Schlame et al., 1993). To ensure correct quantification of molecular species, the isotopic contribution of signals derived from neighboring CL species was compensated by correction for isotopic overlap (data not shown). Furthermore, the experimentally determined response factor of 1.5 (see chapter 2.1.1.1) was used to correct for response differences between the internal standard CL 56:0 and endogenous CL species. To increase the specificity of CL species identification, a threshold was applied to the data set. Only species accounting for >0.5 mol% of the 45 analyzed precursors were considered to be unambiguously identified as CL.

Species	m/z $[M-H]^-$	Possible fatty acid combinations	Species	m/z $[M-H]^-$	Possible fatty acid combinations
CL 64:8	1335.84	16:2	CL 70:8	1419.93	16:2, 18:2
CL 64:7	1337.86	16:2, 16:1	CL 70:7	1421.95	16:2, 16:1, 18:2, 18:1
CL 64:6	1339.87	16:2, 16:1, 16:0	CL 70:6	1423.96	16:2, 16:1, 16:0, 18:2, 18:1, 18:0
CL 64:5	1341.89	16:2, 16:1, 16:0	CL 70:5	1425.98	16:2, 16:1, 16:0, 18:2, 18:1, 18:0
CL 64:4	1343.90	16:2, 16:1, 16:0	CL 70:4	1428.00	16:2, 16:1, 16:0, 18:2, 18:1, 18:0
CL 64:3	1345.92	16:2, 16:1, 16:0	CL 70:3	1430.01	16:2, 16:1, 16:0, 18:2, 18:1, 18:0
CL 64:2	1347.93	16:2, 16:1, 16:0	CL 70:2	1432.03	16:2, 16:1, 16:0, 18:2, 18:1, 18:0
CL 64:1	1349.95	16:1, 16:0	CL 70:1	1434.04	16:1, 16:0, 18:1, 18:0
CL 64:0	1351.96	16:0	CL 70:0	1436.06	16:0, 18:0
CL 66:8	1363.87	16:2, 18:2	CL 72:8	1447.96	18:2
CL 66:7	1365.89	16:2, 16:1, 18:2, 18:1	CL 72:7	1449.98	18:2, 18:1
CL 66:6	1367.90	16:2, 16:1, 16:0, 18:2, 18:1, 18:0	CL 72:6	1452.00	18:2, 18:1, 18:0
CL 66:5	1369.92	16:2, 16:1, 16:0, 18:2, 18:1, 18:0	CL 72:5	1454.01	18:2, 18:1, 18:0
CL 66:4	1371.93	16:2, 16:1, 16:0, 18:2, 18:1, 18:0	CL 72:4	1456.03	18:2, 18:1, 18:0
CL 66:3	1373.95	16:2, 16:1, 16:0, 18:2, 18:1, 18:0	CL 72:3	1458.04	18:2, 18:1, 18:0
CL 66:2	1375.96	16:2, 16:1, 16:0, 18:2, 18:1, 18:0	CL 72:2	1460.06	18:2, 18:1, 18:0
CL 66:1	1377.98	16:1, 16:0, 18:1, 18:0	CL 72:1	1462.07	18:1, 18:0
CL 66:0	1380.00	16:0, 18:0	CL 72:0	1464.09	18:0
CL 68:8	1391.90	16:2, 18:2			
CL 68:7	1393.92	16:2, 16:1, 18:2, 18:1			
CL 68:6	1395.93	16:2, 16:1, 16:0, 18:2, 18:1, 18:0			
CL 68:5	1397.95	16:2, 16:1, 16:0, 18:2, 18:1, 18:0			
CL 68:4	1399.96	16:2, 16:1, 16:0, 18:2, 18:1, 18:0			
CL 68:3	1401.98	16:2, 16:1, 16:0, 18:2, 18:1, 18:0			
CL 68:2	1404.00	16:2, 16:1, 16:0, 18:2, 18:1, 18:0			
CL 68:1	1406.01	16:1, 16:0, 18:1, 18:0			
CL 68:0	1408.03	16:0, 18:0			

Table 1: Putative CL species of yeast mitochondria. The list represents CL species (all combinations of the fatty acids 16:0, 16:1, 16:2, 18:0, 18:1 and 18:2) that were used for CL quantification by product ion analysis. Molecular species are indicated by their fatty acid composition (species), the theoretical m/z of singly charged CL ions $[M-H]^-$ and possible fatty acid combinations.

Product ion analysis of putative CL precursor ions enabled the identification and quantification of 28 molecular CL species in wt and Δtaz1 mitochondria (Figure 7 A). As expected, the CL species profile of wt mitochondria reflected a rather symmetric distribution with a high degree of monounsaturated fatty acids (Schlame et al., 2005). The most prominent CL species were found to be CL 66:4, CL 68:4 and CL 70:4. In contrast, the species pattern in Δtaz1 mitochondria showed an altered profile, characterized by significant reduced levels of unsaturated species, such as CL 64:4, CL 66:4, CL 68:7, CL 68:4, CL 70:7 and CL 70:4, which was compensated by elevated levels of species with a higher degree of saturation such as CL 66:3, CL 66:2, CL 68:3 and CL 68:2.

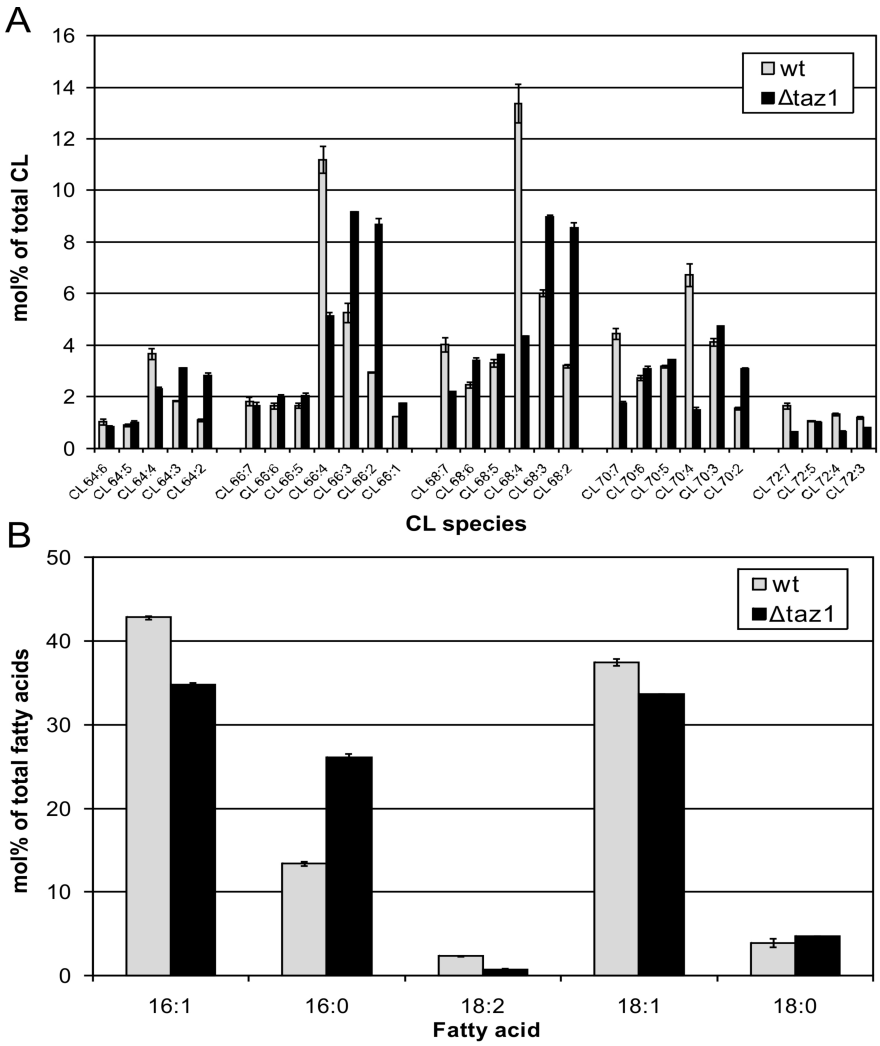

Figure 7: Identification and quantification of endogenous CL species. (A) Phospholipids of wt and Δtaz1 mitochondrial fractions were extracted in the presence of the internal standard CL 56:0 and analyzed by product ion analysis of CL precursors (Table 1). Endogenous CL species were quantified via the corresponding fatty acid fragments. Data represent mean ± average deviation of two independent experiments. (B) Distribution of fatty acids derived from CL species identified in wt and Δtaz1 mitochondria.

The fatty acid distribution, as depicted in Figure 7 B, revealed that the saturated fatty acids 16:0 and 18:0 were specifically enriched in Δtaz1 mitochondria whereas the unsaturated fatty acids 16:1, 18:1 and 18:2 were reduced compared to the wt situation. Interestingly, the most prominent effect occurred on the level of the fatty acid 16:0 which was ~1.8-fold increased in Δtaz1 mitochondria.

Consistent with previous observations (Daum and Vance, 1997), the basal level of all 28 identified CL species in wt mitochondria was quantified to ~15 mol% (Figure 8). CL level in Δtaz1 mitochondria were slightly reduced, accounting to ~12 mol% of phospholipids (Figure 8).

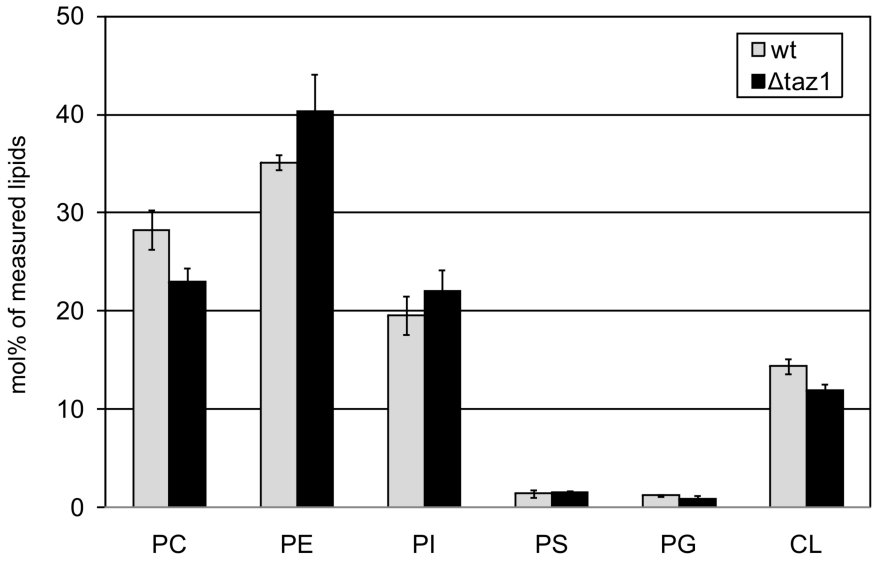

Figure 8: Quantification of phospholipids in wt and Δtaz1 mitochondria. Phospholipids were extracted in the presence of internal lipid standards. For CL quantification, lipid extracts were analyzed by product ion analysis of CL precursors (Table 1). Endogenous CL was quantified via the corresponding fatty acid fragments. Quantification of other lipid classes was done as described in materials and methods. Data represent mean ± average deviation of two independent experiments.

2.1.2 Quantification of DAG

DAG is a low abundant but highly important lipid molecule of biological membranes that has been associated with cellular processes such as protein recruitment and activation (Carrasco and Merida, 2004), signaling (Toker, 2005) and vesicular trafficking (Fernandez-Ulibarri et al., 2007; Kearns et al., 1997; Litvak et al., 2005). To analyze molecular processes that are intimately linked to changes in the level of DAG, applicable methods for their absolute quantification are required. We therefore aimed at the development of a method that allows the identification and quantification of DAG by nano-ESI-MS/MS. To this end, a commercially available DAG species was characterized with respect to its mass spectrometric ionization and fragmentation behavior.

2.1.2.1 Mass spectrometric characterization of DAG molecular species

For glycerolipids such as DAG and TAG it has previously been shown that they form positively charged ammonium adducts when analyzed by atmospheric pressure chemical ionization (APCI) (Mu and Hoy, 2000) and nano-ESI (Schwudke et al., 2006; Murphy et al., 2007). To analyze the ionization and fragmentation behavior of DAG on our system a commercially available DAG species with the fatty acid composition 16:0/18:1 (DAG 34:1) was analyzed in the presence of ammonium acetate. In the TOF-MS mode, DAG 34:1 showed a prominent peak at m/z 612.57 corresponding to its ammoniated form (Figure 9 A). Collision-induced dissociation (product ion analysis) of the precursor at m/z 612.57 resulted in a fragment pattern typically observed for DAGs (Murphy et al., 2007) (Figure 9 B). Four characteristic fragment ions were detected at m/z 595.54, m/z 577.53, m/z 339.3 and m/z 313.28. The fragment at m/z 577.53 resulted from the dissociation of H_2O + NH_3 leading to a characteristic neutral loss of 35 Da (NL 35) (Murphy et al., 2007). The fragments at m/z 313.28 and m/z 339.3 reflected neutral losses of the fatty acids 16:0 and 18:1 together with ammonia (RCOOH + NH_3) (Murphy et al., 2007) leading to positively charged ions that represent monoacylglycerol-H_2O fragments MAG-H_2O 16:0 and MAG-H_2O 18:1. In contrast to previous observations (Murphy et al., 2007) a weak loss of deprotonated ammonia (neutral loss of 17 Da) was detected leading to a protonated DAG molecule at m/z 595.54. Nevertheless, the presence of this ion depends on the collision energy (CE) since it disappeared at higher CE offsets (data not shown).

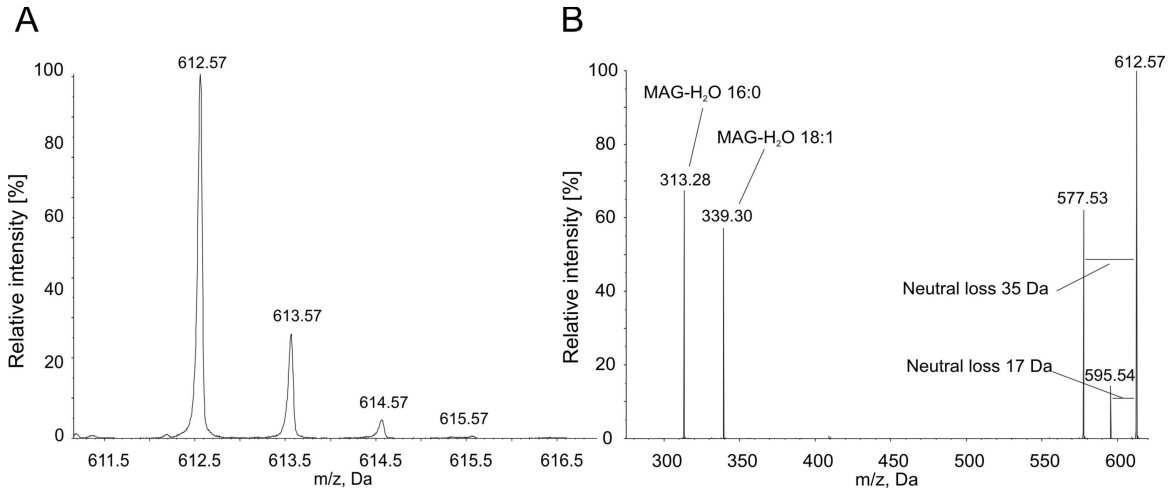

Figure 9: Ionization and fragmentation of DAG. (A) Detection of DAG 34:1 (16:0/18:1) as positively charged ammonium adduct in the TOF-MS mode. (B) Product ion analysis of DAG 34:1 confirmed the typical fragmentation pattern of DAGs. Lipid class specific neutral losses and MAG-H_2O fragments are displayed.

To achieve optimal dissociation conditions for MS/MS experiments the dependence of the collision energy on the intensities of MAG-H_20 and NL 35 fragments was investigated. To cover a broad range of molecular species, commercially available DAGs with the fatty acid composition 14:0/14:0 (DAG 28:0), 16:0/16:0 (DAG 32:0), 16:0/18:1 (DAG 34:1), 17:0/17:0 (DAG 34:0), 18:1/18:1 (DAG 36:2) and 18:0/20:4 (DAG 38:4) were analyzed by product ion analysis. For every species, the CE was ramped from 5 to 55 eV and the peak intensities of MAG-H_2O and NL 35 fragments were monitored (Figure 10 A-F). All DAG species showed a similar correlation between the CE and the intensities of the MAG-H_2O fragments, whereas a CE of 25 eV resulted in most intense signals. In contrast, for NL 35 fragments the dissociation efficiency varied depending on the fatty acid composition of the parent molecule. Whereas for DAG 28:0 and DAG 32:0 a CE of 15 eV resulted in most intense NL 35 derived fragments, species with longer fatty acid chains such as DAG 34:1, 34:0, 36:2 and 38:4 required a CE of 25 eV for optimal dissociation. In general, NL 35 derived fragments displayed lower peak intensities compared to the MAG-H_2O ions. However, DAG 38:4 with the polyunsaturated fatty acid 20:4 exhibited a drastic, ~8-fold lower intensity of the NL 35 derived fragment (Figure 10 F). This characteristic fragmentation behavior did not allow a sensitive analysis of DAG 38:4 by neutral loss scanning for 35 Da (data not shown). In contrast, MAG-H_2O ions showed comparable peak intensities of all analyzed DAG species, thus making MAG-H_2O fragments the preferential ions to scan for in MS/MS experiments.

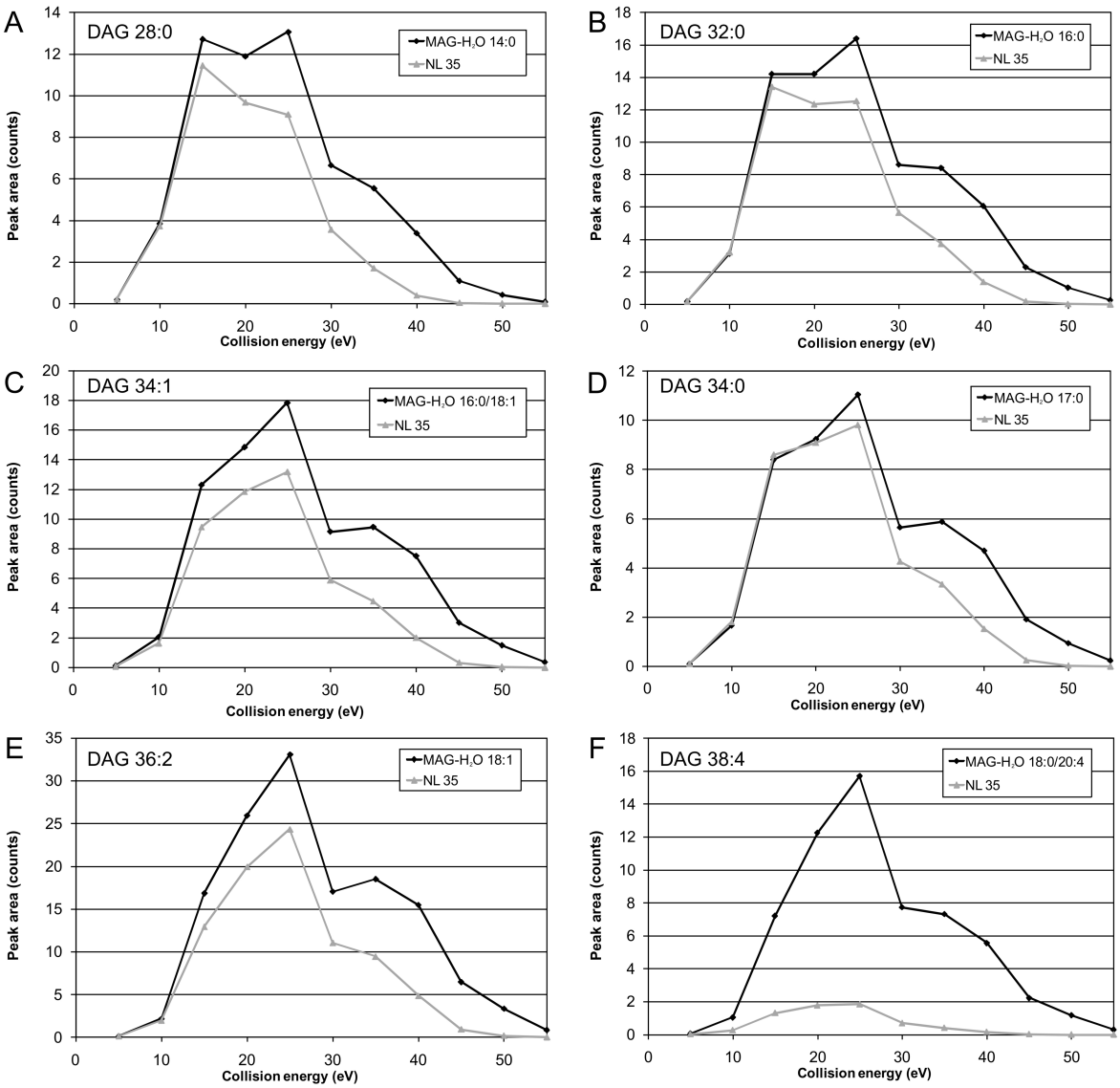

Figure 10: Fragmentation efficiency of DAG molecular species at different CEs. Peak areas of NL 35 and MAG-H_20 fragments are displayed for the indicated CE. For asymmetric DAG species, the peak area sum of two MAG-H_2O fragments is displayed. Data represent mean values ± average deviation of two experiments.

2.1.2.2 Identification and quantification of DAG by MPIS

Multiple precursor ion scanning (MPIS) was successfully developed for the identification and quantification of glycerophospholipids by quadrupole time-of-flight mass spectrometry (Ekroos et al., 2002; Ejsing et al., 2006). In comparison to conventional precursor ion and neutral loss scanning on triple quadrupole instruments, the non-scanning TOF-analyzer allows the acquisition of a virtually unlimited number of precursor ion scans at the same time. This feature was used to perform MPIS of a set of negatively charged fragment ions that are characteristic for glycerophospholipids. The software tool Lipid Profiler (currently

LipidView^{TM}) was developed to cope with MPIS data by comparing MPIS spectra with lipid class specific fragment ions that are stored in a database. Furthermore, the software automatically corrects for isotopic overlap, thus enabling the accurate quantification of lipid classes and lipid species from complex lipid mixtures. Besides being applicable for the identification and quantification of glycerophospholipids, the Lipid Profiler software has also been used for the evaluation of MPIS spectra derived from DAGs and TAGs (Stahlman et al., 2009).

Similar as described (Stahlman et al., 2009), MPIS of 18 DAG-derived MAG-H_2O fragments, that are stored in the Lipid Profiler database (Table 2), was performed in order to facilitate the identification and quantification of endogenous DAG species. To test this approach, an equimolar mixture of commercially available reference standards with the fatty acid composition 14:0/14:0 (DAG 28:0), 16:0/16:0 (DAG 32:0), 16:0/18:1 (DAG 34:1), 18:1/18:1 (DAG 36:2) and 18:0/20:4 (DAG 38:4) was analyzed by MPIS together with DAG 17:0/17:0 (34:0) as internal standard. Lipid species with an odd numbered fatty acid composition have been demonstrated to be distinguishable from endogenous species by MPIS and can therefore serve as internal standards (Ejsing et al., 2006).

MAG-H_2O fragment	m/z
14:1	283.2
14:0	285.2
16:2	309.2
16:1	311.3
16:0	313.3
17:0	327.3
18:3	335.3
18:2	337.3
18:1	339.3
18:0	341.3
20:5	359.3
20:4	361.3
20:3	363.3
20:2	365.3
20:1	367.3
20:0	369.3
22:6	385.3
22:5	387.3

Table 2: DAG-specific MAG-H_20 fragments used for MPIS. The fragments were taken from the Lipid Profiler database.

As depicted in Figure 11 A-F, MPIS allowed the simultaneous identification of DAG species indicated by positively charged DAG parent ions that were detected by the corresponding precursor ion scan for MAG-H_2O ions. Symmetric species such as DAG 28:0 (14:0/14:0), DAG 34:0 (17:0/17:0) and DAG 36:2 (18:1/18:1) were detected in one precursor ion scan. In contrast, asymmetric species such as DAG 34:1 (16:0/18:1) and DAG 38:4 (18:0/20:4) were detected in two different scans.

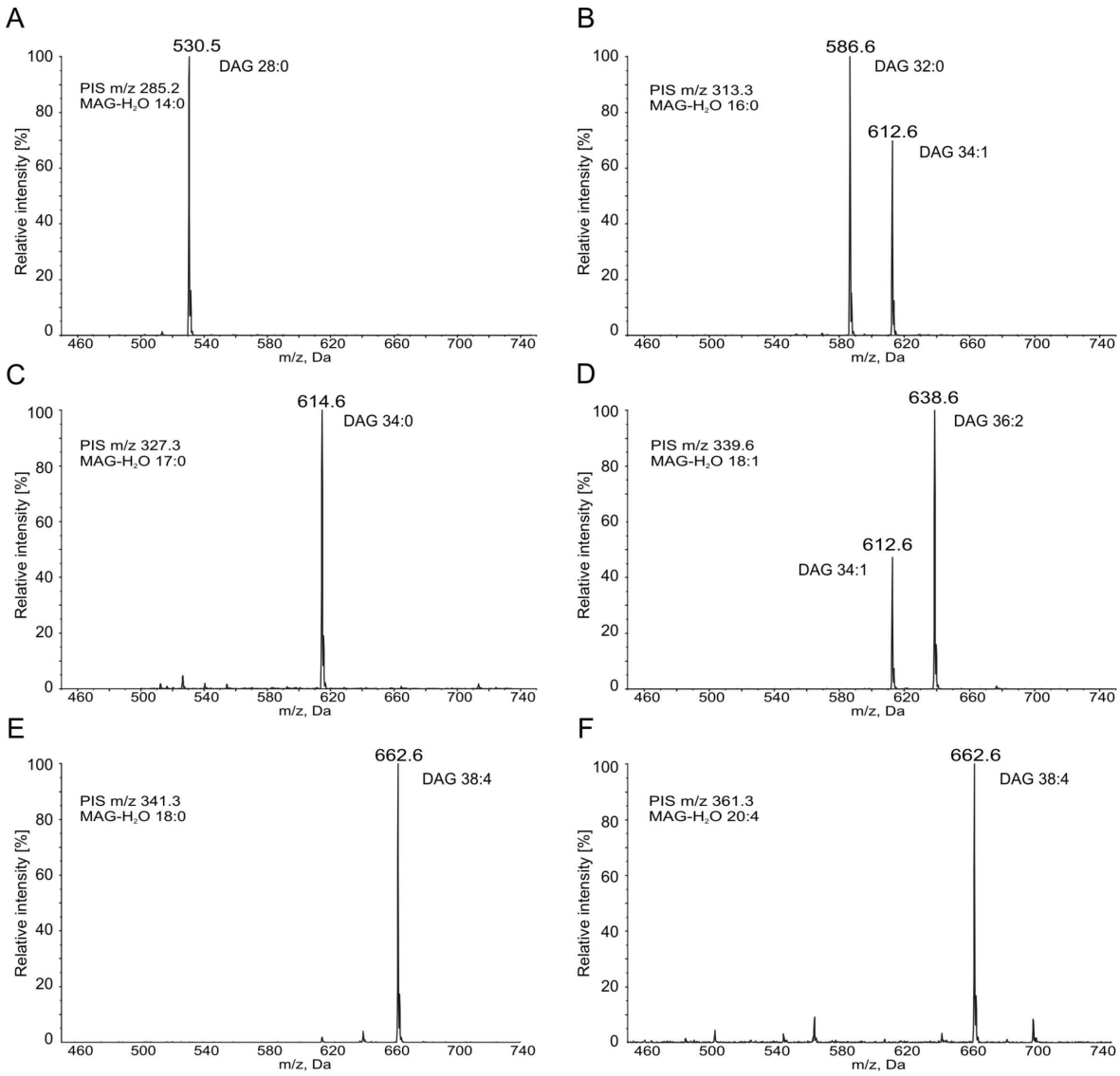

Figure 11: Identification of DAG by MPIS. Six DAG molecular species were prepared in equimolar amounts and analyzed by MPIS for DAG-specific MAG-H_2O fragments (Table 2). Precursor peaks represent positively charged DAG ammonium adducts.

In order to determine response factors (Rfs), DAG reference standards were prepared in different quantities (1-20 pmol) and analyzed together with a constant amount (20 pmol) of the internal standard DAG 34:0 (17:0/17:0) by MPIS. As shown in Table 3, the Rf-values

of all DAG species, except DAG 38:4, were close to 1 with a maximum deviation of about 10% for DAG 28:0 and DAG 32:0. DAG 38:4 was underestimated ~1.7-fold compared to other species.

DAG species	m/z (NH_4^+)	Rf (n=4)
28:0 (14:0/14:0)	530.5	0.91 ± 0.09
32:0 (16:0/16:0)	586.6	0.90 ± 0.12
34:1 (16:0/18:1)	612.6	1.07 ± 0.07
34:0 (17:0/17:0)	614.6	1
36:2 (18:1/18:1)	638.6	1.06 ± 0.09
38:4 (18:0/20:4)	662.6	1.70 ± 0.11

Table 3: Response factors of the internal standard DAG 34:0 (17:0/17:0). Quantification was achieved by MPIS for DAG-specific MAG-H_2O fragments (Table 2). Data evaluation was done with the Lipid Profiler software.

2.1.2.3 Identification and quantification of DAG in Golgi membranes

All experiments so far were performed in a minimal system consisting of defined DAG species, i.e. in the absence of potentially interfering lipid classes. When analyzing crude lipid extracts such as Golgi membranes, it has to be excluded that structurally similar lipids such as TAGs interfere with DAG-specific precursor ion scans. It was reported previously that TAGs display DAG-characteristic MAG-H_2O fragments upon collision-induced dissociation (Mu and Hoy, 2000). We therefore tested the fragmentation behavior of TAGs on the nano-ESI-MS/MS system used in this study. Notably, we found that TAGs did not display DAG-characteristic MAG-H_2O fragments (data not shown), thus the established MPIS method was suitable for the quantification of DAG in crude lipid extracts, unaffected by TAG cross-fragmentation.

Subsequently, MPIS was applied to identify and quantify endogenous DAG in Golgi membranes isolated from HeLa cells. To define the minimum amount of Golgi membranes needed for robust DAG quantification, increasing amounts of Golgi lipid extracts (0.07-15 µg protein) were analyzed by MPIS and DAG levels quantified by the internal standard DAG 34:0 (17:0/17:0). As depicted in Figure 12, DAG quantification showed a linear correlation between ~1-15 µg Golgi protein. In the linear range, the DAG basal level in the Golgi was quantified to ~80-90 pmol/µg protein. Assuming a protein/phospholipid ratio of ~1.2 in the Golgi, this reflects DAG amounts of ~7.6 mol% of phospholipids. In contrast, at protein amounts <1 µg the DAG content was misleadingly overestimated reaching a plateau between 160-500 pmol/µg protein (Figure 12). Taken together, optimal amounts of Golgi membranes that facilitate accurate DAG quantification were found to be in the range

of ~1-15 µg protein. Within the linear range, 9 DAG species were identified in Golgi membranes with the major species being DAG 32:0 and DAG 34:1 followed by less abundant DAG 30:0, DAG 32:1, DAG 34:0, DAG 34:2, DAG 36:0, DAG 36:1 and DAG 36:2 (Figure 13).

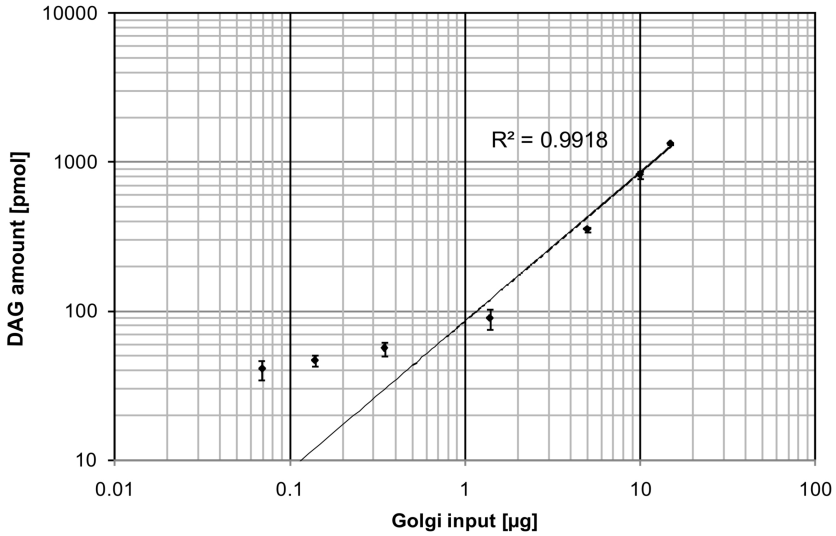

Figure 12: Dynamic range of Golgi DAG quantification. Quantification was done by MPIS for DAG-specific MAG-H_2O fragments (Table 2). Data evaluation was performed with the Lipid Profiler software. Data represents mean values ± average deviation of two independent extractions.

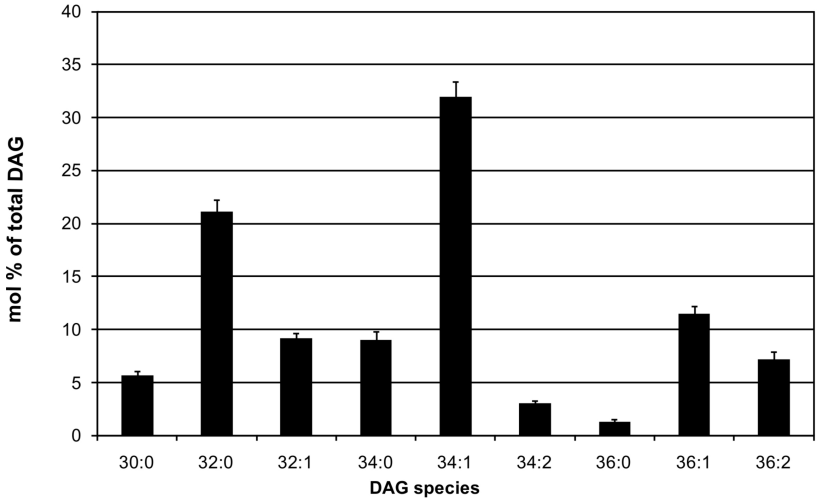

Figure 13: DAG species in Golgi membranes derived from HeLa cells. Identification and quantification was done by MPIS for DAG-specific MAG-H_2O fragments (Table 2). Data evaluation was performed with the Lipid Profiler software. Data represents mean values ± average deviation of five independent extractions each analyzed in duplicate.

Although DAG was unambiguously identified and quantified in Golgi membranes derived from HeLa cells, the observed amounts (80-90 pmol/µg protein) were more than 100-fold higher compared to published data (0.55 pmol/µg protein) (Fernandez-Ulibarri et al., 2007). To solve these discrepancies, the DAG level in several Golgi fractions prepared from rat liver, HeLa or CHO cells were systematically analyzed by MPIS. Noticeable, the DAG quantities in the different Golgi preparations were quite variable, ranging from 5-75 pmol DAG/µg protein which corresponds to ~0.5-7 mol% DAG of phospholipids (data not shown). Nevertheless, even the lowest amount determined (5 pmol/µg protein) was still ~10-fold higher compared to the amount published (0.55 pmol/µg protein) (Fernandez-Ulibarri et al., 2007). To further exclude that the mass spectrometric method over-estimated the DAG contents, Golgi DAG was quantified by an independent assay, the DAG kinase assay (Bielawska et al., 2001). DAG kinase-based quantification was performed by Dr. Inés Fernández-Ulibarri (Research Group: Prof. Dr. Gustavo Egea, Barcelona, Spain) and revealed DAG amounts between ~80-100 pmol/µg protein in Golgi fractions derived from HeLa cells (data not shown). In conclusion, no significant differences were found between the mass spectrometric data and the results obtained by the DAG kinase assay, indicating that the mass spectrometric method produced valid data.

2.1.3 Quantification of PIP and PIP_2

The phosphoinositides PIP and PIP_2 (PIPs) are low abundant but highly important lipid classes of biological membranes that have been associated with cellular processes such as signaling, regulation of membrane traffic, nuclear events and permeability and transport functions of membranes (Di Paolo and De Camilli, 2006). To analyze molecular processes that are intimately linked to changes in the level of PIPs, methods for their identification and quantification are required. We therefore aimed at the development of an approach that allows the quantification of PIPs by nano-ESI-MS/MS. HeLa cells were taken as a model system to investigate (i) the extraction behavior of endogenous PIPs and (ii) identify and quantify molecular PIP and PIP_2 species. Furthermore, commercially available standards were used to characterize the ionization and fragmentation behavior of PIP and PIP_2 in order to set up lipid class specific scans that allow the mass spectrometric analysis.

2.1.3.1 Extraction behavior of endogenous PIP and PIP_2 in HeLa cells

Due to their polar headgroups, PIPs cannot be sufficiently recovered from biological membranes by conventional extraction procedures such as Folch (Folch et al., 1957) or Bligh and Dyer (Bligh and Dyer, 1959). Therefore, modified extraction protocols were introduced decades ago (Dawson and Eichberg, 1965) and continuously optimized and applied for the analysis of PIPs (Michell et al., 1970; Hama et al., 2000; Vickers, 1995; Milne et al., 2005; Pettitt et al., 2006; Wenk et al., 2003; Gray et al., 2003). To make PIPs accessible for mass spectrometric analysis, a previously described two-step extraction procedure for the selective enrichment of PIP and PIP_2 was performed (Gray et al., 2003). During the first extraction, the cell membrane is depleted from relatively apolar lipids by extracting with a mixture of chloroform/methanol (neutral extraction). Finally, negatively charged PIPs, which reside in the membrane during the neutral extraction, are recovered by an acidic extraction using a mixture of chloroform/methanol/HCl.

To determine the extraction behavior of endogenous PIPs, HeLa cells were labeled with *myo*-[^{3}H]-inositol and subjected to a two-step lipid extraction. ^{3}H-inositiol labeled lipids in neutral and the acidic extracts were separated by TLC and visualized by autoradiography. The autoradiogram in Figure 14 A shows the distribution of ^{3}H-PI, ^{3}H-PIP and ^{3}H-PIP_2 between the neutral and the acidic extract. Whereas most of ^{3}H-PI was recovered with the neutral extraction, the phosphoinositides ^{3}H-PIP and ^{3}H-PIP_2 were predominantly present in the acidic extract. Quantification of the spot intensities revealed that PI was recovered with ~16% in the acidic extract, whereas PIP and PIP_2 were enriched with ~58% and

~79% in the acidic extract, respectively (Figure 14 B). Taken together, the labeling experiments demonstrated that the two-step extraction provides an easy and fast approach to selectively enrich endogenous PIPs from cellular membranes.

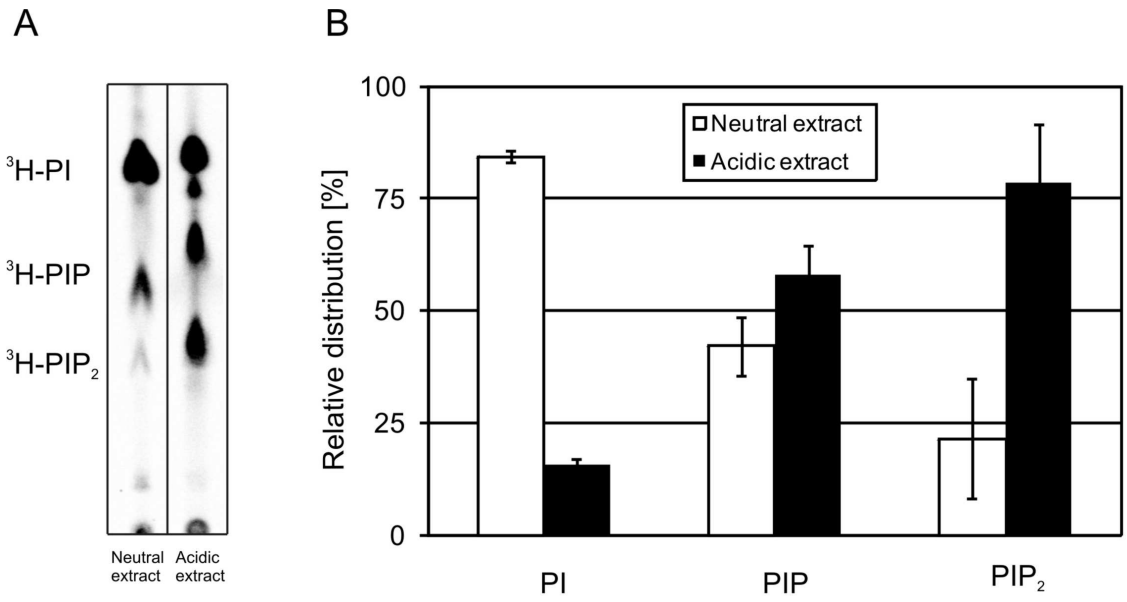

Figure 14: Extraction recovery of endogenous PIPs. HeLa cells were metabolically labeled with *myo*-[^{3}H]-inositol. After two-step lipid extraction, ^{3}H-labeled inositol lipids were separated by TLC and visualized by autoradiography. (A) Autoradiogram showing the distribution of ^{3}H-PI and ^{3}H-PIPs between neutral and acidic lipid extracts. (B) Quantification of the distribution of ^{3}H-PI and ^{3}H-PIPs in neutral and acidic extracts. Data represent mean values ± average deviation of four independent experiments. Note: the spot intensities in the autoradiogram (A) reflect only a proportion of the absolute radioactivity in neutral and acidic extracts. To avoid saturation of the detector, maximal 200 nCi were spotted prior TLC separation. For quantification (B), the spot intensities were extrapolated to determine the absolute amounts of PI and PIPs in lipid extracts.

2.1.3.2 Mass spectrometric characterization of PIP and PIP$_2$ molecular species

To set up a method for the mass spectrometric analysis of PIP and PIP$_2$, the ionization and fragmentation behavior of two commercially available internal standards, PI(4)P and PI(4,5)P$_2$ both with the fatty acid composition 17:0/20:4 (37:4) was investigated. When analyzing in positive ion mode in the presence of 25 mM ammonium acetate in chloroform/methanol/H_2O (1:1:0.05), PI(4)P 37:4 and PI(4,5)P$_2$ 37:4 showed distinct TOF-MS signals at m/z 970.5 (Figure 15 A) and at m/z 1050.5 (Figure 15 B), respectively. The mass differences of 17 Da compared to the calculated, nominal masses of m/z 953.51 for PI(4)P 37:4 and m/z 1033.48 for PI(4,5)P$_2$ 37:4 indicated that both molecules appeared as ammonium adducts (+NH_3). Collision-induced dissociation

(product ion mode) resulted in the formation of two prominent fragments for PIP and PIP_2, respectively (Figure 15 C and D). The fragment ions at m/z 953.5 and m/z 613.5 in the product ion spectra of PI(4)P 37:4 (Figure 15 C) corresponded to neutral losses of ammonia (17 Da) and inositoldiphosphate+NH_3 (357 Da). PI(4,5)P_2 37:4 showed a similar fragmentation pattern resulting in ions at m/z 1033.46 (neutral loss of ammonia) and m/z 613.5 corresponding to the neutral loss of inositoltriphosphate+NH_3 (437 Da) (Figure 15 D).

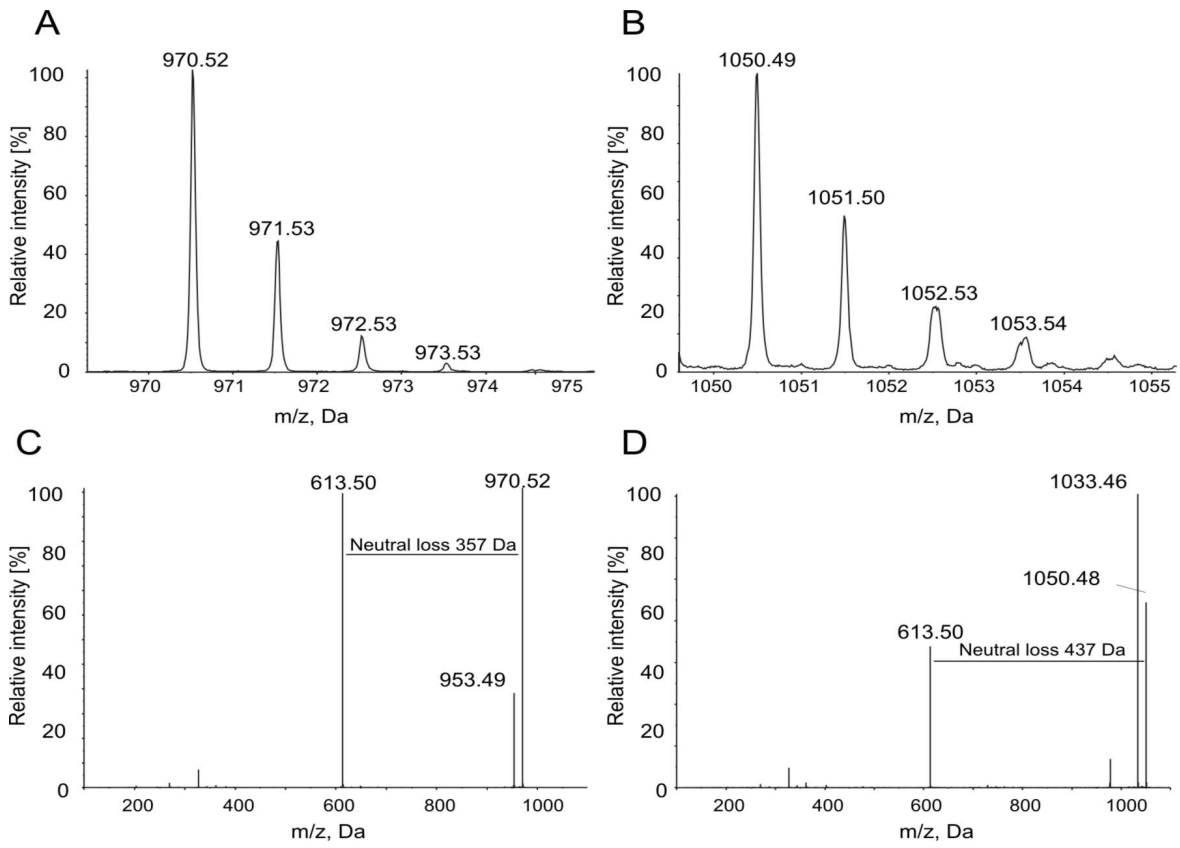

Figure 15: Ionization and fragmentation of PIPs. Detection of PI(4)P 37:4 (A) and PI(4,5)P_2 37:4 (B) as positively charged ammonium adducts in the TOF-MS mode. Product ion analysis of PI(4)P 37:4 (C) and PI(4,5)P_2 37:4 (D). Characteristic neutral losses of inositoldiphosphate+NH_3 (357 Da) and inositoltriphosphate+NH_3 (437 Da) are indicated.

To determine optimum dissociation conditions for MS/MS experiments the dependency of the applied collision energy (CE) on neutral loss derived signals at m/z 613.5 was investigated for both species. As depicted in Figure 16, PI(4)P 37:4 required a relatively low CE of 25 eV for efficient neutral loss of the headgroup fragment (357 Da). In contrast, PI(4,5)P_2 37:4 with one additional phosphate group required a CE of 35 eV for efficient neutral loss of the headgroup fragment (437 Da).

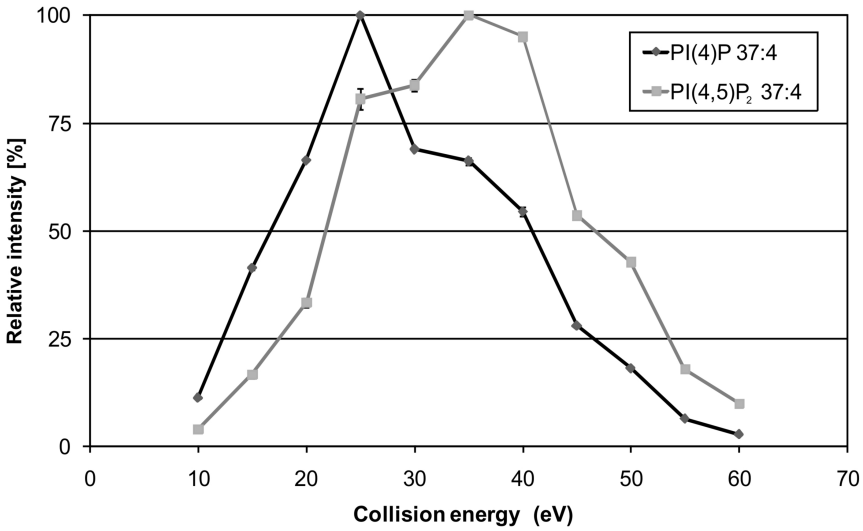

Figure 16: Fragmentation efficiency of PI(4)P 37:4 and PI(4,5)P_2 37:4 at different CEs. The peak intensities of neutral loss derived fragments (m/z 613.5) were normalized to the peak intensity at the optimal collision energy (100% relative intensity). Data represent mean values ± average deviation of two experiments.

2.1.3.3 Identification and quantification of PIP and PIP_2 by neutral loss scanning

To investigate endogenous PIPs by neutral loss scanning, commercially available bovine brain PI(4)P and bovine brain PI(4,5)P_2 were extracted together with the internal standards PI(4)P 37:4 and PI(4,5)P_2 37:4 and analyzed by scanning for neutral losses of 357 Da and 437 Da, respectively (Figure 17). Remarkably, neutral loss scanning enabled the identification of PIP and PIP_2 molecular species, indicated by characteristic profiles of brain PI(4)P (Figure 17 A) and brain PI(4,5)P_2 (Figure 17 B). Collectively, 16 molecular species of bovine brain derived PIPs were unambiguously identified and quantified by neutral loss scanning (Table 4).

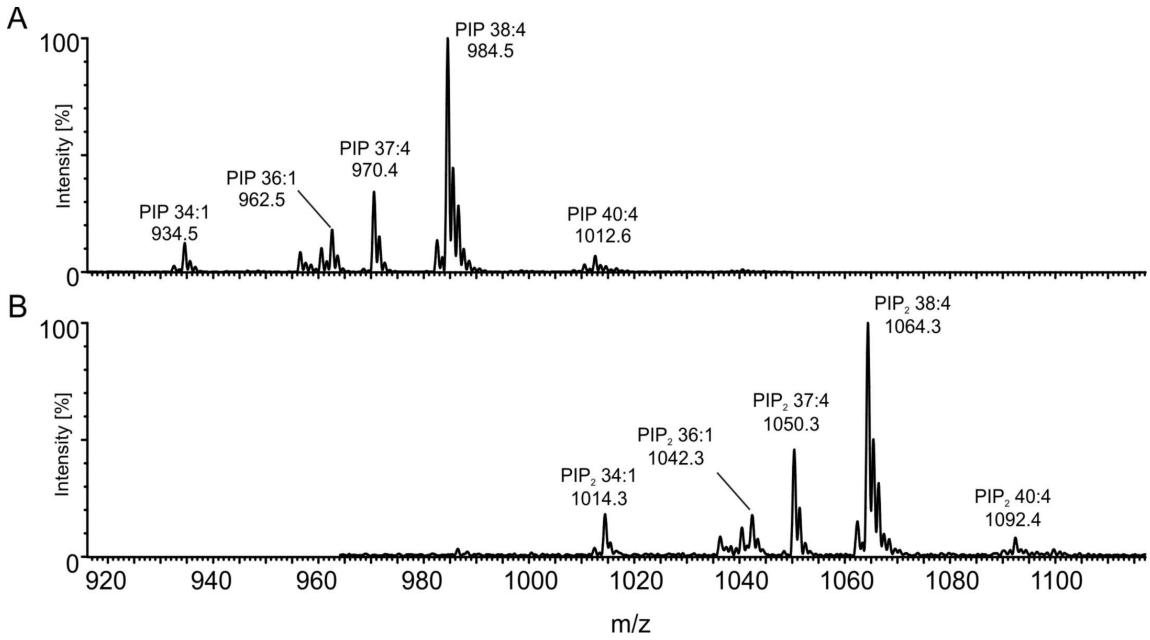

Figure 17: Identification of brain PI(4)P and brain PI(4,5)P_2 species. (A) Characteristic PI(4)P brain profile acquired by scanning for neutral losses of 357 Da. (B) Characteristic PI(4,5)P_2 brain profile acquired by scanning for neutral losses of 437 Da.

Species	PI(4)P bovine brain (NL 357)		PI(4,5)P_2 bovine brain (NL 437)	
	m/z	mol%	m/z	mol%
34:2	932.5	1.6 ± 0.2	1012.5	1.4 ± 0.1
34:1	934.5	6.7 ± 0.1	1014.5	7.6 ± 0.6
36:4	956.5	4.3 ± 0.2	1036.5	4.7 ± 0.0
36:3	958.5	1.2 ± 0.3	1038.5	1.0 ± 0.3
36:2	960.6	4.9 ± 0.7	1040.5	6.5 ± 0.5
36:1	962.6	8.1 ± 0.3	1042.5	8.9 ± 1.0
38:5	982.5	6.7 ± 0.3	1062.5	7.0 ± 0.8
38:4	984.6	47.6 ± 1.0	1064.5	41.2 ± 3.0
38:3	986.6	9.7 ± 0.0	1066.5	9.2 ± 0.1
38:2	988.6	1.6 ± 0.0	1068.6	3.1 ± 0.7
38:1	990.6	0.9 ± 0.2	1070.6	1.2 ± 0.2
40:6	1008.6	0.4 ± 0.1	1088.5	0.7 ± 0.2
40:5	1010.6	1.3 ± 0.2	1090.5	1.5 ± 0.3
40:4	1012.6	3.3 ± 0.1	1092.6	3.2 ± 0.2
40:3	1014.6	1.0 ± 0.0	1094.6	1.8 ± 0.6
40:2	1016.6	0.8 ± 0.2	1096.6	1.0 ± 0.2

Table 4: PI(4)P and PI(4,5)P_2 species identified in bovine brain. The species are indicated by their fatty acid composition, their m/z values (NH_4^+) and their relative abundances in mol%. Data represent mean values ± average deviation of three independent analyses.

To determine response factors (Rfs) between the internal standards and endogenous reference PIPs, different amounts of bovine brain PI(4)P (~50-200 pmol) and PI(4,5)P_2 (~250-1000 pmol) were mixed with constant amounts of PI(4)P 37:4 (~20 pmol) and PI(4,5)P_2 37:4 (~210 pmol). After acidic lipid extraction, the extracts were analyzed by neutral loss scanning on two different triple quadrupole instruments and by product ion analysis of dedicated PIP and PIP_2 species (Table 4) on a quadrupole time-of-flight instrument. Quantification of bovine brain PIPs resulted in comparable Rfs on all instruments (Table 5). For the internal standard PI(4)P 37:4, a Rf of ~1.1 was determined, indicating that endogenous PI(4)P brain species were slightly underestimated. In contrast, quantification of brain PI(4,5)P_2 species was slightly overestimated, indicated by Rf values <1.

	Instrument	PI(4)P bovine brain	PI(4,5)P_2 bovine brain
Internal standard PI(4)P 37:4	QTrap 5500	1.08 ± 0.10 (n=6)	-
	Quattro II	1.14 ± 0.10 (n=3)	-
	QStar Elite	1.05 ± 0.02 (n=6)	-
Internal standard PI(4,5)P_2 37:4	QTrap 5500	-	0.91 ± 0.11 (n=3)
	Quattro II	-	0.85 ± 0.07 (n=3)
	QStar Elite	-	0.84 ± 0.04 (n=5)

Table 5: Response factors of internal standards PI(4)P 37:4 and PI(4,5)P_2 37:4. Rfs were determined by quantification of endogenous PI(4)P and PI(4,5)P_2 derived from bovine brain. Data represent mean values ± average deviation of the indicated number of experiments.

2.1.3.4 Identification and quantification of PIP and PIP_2 in HeLa cells

We next aimed at the identification and quantification of endogenous PIPs in HeLa cells. To this end, HeLa cells were grown to 80-90% confluency and lipids were extracted by a two-step extraction (see chapter 2.1.3.1). For quantification, the internal standards PI(4)P 37:4 and PI(4,5)P_2 37:4 were spiked in defined amounts (50-200 pmol) to the cell sample after the neutral extraction. After acidic extraction, the lipid extract was analyzed by scanning for neutral losses of 357 Da and 437 Da in order to identify and quantify HeLa PIP and PIP_2 (Figure 18). Remarkably, neutral loss scanning enabled the identification of PIP and PIP_2 molecular species in acidic lipid extracts from HeLa cells indicated by characteristic profiles of HeLa PIP (Figure 18 A) and HeLa PIP_2 (Figure 18 B). Collectively, 18 different PIP and PIP_2 molecular species were unambiguously identified in the neutral loss spectra (Table 6).

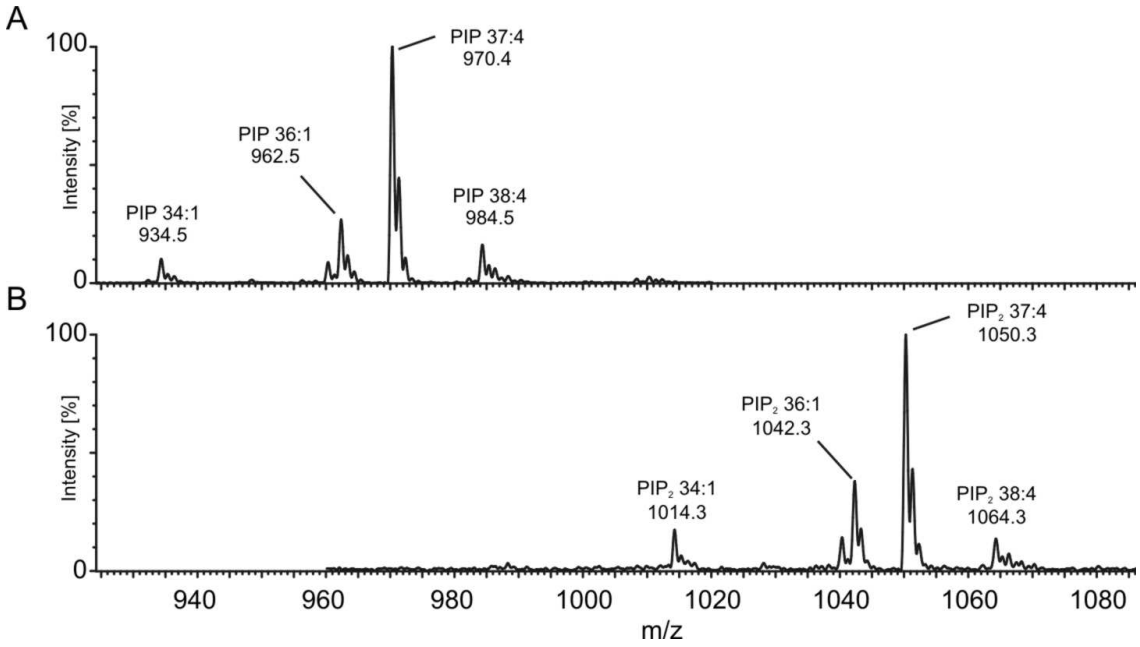

Figure 18: Identification of PIP and PIP_2 species in HeLa cells. (A) Characteristic PIP profile acquired by scanning for neutral losses of 357 Da. (B) Characteristic PIP_2 profile acquired by scanning for neutral losses of 437 Da.

Species	PIP HeLa (NL 357)		PIP_2 HeLa (NL 437)	
	m/z	mol%	m/z	mol%
32:1	906.5	1.0 ± 0.0	986.5	1.8 ± 0.0
32:0	908.5	0.9 ± 0.0	988.5	2.8 ± 0.0
34:2	932.5	1.5 ± 0.1	1012.5	2.0 ± 0.5
34:1	934.5	12.3 ± 0.4	1014.5	12.8 ± 1.2
36:4	956.5	1.5 ± 0.3	1036.5	2.1 ± 0.6
36:3	958.5	1.0 ± 0.1	1038.5	2.0 ± 0.3
36:2	960.6	11.2 ± 0.5	1040.5	11.9 ± 0.6
36:1	962.6	29.8 ± 1.3	1042.5	30.3 ± 2.1
38:5	982.5	2.8 ± 0.3	1062.5	2.3 ± 0.5
38:4	984.6	20.0 ± 1.0	1064.5	15.7 ± 1.9
38:3	986.6	6.7 ± 0.7	1066.5	5.4 ± 0.6
38:2	988.6	3.1 ± 0.1	1068.6	3.1 ± 0.9
38:1	990.6	1.5 ± 0.1	1070.6	1.7 ± 0.5
40:6	1008.6	2.1 ± 0.1	1088.5	1.8 ± 0.5
40:5	1010.6	3.1 ± 0.1	1090.5	3.1 ± 0.3
40:4	1012.6	1.8 ± 0.1	1092.6	2.4 ± 0.4
40:3	1014.6	0.8 ± 0.1	1094.6	1.3 ± 0.5
40:2	1016.6	0.4 ± 0.1	1096.6	1.3 ± 0.3

Table 6: PIP and PIP_2 species identified in HeLa cells. The species are indicated by their fatty acid composition, their masses (NH_4^+) and their relative abundances in mol%. Data represent mean values ± average deviation of six independent analyses.

For absolute quantification of PIP and PIP_2 basal level in HeLa cells the raw pmol-values were adjusted to correct for (i) losses during the neutral extraction (Figure 14) and (ii) response differences between endogenous PIPs and internal standards (Table 5). To compensate for losses during the neutral extraction, the data was multiplied by a factor of 1.72 for PIP (compensates for a loss of 42%) and by a factor of 1.27 for PIP_2 (compensates for a loss of 21%). The data was then multiplied with the response factors 1.14 for PIP and 0.85 for PIP_2. Thus, the absolute amount of PIP in HeLa cells was quantified to 0.34 ± 0.02 mol% of phospholipids (n=6). PIP_2 was quantified slightly higher to 0.49 ± 0.09 mol% of phospholipids (n=6). The amounts were in agreement with previous reports (Mallo et al., 2008).

2.2 Method application

2.2.1 Genetic interactors of prohibitins regulate mitochondrial PE and CL

Genetic interactors of prohibitins (GEP genes) comprise a set of 35 yeast genes that were identified by Dr. Christof Osman (Research Group: Prof. Dr. Thomas Langer, Institute for Genetics, University of Cologne) in a genome wide screen to genetically interact with prohibitins (Osman et al., 2009). Prohibitins are an evolutionary conserved and ubiquitously expressed family of membrane proteins that are essential for cell development in higher eukaryotes. Prohibitins form large ring complexes in inner mitochondrial membranes (Back et al., 2002; Tatsuta et al., 2005) and are involved in mitochondrial processes such as cell proliferation, apoptosis and cristae morphogenesis (Merkwirth et al., 2008; Merkwirth and Langer, 2009a). The molecular mechanisms of prohibitin function and, furthermore, a putative link between prohibitins and mitochondrial lipid homeostasis remained elusive. We aimed at a quantitative analysis of CL in mitochondria derived from GEP mutant cells to figure out whether GEP genes are involved in the regulation of mitochondrial CL. Furthermore, PE, another important mitochondrial lipid class that shares the ability to form non-bilayer structures with CL, was taken into account for quantitative lipid analysis.

2.2.1.1 Gep1 and Ups1 regulate the level of mitochondrial PE and CL

Gep1 and Ups1 comprise a set of proteins that were identified in a genome wide screen to genetically interact with prohibitins (Osman et al., 2009; Osman, 2009). Since the synthetic lethality of ∆phb1∆gep1 cells could be rescued by overexpression of *CHO1,* a first link between these proteins and the homeostasis of mitochondrial phospholipid composition was assigned to Gep1 (data not shown) (Osman et al., 2009). *CHO1* encodes for the PS synthase Cho1 which produces PS, the biosynthetic precursor of mitochondrial PE. Initial lipid analysis, performed by Dr. Christof Osman, revealed that mitochondria from ∆gep1 cells displayed reduced PE levels which were restored upon overexpression of *CHO1* (data not shown) (Osman et al., 2009). Within the array of genetic interactors, two other proteins, Ups1 and Gep2 showed high sequence similarities to Gep1 indicating that these genes could also be involved in the regulation of mitochondrial lipid levels.

To further investigate how Gep1, Ups1 and Gep2 affect the composition of mitochondrial CL and PE, quantitative lipid analysis of mitochondria isolated from ∆gep1, ∆ups1 and ∆gep2 yeast cells was performed (Figure 19 A and B). As expected from initial TLC experiments, the PE level in ∆gep1 mitochondria was strongly reduced, whereas the CL

level remained unaffected in the absence of Gep1. In contrast to *GEP1*, deletion of *GEP2* and *UPS1* did not affect PE levels within mitochondria. However, the lipid analysis revealed a critical role of Ups1 for the regulation of CL levels, since CL was decreased ~7-fold in Δups1 mitochondria but remained unaffected in the absence of Gep1 or Gep2. This data indicates that the accumulation of CL in mitochondria depends on Ups1, whereas Gep1 affects mitochondrial PE level. In contrast, Gep2 does not affect the levels of mitochondrial PE and CL. Notably, deletion of *GEP1* together with *UPS1* (Δgep1Δups1) resulted in elevated CL levels compared to Δups1 mitochondria. PE remained reduced in Δgep1Δups1 mitochondria, demonstrating that the absence of Ups1 does not alleviate the requirement of Gep1 in regulating PE.

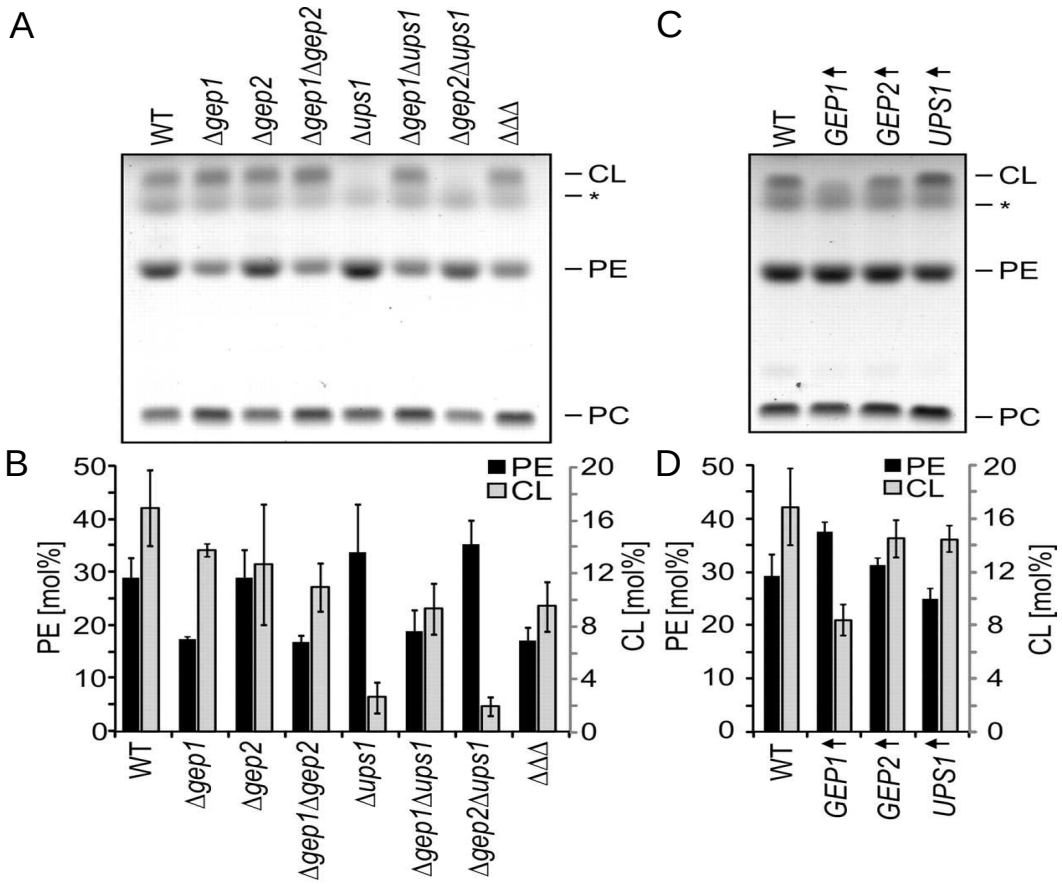

Figure 19: Gep1 and Ups1 affect mitochondrial levels of PE and CL. (A and B) Quantification of PE and CL in mitochondria lacking Gep1, Ups1 and Gep2. Phospholipids were extracted from mitochondria and analyzed by TLC (A) and mass spectrometry (B). Mean values ± standard deviation obtained from at least two independent mitochondrial isolations each analyzed in duplicate are shown in B. The asterisk in A indicates an unidentified lipid species. (C and D) PE and CL levels of mitochondria derived from cells overexpressing Gep1, Ups1 and Gep2. Phospholipids were extracted from mitochondria and analyzed by TLC (C) and mass spectrometry (D). Mean values ± standard deviation obtained from at least two independent mitochondrial isolations each analyzed in duplicate are shown in D.

To further define functional links of PE and CL regulatory pathways, yeast strains, overexpressing Gep1, Gep2, or Ups1 were generated, mitochondria were isolated and subjected to lipid analysis employing TLC and mass spectrometry (Figure 19 C and D). A significantly reduced CL content accompanied by slightly increased PE levels was observed in mitochondria isolated from yeast cells overexpressing Gep1. The overexpression of Gep2 and Ups1 did not significantly affect PE and CL levels in mitochondria.

In summary, these experiments indicate lipid-specific activities of Gep1 and Ups1 proteins for PE and CL and, at the same time, point to common steps in the regulation of both phospholipids within mitochondria. Both, the observed restoration of CL levels in Δups1 cells upon deletion of *GEP1* and the reduction of CL levels upon Gep1 overexpression suggests a competition between Gep1 and Ups1.

2.2.1.2 CL and PE profiles of mitochondria lacking GEP genes

As demonstrated by quantitative mass spectrometry, the proteins Gep1 and Ups1 play a crucial role in the regulation of mitochondrial PE and CL, respectively. Accordingly, other GEP genes may affect PE and CL levels in mitochondrial membranes as well. Therefore, mitochondria were isolated from yeast strains lacking Phb1 or GEP genes, and the levels of PE and CL were quantified by mass spectrometry (Figure 20). Mitochondrial PE and/or CL were affected in the majority of 23 examined strains. Only some strains showed normal PE and almost unaltered CL levels in mitochondria. The latter group included cells lacking assembly factors of the F_O-subunit of the F_1F_O-ATP-synthase, like Atp10 and Atp23, that have been previously found to interact genetically with prohibitins (Osman et al., 2007), or Oxa1, for which a function during F_O-assembly was recently described (Jia et al., 2007). Deletion of *PSD1* or *CRD1* resulted in the expected drastic reduction of the PE or CL content of mitochondrial membranes. Notably, increased PE levels were observed in cells showing a severely reduced CL content. This is in agreement with previous observations of an increase in mitochondrial PE in Δcrd1 cells, and suggested a coordinated regulation of both phospholipids (Zhong et al., 2004). Moreover, membranes isolated from Phb1-deficient mitochondria contained reduced amounts of CL and slightly increased PE levels. Strikingly, the loss of a large number of GEP genes, genetically interacting with prohibitins, led to strongly reduced levels of PE and/or CL. These included genes with functions for mitochondrial morphology and the assembly of β-barrel proteins (*MDM10*, *MMM1*, *MDM31*, *MDM32*, *MDM34*, and *MDM35*; (Merz et al., 2007; Bolender et al., 2008)), genes associated with the assembly of respiratory chain complexes (*COX6*,

YTA10, and *YTA12*), and several uncharacterized open reading frames (*GEP3-6*). Our findings indicate functions of these genes in the mitochondrial lipid metabolism and suggest a critical role of the PE and CL content of mitochondrial membranes for survival of prohibitin-deficient cells.

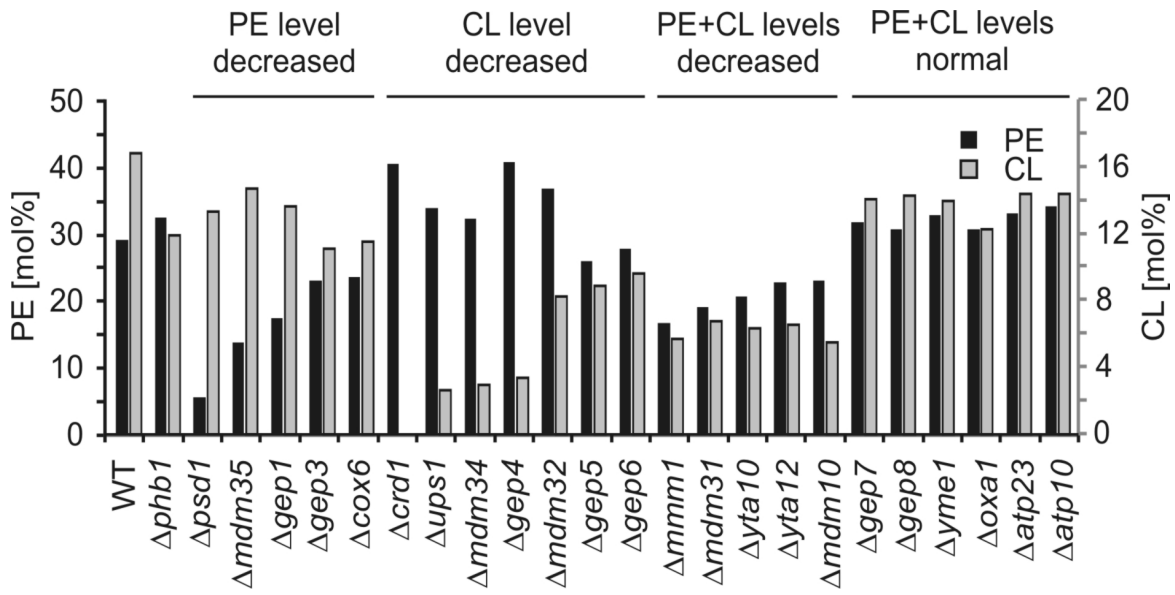

Figure 20: CL and PE profiles of mitochondria lacking GEP genes. CL and PE levels were determined by mass spectrometry in mitochondria isolated from wt, Δphb1 cells and cells lacking various GEP genes. Mean values of two mitochondrial lipid extracts are shown.

2.2.1.3 A role for Gep4 in the biosynthesis of CL

Mitochondria derived from the mutant Δgep4 were further investigated for several reasons. First, Δgep4 mitochondria showed, similar to Δcrd1 mitochondria, drastically reduced levels of CL (Figure 20 and Figure 21), indicating a role of Gep4 in the biosynthesis or regulation of mitochondrial CL. Second, a blast search revealed that Gep4 and homologues in fungal and plant species are characterized by the presence of a hydrolase domain containing a conserved inverted DXDX(T/V) motif (Figure 22). Corresponding motifs were proposed to serve as intermediate phosphoryl-acceptors in various phosphotransferases (Collet et al., 1998). Based on these findings, it was hypothesized that Gep4 might be involved in the biosynthesis of CL by acting as a phosphatase dephoshorylating the lipid intermediate PGP. If this assumption is correct, PGP should accumulate in the absence of Gep4 in mitochondrial membranes. Consequentially, lipid extracts of Δgep4 mitochondria were further investigated in order to identify and quantify the lipid intermediate PGP.

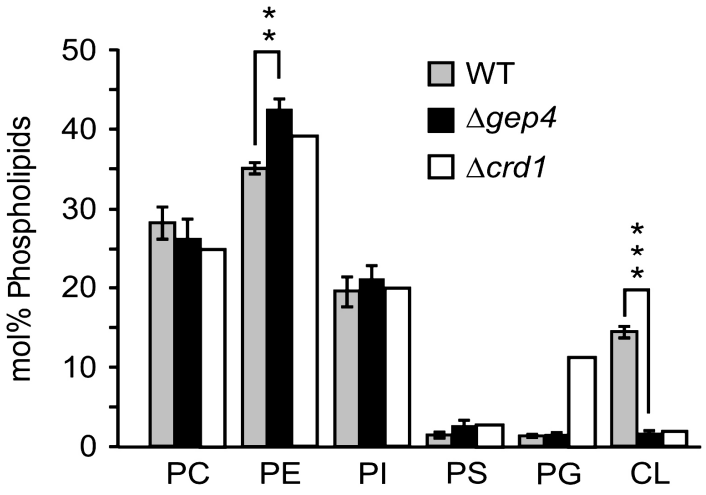

Figure 21: Quantification of phospholipids in wt, ∆gep4 and ∆crd1 mitochondria. Data represent mean values ± standard deviation of three (wt, ∆gep4) and two (∆crd1) independent mitochondrial isolations each analyzed in duplicate. **P<0.005, ***P<0.001.

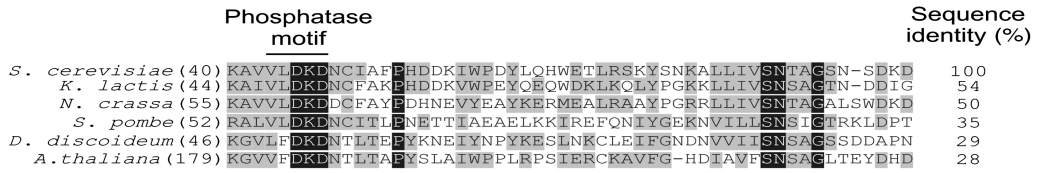

Figure 22: Alignment of proteins homologous to Gep4. The region containing the inverted phosphatase motif DXDX(V/T) is shown.

2.2.1.3.1 PGP accumulates in ∆gep4 mitochondria

It is known since decades that acidic extraction procedures strongly enhance the recovery of PIPs from biological membranes (see 2.1.3.1). PGP, with its two phosphate groups, is structurally related to the phosphoinositide PIP and can therefore be hardly recovered from membranes by conventional extraction procedures such as Folch (Folch et al., 1957) and Bligh and Dyer (Bligh and Dyer, 1959). In order to increase the recovery of PGP from mitochondrial membranes, an acidic lipid extraction was applied to wt, ∆crd1 and ∆gep4 mitochondria and lipid extracts were analyzed by TLC and mass spectrometry (Figure 23). Strikingly, TLC analysis revealed the existence of a lipid class present in ∆gep4 but not in wt and ∆crd1 mitochondria (Figure 23 A). To confirm the identity of this lipid class, the band was recovered from the TLC plate and analyzed by mass spectrometry. Scanning for neutral losses of 269 Da (glyceroldiphosphate+NH_3) unambiguously confirmed the band as PGP (Figure 23 B). The main species were found to be PGP 34:1, PGP 32:1, PGP 34:2 and PGP 32:2. PGP 36:2 and PGP 36:1 were detected to a lower extend.

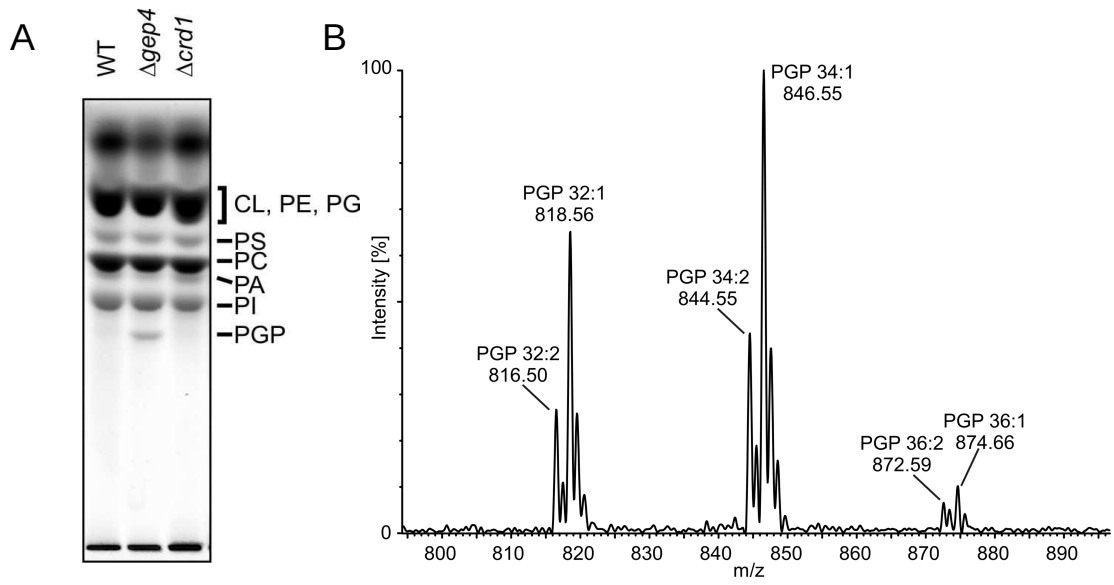

Figure 23: Identification of PGP in Δgep4 mitochondria by TLC and mass spectrometry. (A) Lipids were extracted from mitochondria by acidic extraction and separated by TLC. After isolating the band (indicated with PGP) from the TLC plate, PGP was identified by scanning for neutral losses of 269 Da (B). PGP species are indicated by their fatty acid chain length and saturation state. The m/z values represent positively charged ammonium adducts of PGP.

Mass spectrometric quantification of the identified PGP species revealed minute amounts of PGP in wt and Δcrd1 mitochondria with levels of ~0.02 mol% (Figure 24). Strikingly, in Δgep4 mitochondria, PGP accumulated ~50-fold to ~1.1 mol%, clearly indicating that in the absence of Gep4 dephosphorylation of PGP was inhibited.

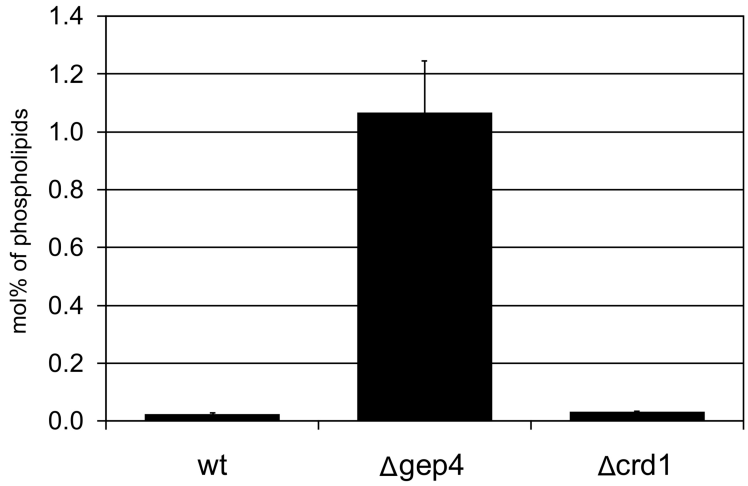

Figure 24: PGP accumulates in Δgep4 mitochondria. Mass spectrometric quantification of PGP in wt, Δgep4 and Δcrd1 mitochondria. Data represent mean values ± standard deviation of three (wt, Δgep4) and two (Δcrd1) independent mitochondrial isolations each analyzed in duplicate.

2.2.1.3.2 Gep4 dephosphorylates PGP *in vitro*

In order to demonstrate that Gep4 dephosphorylates PGP an *in vitro* assay was developed by Dr. Christof Osman. N-terminally hexahistidine tagged Gep4 or Gep4D45N with a mutation in its phosphatase motif were expressed in *E. coli* and purified by Ni-NTA affinity purification (data not shown) (Osman et al., 2010). Gep4 or Gep4D45N were added to liposomes generated from lipid extracts of Δgep4 mitochondria, and PGP and PG levels were monitored upon further incubation of the samples. As shown in Figure 25, PGP was dephosphorylated and PG accumulated in the presence of Gep4. In contrast, PGP remained stable and PG was not detectable when Gep4D45N was added to the liposomes. Taken together, these results demonstrated that Gep4 exerts PGP phosphatase activity.

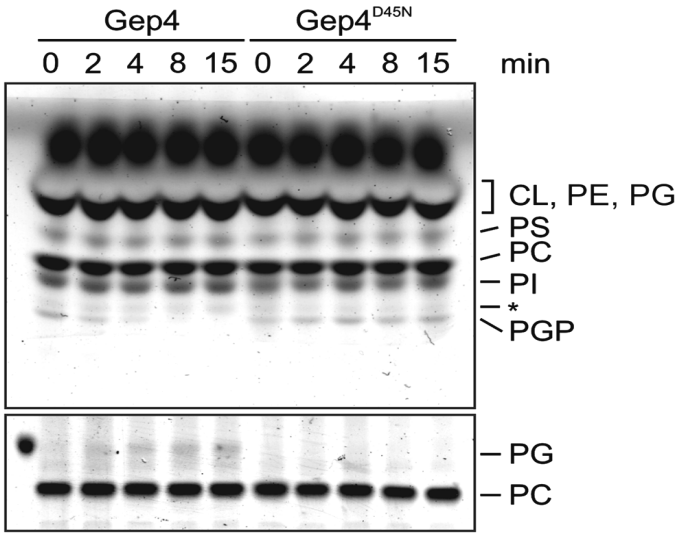

Figure 25: Gep4 dephosphorylates PGP *in vitro*. Purified Gep4 or Gep4D45N were mixed with liposomes generated from Δgep4 mitochondrial lipid extracts and incubated at 25℃ for the indicated time periods. Dephosphorylation of PGP (upper panel) and formation of PG (bottom panel) were monitored. The asterisk indicates an unidentified lipid species.

2.2.2 Ilimaquinone affects DAG level in Golgi membranes

The marine sponge metabolite ilimaquinone (IQ) is known to induce reversible fragmentation of the Golgi complex and therefore used to analyze Golgi integrity and trafficking (Takizawa et al., 1993). Studies on the molecular mechanisms of IQ-induced Golgi vesiculation revealed that lipid modifying enzymes such as phospholipase D (PLD) and PA phosphatase (PAP) play essential roles in the fragmentation process (Sonoda et al., 2007). The lipid products of these enzymes, PA and DAG, have been intimately associated with vesicular transport processes (Riebeling et al., 2009; Siddhanta and Shields, 1998; Fernandez-Ulibarri et al., 2007). A detailed study on how DAG level are affected upon IQ-induced Golgi fragmentation has not been reported so far. We therefore aimed at a quantitative analysis of DAG in IQ-treated Golgi membranes that were kindly provided by our collaboration partner Dr. Josse van Galen (Research Group: Prof. Dr. Vivek Malhotra, Center for Genomic Regulation, Barcelona, Spain).

Golgi membranes (~10-100 µg), treated either with DMSO (control) or IQ in DMSO, were extracted in the presence of the internal standard DAG 34:0 (17:0/17:0) and endogenous DAG species identified and quantified by MPIS as previously described (see chapter 2.1.2.2 and 2.1.2.3). As shown in Figure 26 the DAG basal level in control Golgi membranes were quantified to ~9 pmol/µg protein (~0.8 mol% of phospholipids). Notably, IQ treatment of Golgi membranes resulted in significantly elevated DAG amounts of ~14.5 pmol/µg protein (~1.3 mol% of phospholipids) indicating an increased production of DAG. Furthermore, slightly reduced PA levels in IQ-treated Golgi membranes compared to control Golgi membranes were also observed (data not shown). A reduction of PA is in agreement with a role of PA as DAG precursor, consequently, elevated DAG levels can be attributed to an increased PA phosphatase activity (Sonoda et al., 2007). The distribution of DAG molecular species revealed similar profiles in control and IQ-treated Golgi membranes (Figure 26 B), indicating that IQ is not affecting DAG level in a species specific manner.

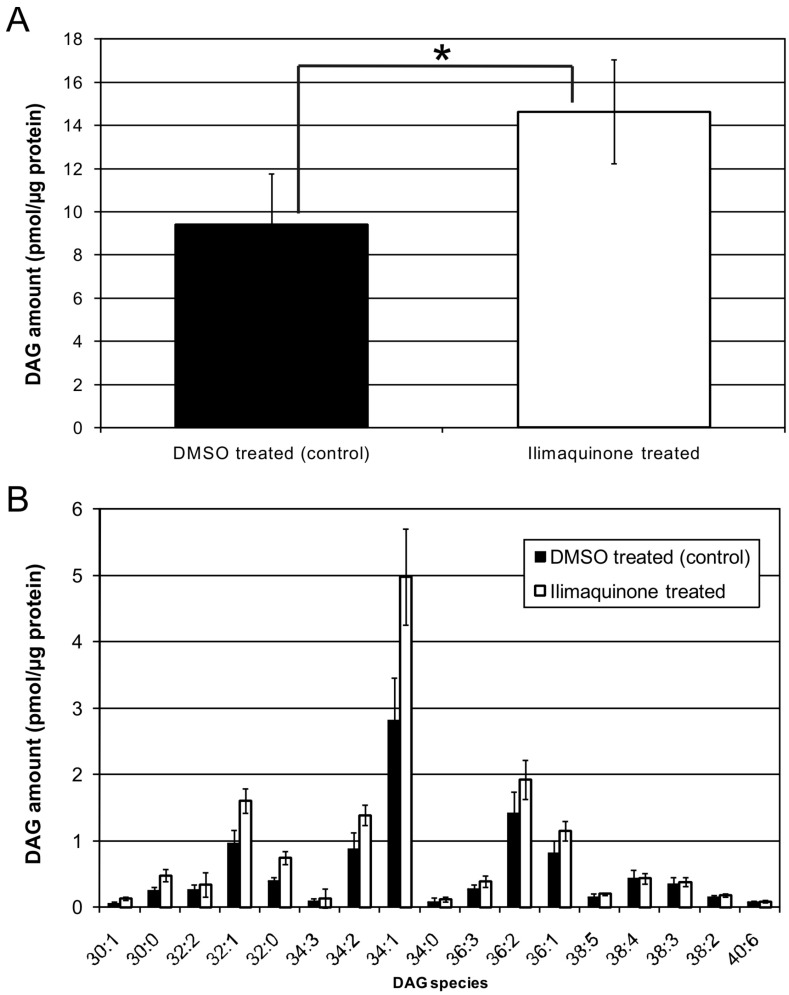

Figure 26: Ilimaquinone treatment of Golgi membranes affects DAG level. (A) Absolute amounts of DAG level in control and IQ-treated Golgi membranes. (B) DAG species identified and quantified in Golgi membranes. Data represents mean values ± average deviation of four independent experiments. *p<0.05.

2.2.3 TCR stimulation affects PIP, PIP_2 and DAG levels in human T cells

Adaptive immunity requires the activation of T cells in order to accomplish the response towards a specific antigen. Activation of T cells is achieved by antigenic stimulation of the T cell receptor (TCR) (Rojo et al., 2008; Smith-Garvin et al., 2009). Activated T cells produce cytokines that are required for the modulation of other immune cells. The expression of many cytokines is triggered through the activation of transcription factors, which themselves are activated *via* intracellular signaling pathways induced by TCR ligation. These intracellular signaling cascades involve, among other factors, the activation of phospholipase Cγ1 (PLCγ1) which cleaves $PI(4,5)P_2$ to generate the second messengers DAG and IP_3 (Feske, 2007). DAG activates protein kinase Cθ (PKCθ), a critical player of the NF-κB pathway, and contributes to AP-1 activation *via* Ras/ERK. IP_3 on the other hand triggers Ca^{2+}-release from the ER leading to calcium entry and NFAT activation. Activation of all three transcription factors (AP-1, NF-κB and NFAT) is needed for the expression of certain cytokines such as the Th1-type cytokines IL-2 and IFNγ.

Our collaboration partner Angelika Schmidt (Research Group: Prof. Dr. Peter H. Krammer, DKFZ, Heidelberg) is particularly interested in the molecular mechanisms of how regulatory T cells (Tregs) suppress cytokine transcription of conventional T cells (Tcons). *In vitro* experiments, employing Tcon and Treg coculture, revealed fast kinetics of Tcon suppression in the presence of Tregs (Oberle et al., 2007). The exact mechanism of suppression, however, is still unknown. In order to address the question whether Tregs affect TCR proximal signaling events in Tcons, particularly at the level of lipids, we aimed for a quantitative analysis of PIP, PIP_2 and DAG levels in Tcons that were suppressed by Tregs.

Initially, to define stimulation conditions that give rise to significant changes in profiles of signaling lipids, PIP, PIP_2 and DAG levels were quantified in stimulated control Tcons (not cocultured with Tregs). Tcons were TCR-stimulated for 0.5 min, 1 min, 3 min and 5 min by anti-CD3 antibodies, costimulation was achieved with anti-CD28 antibodies, and cross-linking antibodies were added in addition to enhance stimulation. ~5-10 x 10^6 cells were taken for each experiment and subjected to a two-step lipid extraction (see chapter 2.1.3.1). DAG quantification was performed in neutral extracts, whereas PIP and PIP_2 level were quantified in acidic extracts. The sole PIP_2 species that could be detected by scanning for neutral losses of 437 Da was PIP_2 38:4 (data not shown). Consequently, PIP 38:4 and DAG 38:4 were analyzed in order to monitor PIP_2-related effects on DAG and PIP. As shown in Figure 27, TCR stimulation induced visible changes in the profiles of

PIP, PIP_2 and DAG in Tcons. PIP 38:4 was constantly increased at any stimulation time accompanied by a slight but stable reduction of PIP_2 38:4. Noticeably, DAG 38:4, which remained relatively unaffected after 0.5 min and 1 min of stimulation, was massively produced after longer stimulation times of 3 min and 5 min indicated by >2-fold elevated levels compared to unstimulated cells of the same donor.

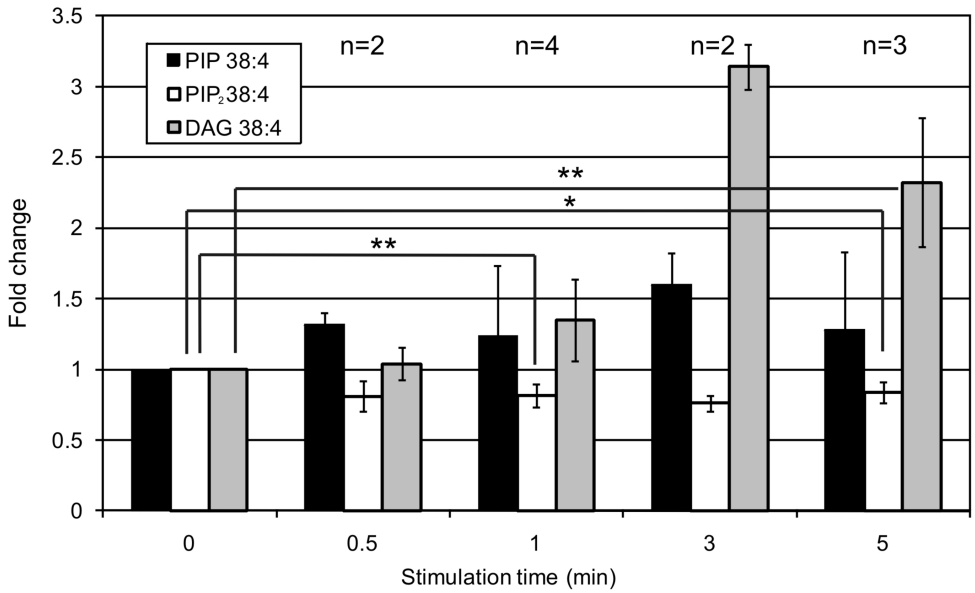

Figure 27: TCR stimulation affects level of signaling lipids in primary human T cells (Tcons). Tcons were left unstimulated or stimulated with crosslinked anti-CD3/CD28 antibodies. DAG and PIPs were extracted by a two-step extraction. Quantification of PIP and PIP_2 was performed in acidic extracts. Quantification of DAG was performed in neutral extracts. PIP, PIP_2 and DAG amounts were normalized to PC (quantified in neutral extracts). Unstimulated cells were set to 1 for each individual donor. Data represent mean values ± standard deviation of the indicated number of individual donors. *$p<0.05$, **$p<0.01$.

Taken together, the mass spectrometric quantification of PIP, PIP_2 and DAG showed that TCR stimulation induces measurable changes in the levels of Tcon signaling lipids under the applied conditions. Whereas PIP and PIP_2 levels were only slightly affected, the amount of DAG increased significantly after longer stimulation times (3 min and 5 min). Therefore, stimulation times of 3 min and 5 min were chosen for further experiments in order to analyze the impact of Tregs on the level of the signaling lipids PIP, PIP_2 and DAG in Tcons (data not shown).

2.3 Quantitative lipid analysis of Golgi membranes and COPI vesicles

COPI vesicles are Golgi-derived transport carriers that operate in the early secretory pathway (Beck et al., 2009). COPI vesicles have been implicated in the retrograde transport of proteins from the Golgi to the ER (Nickel and Wieland, 1998) and are thought to function in bidirectional transport within the Golgi complex (Orci et al., 2000; Orci et al., 1997). Whereas protein transport has been characterized in great detail, less is known about the role of COPI vesicles in transport and sorting of lipids. Brügger *et al* employed nano-ESI-MS/MS for a quantitative lipid analysis of Golgi membranes and COPI vesicles and found that SM and cholesterol are segregated during the formation of COPI-coated vesicles (Brugger et al., 2000). In order to gain deeper insight into vesicle-mediated lipid sorting an extended lipidome analysis of Golgi membranes and COPI vesicles was performed.

2.3.1 Characterization of subcellular fractions and generation of COPI vesicles

Rat liver Golgi membranes were prepared as described (Brugger et al., 2000) with the exception that Golgi fractions were not subjected to a second gradient for further purification. Relative enrichment of Golgi membranes and the degree of cross-contamination with other organelles was determined by measuring the distribution of marker enzymes for Golgi (galactosyltransferase), ER (NADH-cytochrome c reductase), plasma membrane (alkaline phosphodiesterase) and lysosomes/late endosomes (β-N-acetylglucosaminidase). Enrichment of marker enzymes is expressed as the ratio of specific enzyme activity (units/mg protein). Golgi fractions taken for vesicle preparations were characterized by 18-fold enrichment of a Golgi marker, 3.4-fold enrichment of a plasma membrane marker, 0.5-fold enrichment of a lysosome/late endosome marker and 1.3 enrichment of an ER marker.

COPI vesicles were generated *in vitro* in the presence of rat liver cytosol (RLC) and GTPγS. COPI vesicle fractions were analyzed for the presence of mannosidase II (ManII), delta-COP (δCOP), the p24 family member p27 and ADP-ribosylation factor 1 (Arf1) (Figure 28). Typically, ~0.8-1.2% of Golgi donor membranes were converted into COPI vesicles (assessed by the PC content of Golgi membranes and COPI vesicles). Additionally, as a blank control for quantitative lipid analysis, COPI vesicle fractions, obtained from the incubation of donor Golgi membranes in the presence of RLC but in the absence of GTPγS, were prepared. This control was included to compensate for lipid contaminations derived from RLC. RLC was found to contain significant amounts of lipid impurities (~3.5 nmol PC/mg protein) which had the tendency to migrate into COPI

vesicle-enriched fractions and thereby interfering with vesicle-derived lipid signals (data not shown).

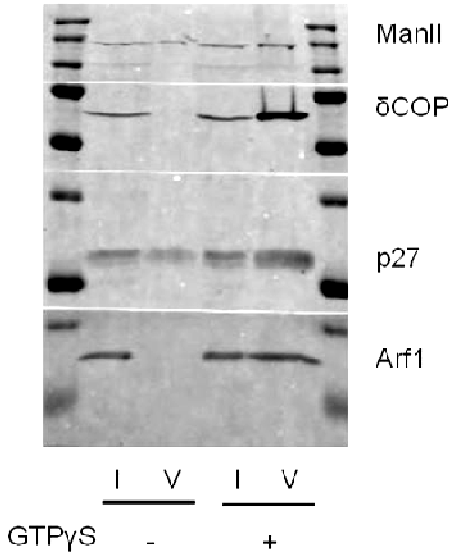

Figure 28: *In vitro* generation of COPI vesicles for quantitative lipid analysis. COPI vesicles were generated from rat liver Golgi membranes in the presence of rat liver cytosol. COPI vesicle fractions were analyzed for the presence of mannosidase II (ManII), delta-COP (δCOP), the p24 family member p27 and ADP-ribosylation factor 1 (Arf1).

2.3.2 Quantitative lipid analysis of subcellular fractions

Brügger *et al* performed a quantitative lipid analysis of PC, SM and cholesterol of donor Golgi membranes and COPI vesicles (Brugger et al., 2000). In the present work an extended lipid analysis, including the lipid classes PE, pl-PE, PI, PS, LPC, LPE and ceramide, was performed (Figure 29). As expected from previous observations (Brugger et al., 2000), cholesterol and SM were found to be depleted in COPI vesicles compared to the donor Golgi membranes. Whereas SM and cholesterol accounted to ~5 mol% and ~10 mol% of lipids in the Golgi, both lipid classes were significantly reduced in COPI vesicles to ~2 mol% and ~5.2 mol%, respectively. In contrast to previous results (Brugger et al., 2000), PC was found to be enriched in COPI vesicles compared to the donor Golgi. PI was also slightly enriched in COPI vesicles whereas PE remained at similar levels in Golgi membranes and COPI vesicles. The lipid classes pl-PE, PS, LPC, LPE and ceramide were all found to be reduced in COPI vesicles compared to Golgi membranes (Figure 29).

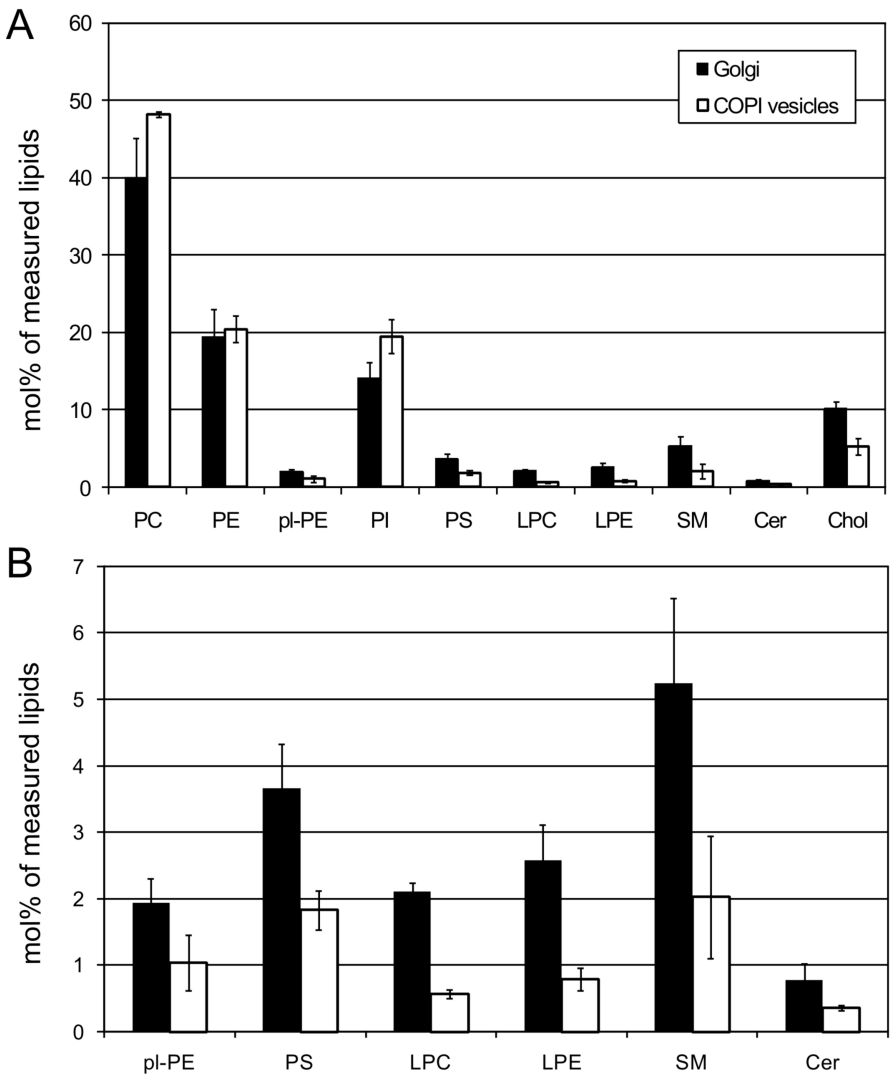

Figure 29: Lipid quantification of Golgi membranes and COPI vesicles. (A) All analyzed lipid classes are displayed. (B) Low abundant lipid classes (<10 mol %) are displayed at a different scale. Data represents mean values ± average deviation of three and two (LPE) independent experiments.

2.3.3 Distribution of lipid species in Golgi membranes and COPI vesicles

Besides changes in the absolute amounts of lipid classes we next asked whether single lipid species were selectively enriched or reduced in COPI vesicles compared to the donor Golgi membrane. The profiles of the molecular species of PC revealed no drastic changes between Golgi and COPI vesicles at a first glance, however, a more careful inspection of the pattern showed very little but apparent differences (Figure 30). The low abundant species PC 32:0 was found to be ~2.4-fold reduced in COPI vesicles accompanied by a very slight reduction of PC 34:2, PC 34:1, PC 36:2 and PC 36:1. In contrast, species with a higher degree of unsaturation such as PC 36:4, PC 38:6, PC 38:5 and PC 38:4 were

slightly enriched in COPI vesicles compared to the donor Golgi membrane. The PS species distribution seemed to follow in part the same tendency, indicated by slightly reduced levels of PS 36:1 and PS 36:2 together with increased levels of PS 38:4 and PS 38:5 in COPI vesicles (Figure 34).

For the phospholipids PE and PI no differences in the species pattern between Golgi and COPI vesicles were observed (Figure 31 and Figure 33). However, the ether lipid species pl-PE 16:0p/20:4 was found to be enriched in COPI vesicles accompanied by a reduction of pl-PE 16:0p/22:4 and pl-PE 18:0p/20:4, respectively (Figure 32). The lysolipid species LPC 16:0 and LPC 18:0 were slightly reduced in COPI vesicles, in contrast LPC 22:4 and LPC 22:0 were found to be strongly enriched in vesicles (Figure 35). The LPE species analysis revealed that saturated LPE 18:0 was enriched in COPI vesicles whereas other LPE species remained largely unaffected (Figure 36). The sphingolipid species SM 24:2 was enriched in COPI vesicles, accompanied by a depletion of SM 26:0 (Figure 37). Saturated ceramide 22:0 was depleted in COPI vesicles whereas ceramide 24:0 was slightly enriched in the vesicles (Figure 38).

Taken together, these results showed for the first time a comprehensive lipidome analysis of Golgi membranes and COPI vesicles derived thereof. We found that SM and cholesterol are segregated during the formation of COPI vesicles which is consistent to previous observations (Brugger et al., 2000). Moreover, the sphingolipid ceramide, the ether lipid pl-PE, the aminophospholipid PS and the lysolipids LPC and LPE were all found to be reduced in COPI vesicles indicating that these lipid classes are segregated together with SM and cholesterol during the formation of COPI vesicles.

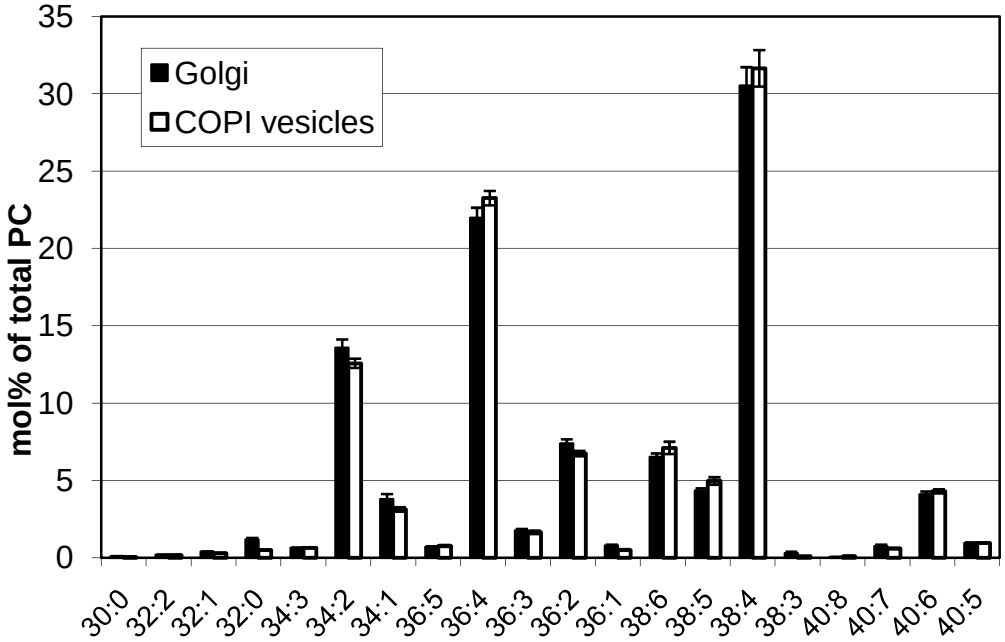

Figure 30: PC species distribution in Golgi membranes and COPI vesicles. Data represents mean values ± average deviation of three independent experiments.

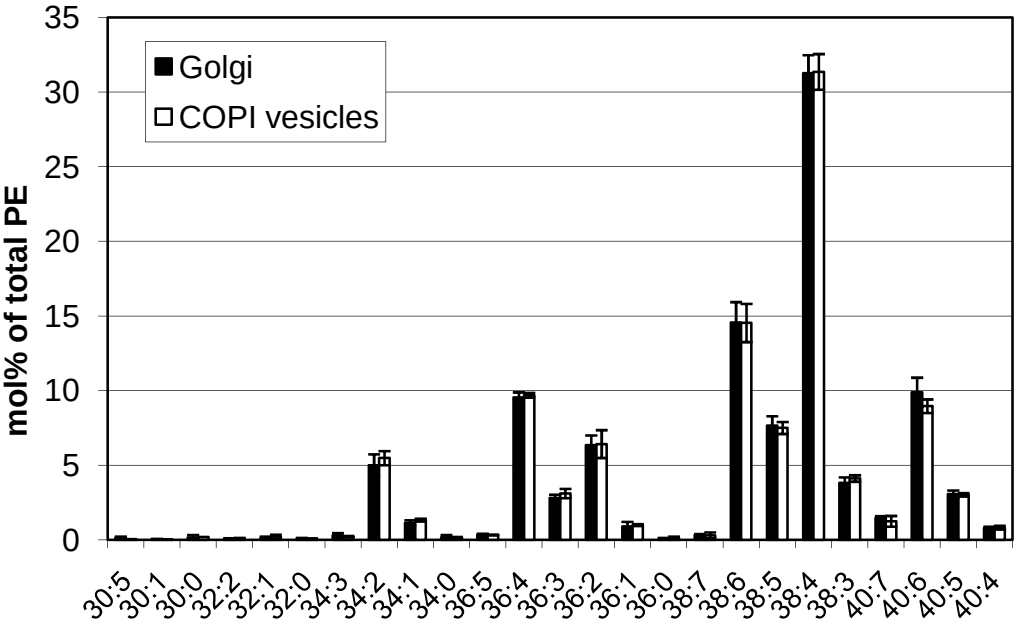

Figure 31: PE species distribution in Golgi membranes and COPI vesicles. Data represents mean values ± average deviation of three independent experiments.

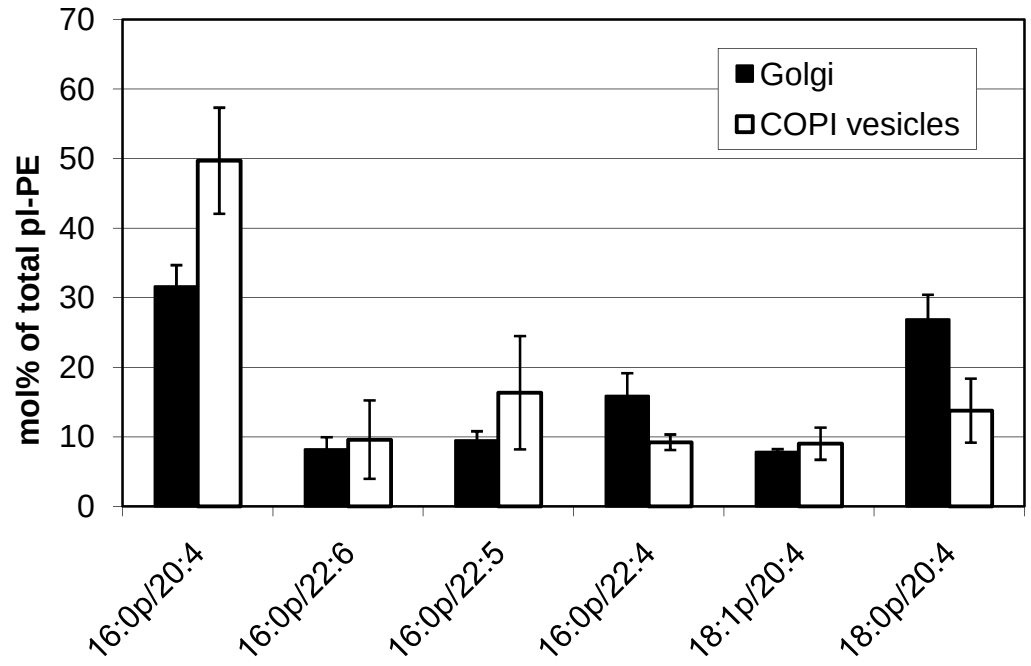

Figure 32: pl-PE species distribution in Golgi membranes and COPI vesicles. Data represents mean values ± average deviation of three independent experiments.

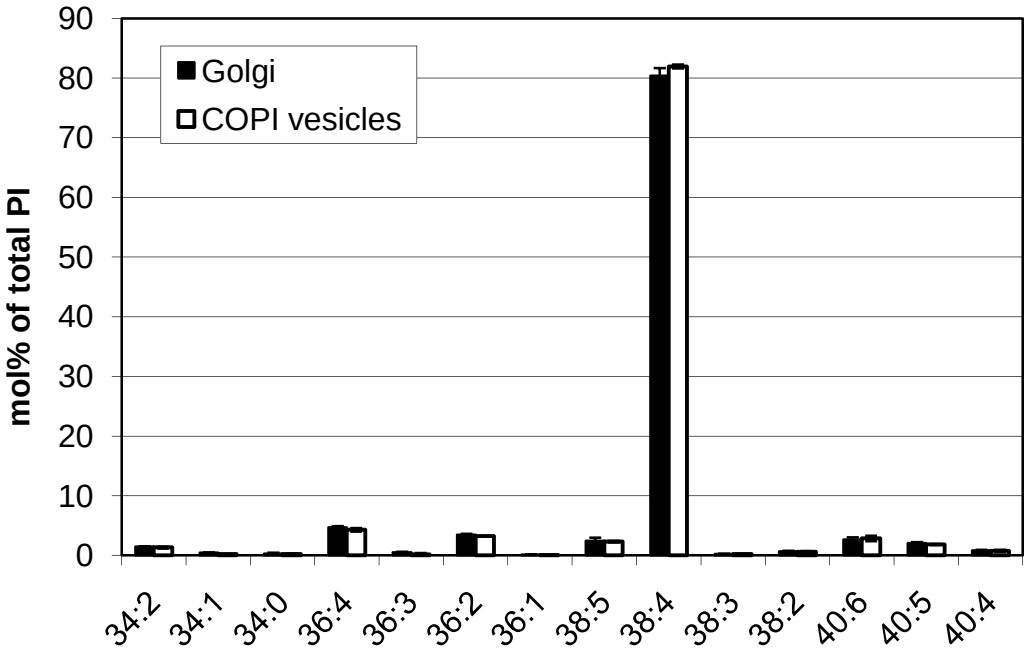

Figure 33: PI species distribution in Golgi membranes and COPI vesicles. Data represents mean values ± average deviation of three independent experiments.

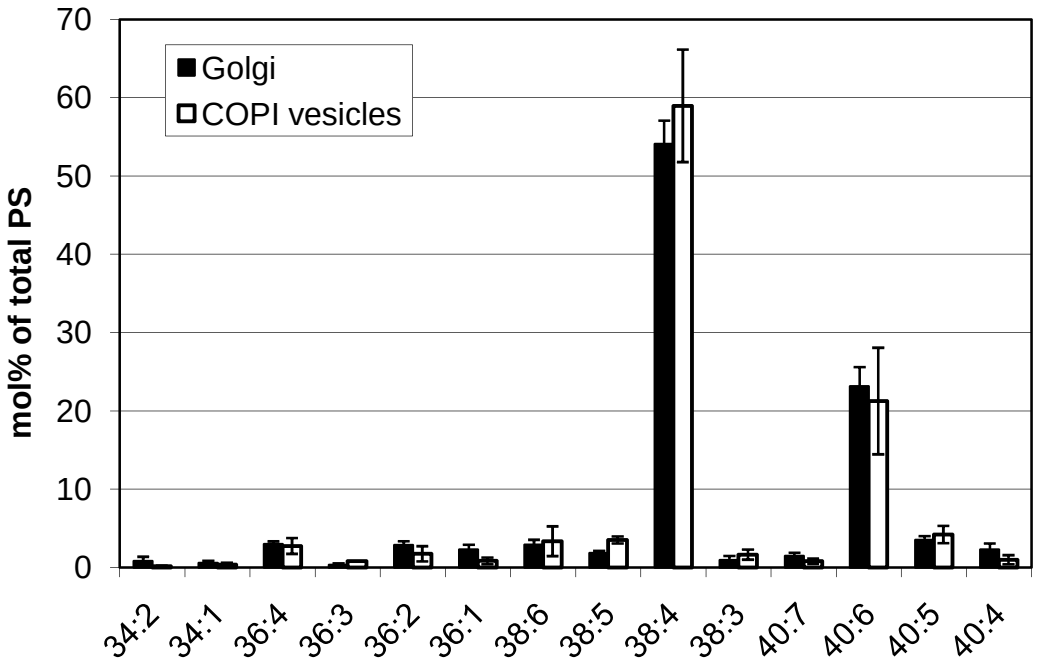

Figure 34: PS species distribution in Golgi membranes and COPI vesicles. Data represents mean values ± average deviation of three independent experiments.

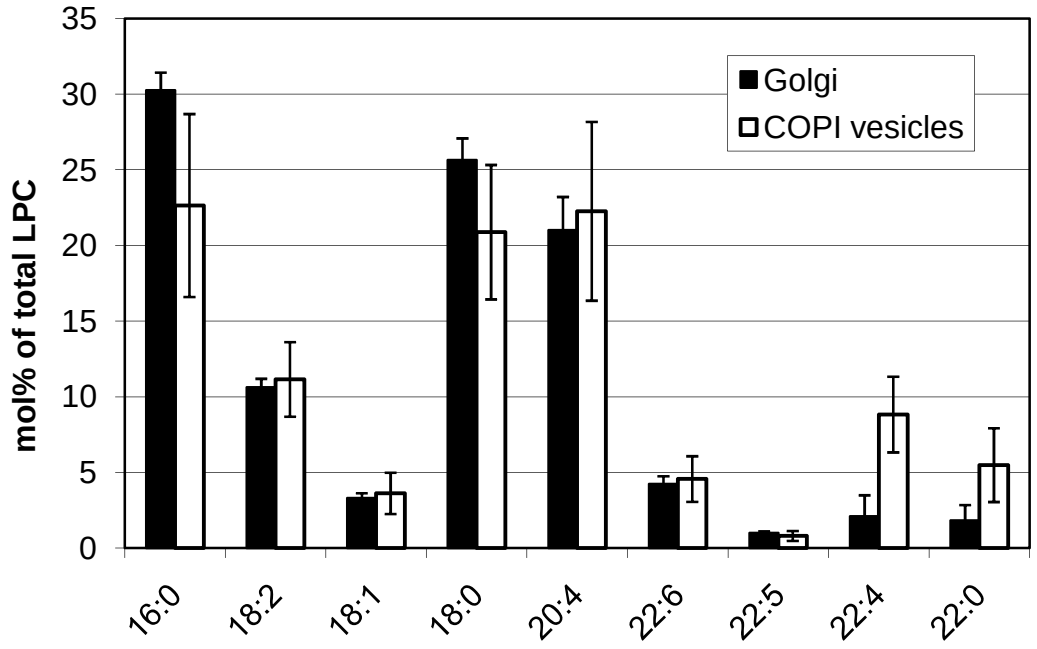

Figure 35: LPC species distribution in Golgi membranes and COPI vesicles. Data represents mean values ± average deviation of three independent experiments.

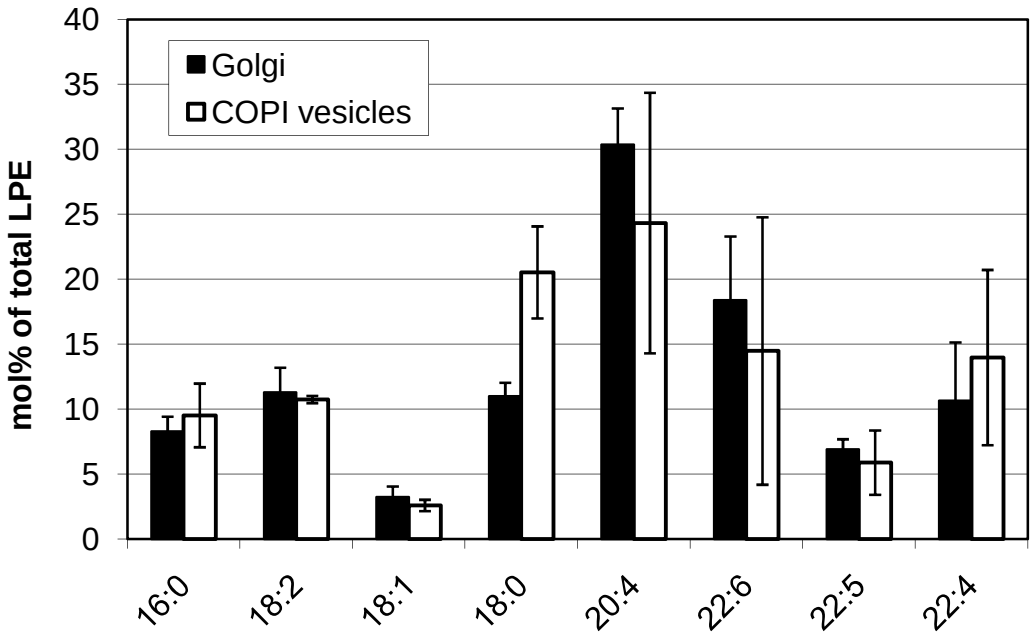

Figure 36: LPE species distribution in Golgi membranes and COPI vesicles. Data represents mean values ± average deviation of two independent experiments.

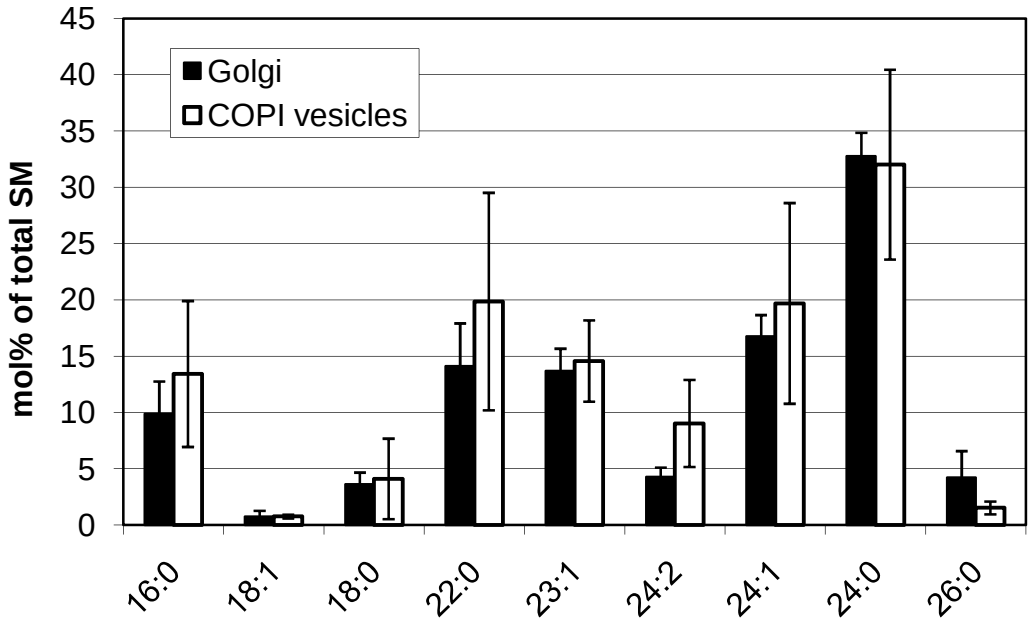

Figure 37: SM species distribution in Golgi membranes and COPI vesicles. Data represents mean values ± average deviation of three independent experiments. Note: the SM species data is derived from SM analysis after mild alkaline hydrolysis of PC species that appear in the same mass spectrometric scan (PIS m/z 184). Since SM 16:0 was hardly detectable after alkaline hydrolysis, the data for SM 16:0 was taken from the PIS m/z 184 scan before alkaline hydrolysis.

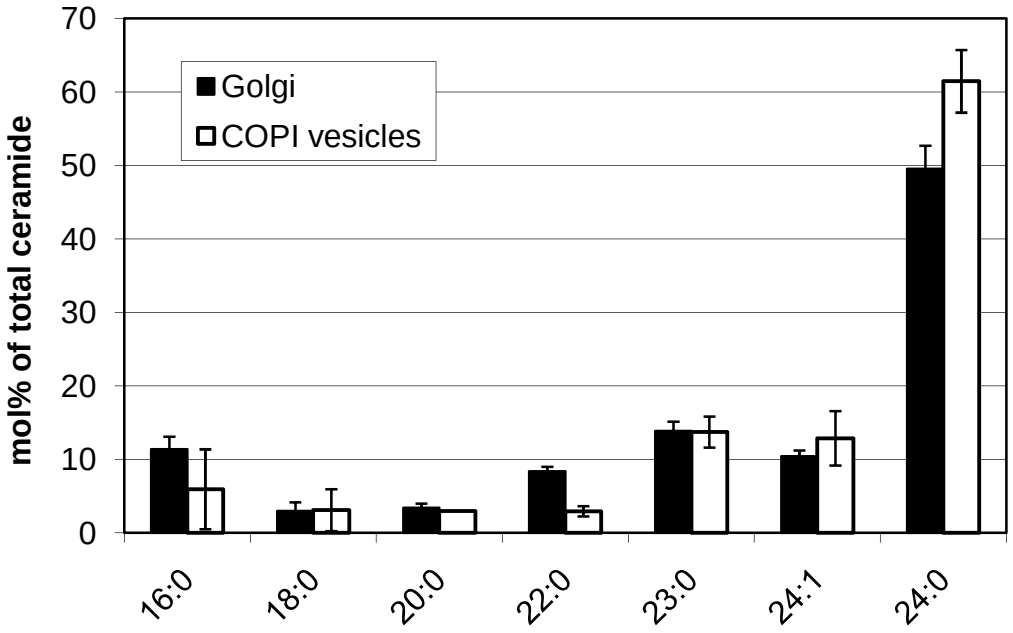

Figure 38: Ceramide species distribution in Golgi membranes and COPI vesicles. Data represents mean values ± average deviation of three independent experiments.

3 Discussion

Within the course of this thesis, nano-ESI-MS/MS for automated lipid analysis was set up (Ejsing et al., 2006) and employed to establish methods for the quantification of CL, DAG, PIP and PIP_2. The methods were applied in order to address scientific questions related to mitochondria, the Golgi complex and primary human T cells. Additionally, a quantitative lipidome analysis of Golgi membranes and COPI vesicles was performed in order to gain insight into COPI vesicle-mediated lipid sorting.

3.1 Method development

3.1.1 Quantification of CL

To study the impact of GEP genes on mitochondrial lipids, a method for the identification and quantification of CL molecular species was established. To this end, two CL species, CL 56:0 and CL 72:4 were characterized with respect to their mass spectrometric behavior similar as described (Han et al., 2006). The suitability of CL 56:0 as internal standard for CL quantification was shown in other studies as well (Valianpour et al., 2002; Valianpour et al., 2005; Sparagna et al., 2005). CL has previously been analyzed as singly (Sparagna et al., 2005) or doubly charged ion (Valianpour et al., 2002; Han et al., 2006; Garrett et al., 2007). When infused in solvents consisting of chloroform/methanol (Han et al., 2006) or methanol (this study), CL favors the doubly charged ionization state rather than the singly charged state. Interestingly, Sparagna *et al* found that the charge state of CL is also affected by the instrument design of the mass spectrometer (triple quadrupole or quadrupole time-of-flight), irrespective of the solvent system used for the infusion (Sparagna et al., 2005). When analyzing CLs on a quadrupole time-of-flight mass spectrometer (nano-ESI), we found that the distribution of singly and doubly charged CL ions can be influenced by changing the composition of the solvent system. The addition of ammonium acetate and piperidine supported the singly charged state of CL. Monitoring on singly charged CLs was assumed to be advantageous for the analysis of crude lipid mixtures in order to avoid interference with glycerophospholipids such as PE, PA and PG that appear in the same mass range. Furthermore, a titration analysis revealed that the quantification limit of singly charged CLs in the product ion mode (~1 nM) was 10-fold lower than any other reported quantification limit for CL analysis (Han et al., 2006; Valianpour et al., 2002). Besides being very sensitive the product ion mode features more advantages. First, the system is less susceptible to detector saturation, thus increasing the dynamic range towards higher sample concentrations. Second, fragmentation of lipid precursors reveals additional information about the fatty acid composition of the parent

CL molecules, which is in particular important for the analysis of CL fatty acid remodeling (Xu et al., 2003).

A titration analysis of CL 72:4 in lipid extracts of ∆crd1 mitochondria demonstrated that product ion analysis of singly charged ions facilitates the quantification of CLs in the presence of crude lipid mixtures. In summary, 28 CL species were identified in yeast mitochondria, thus representing a comprehensive spectrum of CL species that could be identified by the established method. The basal level of CL in wt mitochondria was quantified to ~15 mol% of phospholipids which is in accordance with previous findings (Daum and Vance, 1997).

3.1.2 Quantification of DAG

The mass spectrometric analysis of DAG 34:1 confirmed that DAG forms positively charged ammonium adducts that, upon collision-induced dissociation, display lipid class specific fragments derived from neutral losses of H_2O + NH_3 (35 Da) and fatty acid fragments RCOOH + NH_3 (Murphy et al., 2007). The latter neutral loss fragments result in characteristic MAG-H_2O ions, that, due to a better dissociation efficiency, were chosen to set up DAG-specific MPIS as described (Stahlman et al., 2009). For quantification, the internal standard DAG 34:0 (17:0/17:0) was used (Stahlman et al., 2009; Ejsing et al., 2009).

Although scanning for neutral losses of 35 Da allowed the identification of DAGs (data not shown), not all molecular species were detected with the same sensitivity. This was in particular the case for DAG 38:4 which showed a drastically reduced NL 35 fragmentation efficiency compared to all other examined DAG species. Most likely, this effect can be attributed to the polyunsaturated fatty acid 20:4 that might influence the fragmentation behavior of polyunsaturated species. Further experiments are required to reveal additional information about the mass spectrometric dissociation behavior of DAG 38:4. Several scenarios should be considered: (i) DAG fragmentation is generally affected by the saturation state of the fatty acids. The inspection of species containing fatty acids with different degrees of unsaturation (e.g. DAG 36:3 and DAG 40:6) will shed light on this issue. (ii) Although DAG species used in this study were supposed to be sn-1,2 positional isomers, DAGs tend to isomerize to more stable sn-1,3 isomers by transposition of the fatty acid group during storage and sample processing. Thus, it is possible that DAG 38:4 is more susceptible to isomerization and that this, in consequence, affects the

fragmentation behavior. The isomerization state of DAG species should therefore be carefully determined in future studies (Rosati et al., 2007).

To demonstrate that endogenous DAG can be identified and quantified, the established MPIS method was applied to Golgi membranes. The analysis of several Golgi fractions revealed quite variable DAG amounts between 5-100 pmol/µg protein. These amounts are in overall agreement with previously reported data of ~32-70 pmol DAG/µg protein in rat liver Golgi membranes (Stremmel and Debuch, 1979). Similar results were reported for yeast-derived trans-Golgi network (TGN) fractions where DAG was quantified to ~8.5 mol% of lipids which reflects ~90 pmol/µg protein (Klemm et al., 2009). However, our observations together with the reported data are still discrepant to very low DAG amounts that were reported for Golgi fractions derived from HeLa cells (0.55 pmol/µg) (Fernandez-Ulibarri et al., 2007). Further studies are required in order to solve these discrepancies since we have currently no explanation for the quantitative differences.

Given the fact that purified Golgi fractions contain large amount of neutral lipids (Zambrano et al., 1975; Keenan and Morre, 1970; Yunghans et al., 1970; Stremmel and Debuch, 1979) it was not surprising to detect high DAG levels in Golgi membranes. Neutral lipids in Golgi fractions are derived from lipid droplets and lipoprotein particles that are secreted from the Golgi (Hess et al., 1979). Such particles contain huge amounts of TAG that could be degraded to DAG by lipases (Smirnova et al., 2006) during the Golgi preparation process. Thus, a possible explanation for the variability in DAG levels could be due to different amounts of lipid droplets or lipoprotein particles that co-migrate into the Golgi fraction.

3.1.3 Quantification of PIP and PIP_2

To specifically enrich PIPs from HeLa cells, a two-step extraction procedure (Gray et al., 2003) was performed and the extraction behavior of PIPs was investigated by auto-radiography. The finding that PIP and PIP_2 were recovered with 58% and with 79% in acidic extracts of HeLa cells is not consistent with observations by Gray *et al* who reported recoveries of 74% PIP and 94% PIP_2 in acidic extracts of astrocytoma cells (Gray et al., 2003). These discrepancies in the extraction behavior of PIP and PIP_2 are most likely due to the different cell types used for the extraction analysis. Astrocytoma cells contain large amounts of cerebrosides, sulfatides and plasmalogens (Norton et al., 1975) whereas HeLa cells do not. Such differences in the membrane lipid composition might explain a greater loss of PIPs during the neutral extraction in HeLa cells and consequently lower

yields in the acidic extract. Further studies are required in order to clarify the extraction behavior of endogenous PIPs from different cell types.

All available mass spectrometric methods for the measurement of PIPs rely on the analysis of PIPs in negative ionization mode (Wenk et al., 2003; Milne et al., 2005; Pettitt et al., 2006) what should be beneficial because of the negatively charged phosphate groups. However, we found that negatively charged PIPs showed a variable ionization behavior on our nano-ESI-MS/MS system (data not shown). Consequently, it was not possible to create conditions that resulted in a constant stream of either singly or doubly charged PIPs. Negatively charged PIPs were rather fluctuating between the singly and the doubly charged state and thus did not allow robust analysis (data not shown). In contrast, positively charged ammonium adducts (presented in this study) resulted in a stable ionization behavior of PIP and PIP_2 and thus allowed the identification and quantification of PIPs in positive ionization mode. Collision-induced fragmentation of PI(4)P 37:4 and PI(4,5)P_2 37:4 ammonium adducts revealed lipid class specific neutral losses of 357 Da (PIP) and 437 Da (PIP_2), respectively. The identification and quantification of PIP and PIP_2 by neutral loss scanning was confirmed by profiling of complex PI(4)P brain and PI(4,5)P_2 brain mixtures. As proof of principle, it was demonstrated that a selective two-step extraction allowed the mass spectrometric analysis of PIP and PIP_2 in HeLa cells. The quantified amounts of 0.34 mol% PIP and 0.49 mol% PIP_2 were in agreement with previous reports (Mallo et al., 2008).

Although PIP_3 was detected in HeLa cells (data not shown), attempts to quantify PIP_3 in a robust manner failed so far. PIP_3 is an extremely low abundant lipid class accounting to <0.0002 mol% of phospholipids in HeLa cells (Mallo et al., 2008). Besides the extreme low abundance, another difficulty of PIP_3 analysis results from a reduced ionization efficiency that correlates with the number of phosphate groups (Wenk et al., 2003; Pettitt et al., 2006). Therefore, to compensate for low abundances and for reduced ionization efficiencies of PIP_3, more starting material (>10 x 10^6 cells) will be needed for future experiments.

3.2 Method application

3.2.1 Genetic interactors of prohibitins regulate mitochondrial PE and CL

Although almost all enzymes of lipid biosynthetic pathways have been identified in yeast mitochondria, little is known about regulatory mechanisms that control and maintain mitochondrial lipid composition. During this study, we focused on PE and CL, two phospholipids that are important for mitochondrial function and membrane biogenesis. PE and CL can substitute for each other which is supported by the finding that PE and CL biosynthetic pathways are synthetic lethal in yeast (Gohil et al., 2005). Compensatory effects of PE and CL can be attributed to the ability of both lipids to form hexagonal phase (non-bilayer) structures in membranes (Cullis and de Kruijff, 1978; Vasilenko et al., 1982; Dowhan, 1997). Non-bilayer lipids are discussed to be involved in the lateral stabilization and movement of proteins (Cullis and de Kruijff, 1979; Schlame et al., 2000; van den Brink-van der Laan et al., 2004; Dowhan, 1997; Pfeiffer et al., 2003) and membrane fusion events (Verkleij et al., 1984). Contact sites between the inner and outer mitochondrial membrane are enriched in CL and PE (Daum and Vance, 1997; Ardail et al., 1990), thus supporting the idea that both lipids are involved in the transport of proteins and lipids through contact sites. Moreover, PE and CL cluster have been identified in bacteria where they may function as membrane organizers required for cell division and sporulation (Nishibori et al., 2005; Matsumoto et al., 2006; Kawai et al., 2004).

Mass spectrometric quantification of CL and PE in mitochondria derived from yeast deletion mutants whose genes were identified in a screen to genetically interact with prohibitins (GEP genes) revealed regulators that are required for normal PE (Psd1, Mdm35 and Gep1), normal CL (Ups1, Mdm34, Gep4, Mdm32 and Crd1) or normal PE and CL levels (Mmm1, Mdm31, Yta10, Yta12, Cox6, Gep3, Gep5 and Gep6) (Figure 39) (Osman et al., 2009) and reviewed in (Gohil and Greenberg, 2009).

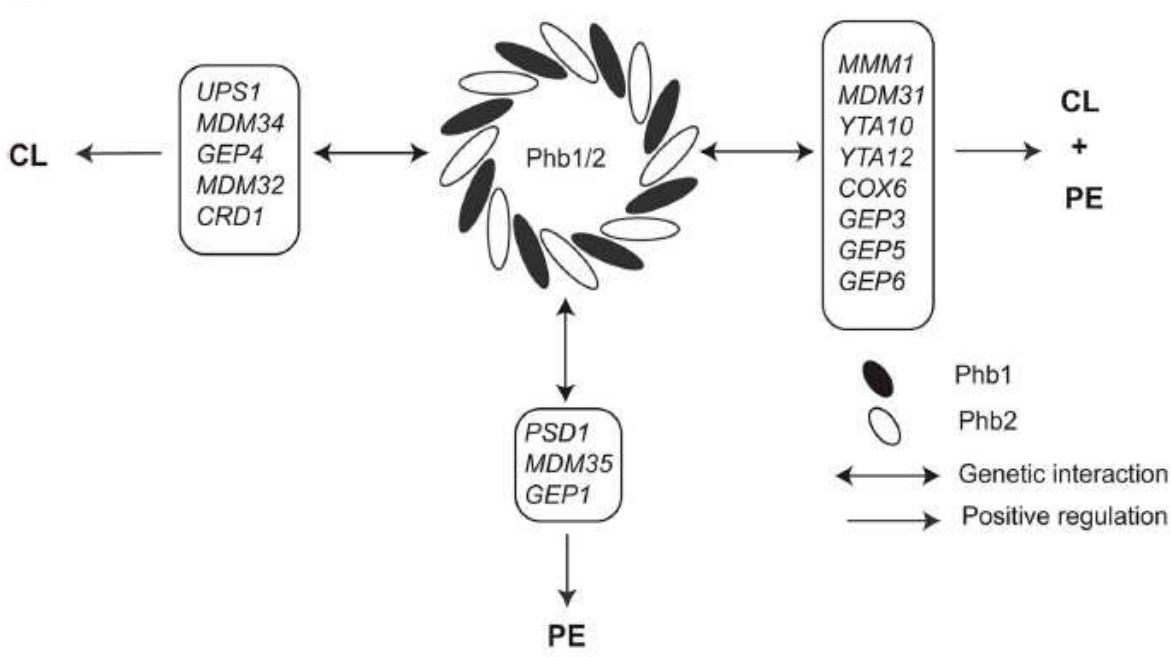

Figure 39: Genetic interactors of prohibitins (GEP genes) regulate the levels of PE and CL. GEP genes consist of three classes that are involved in the regulation of PE, CL or both PE and CL in yeast mitochondria. Taken from Gohil and Greenberg 2009.

Within the set of identified GEP genes, two proteins, Gep1 and Ups1 were analyzed in detail to study their function in regulating mitochondrial PE and CL. The data revealed that the accumulation of PE depends on Gep1, whereas Ups1 controls CL level in mitochondria. Strikingly, CL was found to be reduced upon overexpression of Gep1 and PE was slightly reduced upon overexpression of Ups1 (Figure 19). This suggests a competition between Gep1 and Ups1 and supports the idea that mitochondrial PE and CL levels are regulated coordinately by Gep1 and Ups1. Consistently, deletion of *GEP1* in Δups1 cells restored mitochondrial CL level (Figure 19).

Recent studies showed that Ups1 and Gep1 (also termed Ups2) regulate mitochondrial CL antagonistically and furthermore, a critical connection between the regulation of CL by Ups1 and Gep1 and the assembly state of the TIM23 translocase was discovered (Tamura et al., 2009). Other studies demonstrated that the ability of Ups1 and Gep1 to regulate CL and PE depends on Mdm35, which was found to protect Ups1 and Gep1 against proteolysis by the protease Yme1 and the peptidase Atp23 (Potting et al., 2010).

Although a plethora of data indicates a coordinated regulation of PE and CL level by Gep1 and Ups1, the underlying molecular mechanisms remain to be determined. The observation that the absence of both, Gep1 and Ups1 (Δgep1Δups1) only slightly affect

mitochondrial PE and CL levels makes it unlikely that both proteins are enzymes of biosynthetic PE and CL pathways. This assumption was confirmed for Gep1, as it was shown to be dispensable for PE synthesis but rather controls the stability of PE (data not shown) (Osman et al., 2009). Therefore, Gep1 most likely regulates the degradation of PE by inhibiting a lipase or, alternatively, Gep1 plays a role in export of PE from mitochondria. The scenario that Gep1 regulates PE export is consistent with the fact that significant amount of cellular PC (produced in MAMs and the ER) is derived from mitochondrial PE (Daum and Vance, 1997). Interestingly, ∆gep1 mitochondria contained slightly elevated levels of PC (Figure 19 A), which could be the result of MAM/ER-produced PC that is re-imported to mitochondria. The role of Ups1 in maintaining physiological CL level is currently less clear, and further experiments are required to examine whether Ups1 affects CL biosynthesis or degradation. Two possible mechanisms of Ups1-dependent CL regulation can be envisaged: (i) Ups1 controls enzymes of the CL biosynthetic pathway, e.g. by the inhibition of Crd1 or Gep4, or (ii) Ups1 protects mitochondrial CL from degradation by the inhibition of a CL-specific lipase.

Taken together, the mass spectrometric quantification of CL and PE in GEP mutants revealed a critical connection between prohibitins, GEP genes and the regulation of mitochondrial lipid levels. Consequently, reduced levels of mitochondrial PE and CL also affect mitochondrial structure by affecting the lipid composition as well as protein stability in membranes. Ring-like prohibitin complexes may therefore function as membrane organizers that influence the distribution of PE and CL in mitochondrial membranes. The synthetic lethality of Psd1 and Crd1 with prohibitins supports the idea that prohibitins are required to maintain inner membrane integrity when mitochondrial PE and CL levels are decreased. PE and CL clusters have been observed in bacterial membranes (Matsumoto et al., 2006). It is tempting to speculate that such domains also exist in mitochondria. Such clusters could be involved in generating and maintaining contact sites between inner and outer mitochondrial membranes that are enriched in CL and PE (Daum and Vance, 1997; Ardail et al., 1990). In case of low PE and CL levels, prohibitins might compensate for the loss of these lipids by maintaining contact sites and consequently mitochondrial integrity and function. This scenario is in agreement with a putative scaffolding function of prohibitins (Merkwirth and Langer, 2009b; Langhorst et al., 2005).

Although almost all enzymes of CL biosynthesis are known in yeast, there are still players that need to be identified. The unknown gene *GEP4* was identified as a GEP gene that is required for normal CL levels in mitochondria (Figure 20 and Figure 21). The finding that the encoded protein Gep4 contains a phosphoryl-acceptor motif suggested that Gep4

might be involved in the biosynthesis of mitochondrial CL by acting as a PGP phosphatase. Mass spectrometric identification and quantification revealed a ~50-fold accumulation of PGP in ∆gep4 mitochondria. This observation was an important result, stimulating further experiments that lead to the identification of Gep4 as a phosphatase required for CL synthesis (Osman et al., 2010).

3.2.2 Ilimaquinone affects DAG level in Golgi membranes

Ilimaquinone (IQ) is a marine sponge metabolite that induces fragmentation of the Golgi complex (Takizawa et al., 1993) and is therefore used to analyze Golgi integrity and trafficking (Jamora et al., 1997; Acharya et al., 1995; Taylor et al., 1994; Veit et al., 1993). There is evidence that IQ´s ability to vesiculate the Golgi complex can be attributed to an interaction of IQ with methylation enzymes (Casaubon and Snapper, 2001; Radeke et al., 1999). Other studies demonstrated that Golgi-associated phospholipase D (PLD) (Ktistakis et al., 1996; Ktistakis et al., 1995) is required for IQ-induced Golgi fragmentation (Sonoda et al., 2007). The authors concluded from their results that activation of PLD generates PA that is further converted by PA phosphatase (PAP) to DAG which binds and activates protein kinase D (PKD) followed by Golgi vesiculation. Although there is compelling evidence that IQ stimulates the production of DAG in Golgi membranes, this has not yet been confirmed by quantitative lipid analysis.

Quantitative lipid analysis of Golgi membranes showed that DAG level indeed elevated upon IQ treatment (Figure 26). Accordingly, this finding is in agreement with the scenario that activation of PLD and PAP results in elevated DAG levels in Golgi membranes. In future studies it will be interesting to see whether IQ additionally affects other lipids. If so, the main question will be, whether IQ alters Golgi lipid levels by activating other lipid modifying enzymes or if IQ mediates Golgi fragmentation through a direct interaction with Golgi membranes. A direct interaction between Golgi membranes and the Golgi-vesiculating agent norrisolide has recently been observed (Guizzunti et al., 2010).

3.2.3 TCR stimulation affects PIP, PIP_2 and DAG levels in human T cells

Identification and quantification of PIP, PIP_2 and DAG under different cellular conditions was demonstrated by the analysis of TCR-stimulated conventional human T cells (Tcons). The aim of this experiment was to determine conditions that give rise to significant changes in the level of the signaling lipids PIP, PIP_2 and DAG in order to address the future question whether regulatory T cells (Tregs) affect TCR proximal signaling events in Tcons with regard to the lipid composition.

It was found that TCR stimulation of Tcons by adding anti-CD3/CD28 antibodies resulted in significantly increased DAG levels after 3 min and 5 min (Figure 27) which was consistent with kinetics of PLCγ1 and PKCθ activation (observation by Angelika Schmidt, Research Group: Prof. Dr. Peter H. Krammer, DKFZ, Heidelberg). Furthermore, PIP_2 levels were constantly and significantly reduced upon TCR stimulation (Figure 27) which was consistent to activated PLCγ1 (observation by Angelika Schmidt). Noticeably, the accumulation of DAG was only concomitant to a reduction of PIP_2 after 1 min stimulation time. In contrast, stimulation for 3 min and 5 min tremendously increased DAG levels, whereas PIP_2 did not drop to the same extend. Two possibilities can be envisaged to explain this effect. First, the re-synthesis rate of PIP_2 is especially increased after 3 min and 5 min stimulation. This scenario is supported by elevated levels of PIP, the precursor of PIP_2 biosynthesis. Furthermore, the synthesis rate of PIPs is known to be massively increased upon TCR stimulation (Zaru et al., 2001). Second, DAG can be generated from other lipid precursors as well. Although it is widely accepted that TCR stimulation triggers PLCγ1 that cleaves plasma membrane anchored $PI(4,5)P_2$, there is evidence that activation of Ras/MAPK pathways by DAG can also occur at the Golgi complex (Mor and Philips, 2006). Thus other lipid precursors might contribute to the production of DAG, such as PC that can be converted to DAG by the action of PLD and PA phosphatase, enzymes that have previously been linked to TCR signaling (Mor et al., 2007).

To clarify the source of DAG in the Tcon subset used in this work, the analysis of PIP_2 derived inositol-phosphate intermediates will be required in future studies. Furthermore, it will be interesting to see whether Treg-induced suppression of Tcons is achieved by affecting proximal signaling events that include PIP, PIP_2 and especially DAG levels, or whether Tregs regulate suppression of Tcons by affecting downstream signaling events.

3.3 Quantitative lipid analysis of Golgi membranes and COPI vesicles

3.3.1 Characterization of subcellular fractions and generation of COPI vesicles

According to enzymatic assays, the Golgi fraction was 18-fold enriched in a Golgi marker which was significantly less Golgi enrichment compared to previous observations (90-fold enrichment) (Brugger et al., 2000). The contributions of plasma membrane and endoplasmatic reticulum to the Golgi fraction was comparable to previous reports, however, lysosome/late endosome-derived impurities were found to be lower than previously observed (Brugger et al., 2000). The discrepant Golgi enrichment factors can most likely be attributed to differences in the Golgi purification protocols. Whereas Brügger *et al* subjected Golgi membranes to a two-step purification (Brugger et al., 2000), a second purification step was omitted in this study. Furthermore, it is known that the presence of protease inhibitors during Golgi purification (this study) can lower the apparent purification factors (Hui et al., 1998). Another explanation is that the Golgi fraction used for this study contains only low amounts of TGN-cisternae which would explain a reduced activity of TGN-located galactosyltransferase.

For the upcoming discussion several things should be kept in mind when comparing the data presented here with previous observations (Brugger et al., 2000). First, Golgi fractions used in the present study and in the previous study (Brugger et al., 2000) are not comparable in terms of purity. Thus, any observed differences in lipid class and lipid species distribution between donor Golgi membranes and COPI vesicles can be the result of slightly different lipid compositions of the donor Golgi membranes used. Second, COPI vesicles were prepared in the presence of rat liver cytosol in this study, whereas previously bovine brain cytosol was used for the generation of COPI vesicles (Brugger et al., 2000). Thus, any observed effect can likely be attributed to different cytosolic compositions that might result in the formation of different types of COPI vesicles.

3.3.2 Quantitative lipid analysis of subcellular fractions

The quantitative lipid data of Golgi membranes is in overall agreement with previous data (Yunghans et al., 1970; Keenan and Morre, 1970; Zambrano et al., 1975; Fleischer et al., 1974). Quantitative lipid analysis of COPI vesicles revealed that SM was reduced ~2.5-fold from ~5 mol% in the Golgi to ~2 mol% in COPI vesicles (Figure 29). Cholesterol was reduced ~2-fold from ~10 mol% in the Golgi to ~5 mol% in COPI vesicles (Figure 29). The depletion factors are in line with earlier findings that revealed a ~3.3-fold and

~1.6-fold reduction of SM and cholesterol, respectively (Brugger et al., 2000). COPI vesicles were also found to contain low levels of pl-PE, PS, LPC, LPE and ceramide compared to the donor Golgi. Two lipid classes, PC and PI, were specifically enriched in COPI vesicles whereas PE was not affected during vesicle formation. Consequentially, the lipid composition of COPI vesicles reflects an “ER-like” pattern, characterized by low amounts of SM, cholesterol and PS and high amounts of PC and PI (van Meer et al., 2008; van Meer, 1998).

3.3.3 Distribution of lipid species in Golgi membranes and COPI vesicles

The profiles of PC molecular species revealed no drastic changes between Golgi membranes and COPI vesicles at a first glance. However, a more careful inspection of the profiles revealed very little but apparent changes that were contradictory to previous observations that showed an enrichment of PC 34:1 and PC 40:6 in COPI vesicles accompanied by a reduction of PC 40:7 (Brugger et al., 2000). In contrast, this study revealed that saturated PC 32:0 was significantly reduced in COPI vesicles, indicating that PC 32:0 is segregated together with SM and cholesterol in liquid-ordered phases during COPI vesicle budding. Interestingly, detergent resistant membranes (DRMs) contain, besides high amounts of SM and cholesterol, elevated levels of PC 32:0 (Brugger et al., 2004; Hein et al., 2008). Furthermore, saturated PC species show high affinity to SM and cholesterol rich domains at the PM (Harder and Sangani, 2009). The data suggested that other PC species are also sorted, but to a lower extent than PC 32:0. In general, PC species with a higher degree of saturation (PC 34:1, PC 34:2, PC 36:1 and PC 36:2) seemed to be slightly retained in the Golgi. In contrast, the small enrichment of unsaturated species (PC 36:4, PC 38:6, PC 38:5 and PC 38:4) in COPI vesicles was consistent with the enrichment of polyunsaturated PI 38:4 in COPI vesicles. The small, but obvious changes in the PC species profiles of COPI vesicles compared to the donor Golgi membrane supports the idea that COPI vesicles are involved in a fine-tuned sorting process of PC species along the secretory pathway.

On the level of SM species, we could not confirm an enrichment of SM 18:0 and a reduction of SM 24:0 and SM 24:1 in COPI vesicles as observed previously (Brugger et al., 2000). However, it was found that SM 24:2 is enriched in COPI vesicles accompanied by a reduction of SM 26:0 (Figure 37). Furthermore, changes in the species profiles of other lipid classes such as pl-PE, LPC, LPE and ceramide seemed to follow only in part the observed effect for PC species. The reduction of saturated LPC 16:0 and LPC 18:0 in vesicles was consistent with observations by Keenan *et al,* that LPC 16:0 and LPC 18:0

are enriched at the PM (Keenan and Morre, 1970). Interestingly, saturated LPE 18:0, that is supposed to be concentrated at the PM (Keenan and Morre, 1970) was found enriched in COPI vesicles.

3.3.4 Mechanisms of segregation

Based on the given data, two different mechanisms of lipid segregation during the formation of COPI vesicles can be envisaged (Brugger et al., 2000; Nickel et al., 1998a): (i) a dynamic segregation of lipids concomitant with COPI vesicle generation based on the molecular mechanisms of vesicle budding, and (ii) segregation of lipids before the budding process. Given the fact, that COPI vesicles comprise a liquid-disordered lipid composition and recent *in vitro* observations that COPI coat assembly is adapted to liquid-disordered domains at the Golgi complex (Manneville et al., 2008) the “segregation before budding” scenario seems more likely. Furthermore, the existence of SM-enriched microdomains at the Golgi complex (Gkantiragas et al., 2001) supports a “segregation before budding” situation.

The characteristic, “ER-like” lipid composition of COPI vesicles might be interpreted in a way that COPI vesicles are exclusively involved in retrograde transport pathways. This scenario is in accordance with cisternal maturation (Glick et al., 1997; Bonfanti et al., 1998; Matsuura-Tokita et al., 2006) or rapid partition (Patterson et al., 2008) of Golgi cisternae, where COPI vesicle would play a major role in the retrograde transport of lipids to the ER. Exclusive retrograde transport of COPI vesicles is supported by several findings (Bannykh and Balch, 1997; Mironov et al., 1997; Gaynor et al., 1998), however, there is strong evidence for a role of COPI vesicles in anterograde transport (Nickel et al., 1998b; Orci et al., 1997; Orci et al., 2000; Volchuk et al., 2000). Nevertheless, high amounts of ER lipids in COPI vesicles do not exclude anterograde traffic since low amounts of SM and cholesterol in vesicles may still be sufficient for an anterograde net transport of these lipids. Additionally, alternative lipid transport mechanisms, such as Golgi-independent cholesterol transport (Urbani and Simoni, 1990) or lipid transport via contact sites and lipid transfer proteins (Holthuis and Levine, 2005; Lev, 2010) should be considered as significant contributors to lipid transport and sorting processes.

Taken together, the presented data comprises an extended lipidome analysis of COPI vesicles in comparison to donor Golgi membranes. The analysis provided evidence that COPI vesicles display an “ER-like” lipid composition and supports the idea that COPI vesicle formation takes place at liquid-disordered domains in the Golgi complex. It will be

fascinating to see whether distinct populations of COPI vesicles, that are either characterized by different coatomer isoforms (Moelleken et al., 2007; Wegmann et al., 2004) or by different cargo (Orci et al., 1997; Lanoix et al., 2001; Malsam et al., 2005) are involved in the selective transport of lipid classes and lipid species. Moreover, analyzing the lipid composition of other transport carriers such as COPII- and clathrin-coated vesicles will expand our understanding of intracellular lipid transport and sorting.

4 Materials and methods

4.1 Materials

4.1.1 Chemicals and materials

Following chemicals and materials were used unless stated otherwise:

Product (Order Number)	Company
Acetic acid, AnalaR Normapur (# 20104.334)	VWR International
Aceton, pro analysis (# 1.00014.1000)	Merck, Darmstadt
Acetyl chloride (# 23,957-7)	Sigma-Aldrich, Taufkirchen
Ammonium acetate (# 09690)	Sigma-Aldrich, Taufkirchen
Ammonium hydrogencarbonate	Merck, Darmstadt
Ammonium hydroxide, 25% NH_3 (# UN 2672)	J.T. Baker, USA
Ammonium molybdate (# 09878)	Sigma-Aldrich, Taufkirchen
ART-Tips 1000 µl reach (# 2079)	Molecular Bioproducts
ART-Tips 200 µl (# 2069)	Molecular Bioproducts
Ascorbic acid (# 3525.1)	Roth, Karlsruhe
Chloroform (# 25690)	Sigma-Aldrich, Taufkirchen
Cuvettes, polystyrol (# 67.742)	Sarstedt, Nümbrecht
DMEM (# T041-05)	Biochrom, Berlin
DMEM, inositol-free (# A8164)	AppliChem, Darmstadt
EDTA (# 147850010)	Acros Organics, USA
ESI-Chip for Triversa Nanomate (# HD_D_384 incl. sample tip rack, A15, 384, P/N: 1004763).	Advion Biosciences, Norwich, UK
Glass vials, 1.5 ml (# 2-7201) + Teflon lined screw caps	Neolab, Heidelberg
Glass vials, 4 ml, (# 2-7231) + Teflon lined screw caps	Neolab, Heidelberg
HPLC-grade H_2O, Chromanorm (# 23595.328)	VWR International
Hydrochloric acid 37%, pro analysis	Merck, Darmstadt
Methanol (# 65543)	Sigma-Aldrich, Taufkirchen
myo-[^{3}H]-inositol, 1 mCi/ml (# TRK912)	GE Healthcare, USA
Nanoflow probe tips (# M956230AD1)	Teer Coatings Ltd, Droitwich, UK
Pasteur capillary pipettes, 150 mM length	WU, Mainz
PBS (# L182-05)	Biochrom, Berlin
Perchloric acid 70-72% (# 1.00519.1001)	Merck, Darmstadt
Piperidine (# 41,102-7)	Sigma-Aldrich, Taufkirchen
Pipette tips, 10 µl (# 771290)	Greiner Bio-One
Potassium oxalate (# 1.05072.1000)	Merck, Darmstadt
Safe lock cups 1.5 ml (# 0030 120.094)	Eppendorf, Hamburg
Safe lock cups 2 ml (# 0030 120.068)	Eppendorf, Hamburg
Schott glass tubes (# 231751459)	Duran Group, Mainz
Thermowell™ sealing tape (# 6569)	Corning Incorporated, UK
TLC plates, Silica 60, 20x20 cm (# 1.05721.0001)	Merck, Darmstadt
Trichloracetic acid, Biochemica (# A1431)	AppliChem, Darmstadt
Triethylamine for β-imager (# 90340)	Sigma-Aldrich, Taufkirchen
Well plates 96, colorless (# 0030 128.648)	Eppendorf, Hamburg
Wheaton glass tubes (# 9-0611)	Neolab, Heidelberg

4.1.2 Lipids

Following internal standards and reference standards were purchased from Avanti Polar Lipids (Alabaster, USA): CL 14:0/14:0/14:0/14:0 (# 750332C), CL 18:1/18:1/18:1/18:1 (# 710335C), DAG 14:0/14:0 (# 800814C), DAG 16:0/16:0 (# 800816C), DAG 16:0/18:1 (# 800815C), DAG 18:1/18:1 (# 800811C), DAG 18:0/20:4 (# 800818C), PI(4)P 17:0/20:4 (# LM-1901), PI(4,5)P_2 17:0/20:4 (# LM-1904), Brain PI(4)P (# 840045P), Brain PI(4,5)P_2 (# 840046P), LPC 17:1 (# LM-1601), LPE 17:1 (# 110699), PI 16:0/16:0 (# 850141P), standards for PC mix (PC 13:0/13:0 (# 850340C), PC 14:0/14:0 (# 850345C), PC 20:0/20:0 (# 850368C), PC 21:0/21:0 (# 850370C)) and cholesterol (# 700000P). Unsaturated standards for PG mix (28:2, 40:2 and 44:2), PE mix (28:2, 40:2 and 44:2) and PS mix (28:2, 40:2 and 44:2) were synthesized and purified via HPLC as described (Koivusalo et al., 2001), DAG 17:0/17:0 (# 32-1702) was purchased from Larodan (Malmö, Sweden), D_6-cholesterol (# 2607-0.1) was obtained from Cambridge Isotope Laboratories (Andover, USA).

4.1.3 Instruments

Following instruments were used unless stated otherwise:

Instrument	Company
Quattro II (triple quadrupole mass spectrometer)	Micromass, Manchester, UK
QStar® Elite (quadrupole time-of-flight mass spectrometer)	Applied Biosystems, Darmstadt
AB Sciex QTrap® 5500 (linear ion trap triple quadrupole mass spectrometer)	Applied Biosystems, Darmstadt
Triversa Nanomate	Advion Biosciences, Norwich, UK
Liebisch evaporator and heating device	Liebisch GmbH & Co. KG, Bielefeld
Beta imager	Biospace, France
Scintillation counter	Perkin Elmer, USA

4.2 Methods

4.2.1 Cell culture and *myo*-[^{3}H]-inositol labeling

Labeling of HeLa cells was performed similar as described (Hama et al., 2004). Briefly, HeLa cells (# ATCC CCL-2.1) were maintained in 10-cm dishes in DMEM (including 10% fetal calf serum, 100 µg/ml penicillin, 100 µg/ml streptavidin and 2 mM glutamine) in 5% CO_2 at 37°C in a humidified incubator. Cells were grown to ~50-60% confluence, the medium was replaced by inositol-free DMEM (including 10% fetal calf serum, 100 µg/ml penicillin, 100 µg/ml streptavidin and 2 mM glutamine) and the labeling started by the addition of *myo*-[^{3}H]-inositol to a final concentration of 10-20 µCi/ml. The labeling time was typically 24-88 h until the cells reached levels of ~80-90% confluence.

4.2.2 Phosphorus assay (micro determination)

Lipid phosphorus content was determined according to Rouser *et al* (Rouser et al., 1970). Endogenous lipids were extracted (see chapter 4.2.6.1) and subsequently subjected to the phosphorous assay. Commercially available lipids were directly subjected to the phosphorous assay. Briefly, lipids were provided in Teflon-sealed glass vials, dried and hydrolyzed for 40 min at 180°C after the addition of 300 µl perchloric acid. After cooling down, 1 ml water and 0.8 ml of a freshly prepared mixture containing 0.625% ammonium molybdate and 2.5% ascorbic acid was added followed by incubation for 5 min at 100°C. After cooling down, the mixture was transferred to a cuvette and the absorption was measured at 797 nm. Quantification of sample phosphate amount was achieved by comparing to a calibration line. For the calibration line, 0, 2, 5, 10, 20, 30 and 40 nmol phosphate was provided from a 0.4 mM KH_2PO_4 solution. Calibration samples were processes in parallel to the lipid samples except that they were not subjected to lipid extraction.

4.2.3 Preparation of lipid standards

Standards delivered as powder were dissolved in chloroform except for PI(4)P 37:4, PI(4,5)P_2 37:4, brain PI(4)P and brain PI(4,5)P_2, which were dissolved in chloroform/ methanol/H_2O (1:1:0.2, v/v/v). D_6-cholesterol and cholesterol was dissolved in methanol. The concentration of phospholipid solutions was determined by the phosphorous assay. Lipid stocks were diluted to final concentrations of 1-12.5 µM. PI(4,5)P_2 17:0/20:4 was kept at concentrations of 30-50 µM.

4.2.4 Preparation of primary human T cells and TCR stimulation

All experiment concerning the preparation of primary human T cells (Tcons) and TCR stimulation were performed by Angelika Schmidt (Research Group: Prof. Dr. Peter H. Krammer, DKFZ, Heidelberg). Human peripheral blood leucocytes (PBLs) were purified from Buffy coats by Biocoll™ (Biochrom, Berlin, Germany) gradient centrifugation followed by plastic adherence to deplete monocytes. $CD4^+CD25^-$ Tcon were isolated by magnetic cell sorting (MACS) using the CD4-Isolation kit II and additionally depleted from $CD25^+$-cells with 8µl of anti-CD25 MACS beads per 10^7 cells (Miltenyi Biotech). Tcons were rested overnight in X-Vivo 15 medium (Cambrex) supplemented with 1% Glutamax. Tcon were taken up in pre-warmed X-Vivo 15 medium (37°C) to ~10^7 cells/ml and stimulated by addition of soluble anti-CD3 (0.2 µg/ml), anti-CD28 (2 µg/ml) and goat anti-mouse crosslinker (2 µg/ml) antibodies for indicated time periods at 37°C/ 5% CO_2. Stimulation was stopped by the addition of ice-cold MACS-buffer and cells were passed

over a LS-column (Miltenyi) on ice to mimic a coculture separation procedure. After centrifugation (1,000 x g, 5 min at 4°C), Tcons were w ashed with PBS and lysed in 0.6 ml 0.5 M TCA.

4.2.5 Purification of Golgi membranes and COPI vesicles

Golgi membranes and COPI vesicles were provided by Dr. Vincent Popoff (Research Group: Prof. Dr. Felix Wieland, BZH, Heidelberg). Purification of Golgi membranes was performed as described (Hui et al., 1998). Enzyme marker analyses (NADH-cytochrome c reductase, alkaline phosphodiesterase and β-N-acetylglucosaminidase) were performed by Ingrid Meißner (Research Group: Prof. Dr. Felix Wieland, BZH, Heidelberg). The galactosyltransferase assay was done as described (Roth and Berger, 1982). COPI vesicles were prepared from 360 µg (6 x 60 µg) purified Golgi membranes in the presence of rat liver cytosol (RLC) and GTPγS according to the protocol of Dr. Rainer Beck (Research Group: Prof. Dr. Felix Wieland, BZH, Heidelberg). As a blank control for quantitative lipid analysis, COPI vesicle fractions, obtained from the incubation of 360 µg (6 x 60 µg) Golgi membranes in the presence of RLC but in the absence of GTPγS, were prepared.

4.2.6 Lipid extraction procedures

4.2.6.1 Lipid extraction from GEP mitochondria for PE and CL analysis

Yeast cell culture, isolation and purification of mitochondria was performed by Dr. Christof Osman (Research Group: Prof. Dr. Thomas Langer, University of Cologne) as described (Osman, 2009; Osman et al., 2009). Mitochondrial lipids were extracted and phosphate concentration was determined by the phosphorous assay. For mass spectrometric analysis 1.5 nmol phospholipids were extracted in Teflon-sealed glass vials in the presence of 50 pmol CL 56:0 and 50 pmol PE mix. Briefly 1.875 ml chloroform/ methanol/37% HCl (40:80:0.6, v/v/v) and x µl sample was added to the lipid standards. After vortexing for 20 sec, water (500 µl – x µl sample) was added followed by vortexing. After the addition of 500 µl chloroform and 500 µl water, the sample was vortexed followed by centrifugation to induce a phase separation (200 x g, 2 min at 4°C). The lower chloroform phase was transferred to a second glass vial and the remaining aqueous phase and the chloroform phase were re-extracted after the addition of 500 µl chloroform and 500 µl water. The washed chloroform phase of the second vial was transferred to a third vial and the chloroform phase of the initial vial was combined with the aqueous phase of the second vial followed by re-extraction. After phase separation, the chloroform phase of the second vial was combined with the chloroform phase of the third vial and

evaporated by a gentle stream of argon at 37°C. Lipids were dissolved in 10 mM ammonium acetate in methanol (PE analysis) or 5 mM ammonium acetate and 0.05% piperidine in methanol (CL analysis) and analyzed by mass spectrometry.

For TLC analysis, 1 mg mitochondria were mixed with 1.5 ml chloroform/methanol (1:1, v/v) and vigorously shaken for 60 min. 300 µl water was added and samples were vortexed for 60 s. After centrifugation (1.000 rpm, 5 min) and removal of the aqueous phase, the organic phase was washed with 250 µl methanol/H_2O (1:1, v/v). Samples were then dried under a constant stream of argon. Lipids were dissolved in chloroform, phosphate concentration was determined according to Rouser *et al*, and samples were subjected to TLC analysis. TLC plates (HPTLC; Merck & Co., Inc.) were developed with chloroform/methanol/25% ammonia (50:50:3, v/v/v) followed by staining with 470 mM $CuSO_4$ in 8.5% *o*-phosphoric acid and incubation for 10 min at 180°C .

4.2.6.2 Lipid extraction from wt, ∆gep4 and ∆crd1 mitochondria

Mitochondrial fractions were pelleted for 20 min (13,800 x g and 4°C) and resuspended in 150 mM ammonium hydrogencarbonate (NH_4HCO_3) buffer. The amount of phospholipids was determined by the phosphorus assay. For mass spectrometry, 1.5-3 nmol phospholipids per sample was extracted as described in chapter 4.2.6.1 in the presence of internal standards providing spike amounts of 100 pmol PC mix, 80 pmol PE mix, 80 pmol PI 32:0, 50 pmol PS mix, 25-50 pmol PG mix and 50 pmol CL 56:0. Dried lipid samples were prepared for mass spectrometry as described chapter 4.2.6.1.

For PGP quantification, 1.5-3 nmol phospholipids were extracted in the presence of 25-50 pmol PG mix in Eppendorf tubes. Briefly, 750 µl chloroform/methanol/37% HCl (40:80:1, v/v/v) was added to the samples followed by 15 min incubation at RT. Samples were vortexed for 30 sec every 3 min. Phase separation was induced by the addition of 250 µl chloroform and 450 µl 0.1 M HCl followed by 1 min vortexing and centrifugation (6,500 x g, 2 min at 4°C). The organic phase was transferred into a new Eppendorf tube and evaporated. Dried lipids were dissolved in 25 mM ammonium acetate in chloroform/methanol/H_2O (1:1:0.05) and analyzed by mass spectrometry.

For TLC analysis, 0.5 mg mitochondria were pelleted, resuspended in 750 µl chloroform/methanol/37% HCl (40:80:1, v/v/v) and vigorously shaken for 15 min at 25°C. Samples were transferred to ice, 250 µl cold chloroform and 450 µl cold 0.1 M HCl were added and samples were vortexed for 1 min at 25°C. After centrifugation at 7,500 x g for 2 min at

4℃, the organic phase was transferred to a new Epp endorf tube and samples were dried under a constant stream of argon. For one-dimensional separation of PGP, 12 nmol phospholipids were spotted on TLC plates that were developed with ethylacetate/ 2-propanol/ethanol/6% ammonia (3:9:3:9, v/v/v/v) (Hegewald, 1996).

4.2.6.3 Phosphoinositide extraction from *myo*-[^{3}H]-inositol labeled HeLa cells

Cell harvesting and phosphoinositide extraction was performed as described (Wenk, 2007). Briefly, after transferring the cells (~5 x 10^6) to ice and removal of the medium, cells were washed two times with 10 ml cold PBS. After adding 1.2 ml cold 0.5 M TCA, the cells were immediately scraped off the dish, transferred to an Eppendorf tube and vortexed for 10 sec followed by 5 min incubation on ice. After centrifugation (13,800 x g, 2 min at 4℃), the supernatant was discarded and the pellet washed two times with 1 ml cold 5% TCA/ 1 mM EDTA. For neutral extraction, the pellet was resuspended in 1 ml chloroform/methanol (1:2, v/v) and incubated for 10 min at RT. The sample was vortexed for 30 sec every 3 min. After precipitation (13,800 x g, 2 min at 4℃), the supernatant was transferred to a new Eppendorf tube. For acidic extraction, the remaining pellet was resuspended in 750 µl chloroform/methanol/37% HCl (40:80:1, v/v/v) and incubated for 15 min at RT while vortexing the sample for 30 sec every 5 min. After transferring the tube to ice, 250 µl cold chloroform and 450 µl cold 0.1 M HCl was added followed by 1 min vortexing and centrifugation (6,500 x g, 2 min at 4℃). The lower organic phase was transferred to a new tube. Before drying, ~1 vol% of the neutral and the acidic extract was subjected to scintillation counting to determine the radioactivity. Based on the sum of radioactivities in the neutral extract (100 vol%) and the acidic extract (100 vol%), a typical *myo*-[^{3}H]-inositol incorporation of 0.5-1.5% was calculated compared to the starting labeling amount (100-200 µCi). The organic phases were dried and stored at -20℃ until further processing.

For TLC analysis, plates were covered with 1% (w/v) potassium oxalate and 2 mM EDTA in 50% methanol followed by drying for 10-15 min with a blow-dryer. Dried lipid extracts were dissolved in appropriate volumes (20-300 µl) of chloroform/methanol/H_2O (1:1:0.2, v/v/v) to a final concentration of ~5-15 nCi/µl. 50-200 nCi were spotted on TLC-plates and dried (Note: to avoid saturation of the beta imager detector, only a proportion of each extract was spotted on the plates). The plates were developed with chloroform/ acetone/methanol/acetic acid/H_2O (64:30:24:30:13, v/v/v/v/v) for 1.5-2 h. After drying, ^{3}H-PI and ^{3}H-PIPs were visualized by the beta imager (24 h acquisition). Data evaluation

was performed with the β-vision+ software (Biospace). The spot activities (cpm) of ^{3}H-PI and ^{3}H-PIPs were used to determine the distribution of ^{3}H-PI, ^{3}H-PIP and ^{3}H-PIP_2 in neutral and acidic extracts.

4.2.6.4 Phosphoinositide extraction from HeLa cells

HeLa cells were grown in DMEM to 80-90% confluence in a 10-cm dish (~5 x 10^6 cells). Cell harvesting was done as described (chapter 4.2.6.3). Aliquots (1-10 vol%) were taken from the homogenate (second wash step with 1 ml 5% TCA/ 1 mM EDTA), lipids extracted and quantified by the phosphorous assay. Typically, 100-250 nmol phospholipids were subjected to a two-step lipid extraction in Eppendorf tubes. For neutral extraction, the pellet was resuspended in 1 ml chloroform/methanol (1:2, v/v) and incubated for 10 min at RT. The sample was vortexed for 30 sec every 3 min. After precipitation (13,800 x g, 2 min at 4°C), the supernatant was transferred to a new Eppendorf tube. 270 pmol PI(4)P 37:4 and 625 pmol PI(4,5)P_2 37:4 were added to the pellet followed by acidic extraction. Briefly, the pellet was resuspended in 375 µl chloroform/methanol/37% HCl (40:80:1, v/v/v) and incubated at RT for 15 min, vortexing every 5 min for 30 sec. After transferring the tube to ice, 125 µl cold chloroform and 225 µl cold 0.1 M HCl were added followed by 1 min vortexing. Phase separation was induced by centrifugation (6,500 x g, 2 min at 4°C) and the lower organic phase was immediately transferred to a new tube and kept on ice until further processing. For mass spectrometric analysis, 10 µl of the organic phase was diluted 1:2 with 50 mM ammonium acetate in chloroform/methanol (1:1, v/v).

4.2.6.5 Lipid extraction from HeLa Golgi membranes for DAG quantification

Preparation of Golgi membranes from HeLa cells was performed by Dr. Frank Anderl (Research Group: Prof. Dr. Felix Wieland, BZH, Heidelberg) as described in his PhD thesis (Anderl, 2008). Lipid extraction from Golgi membranes was done as described in chapter 4.2.6.1 in the presence of 80 pmol DAG 17:0/17:0. Dried lipids were dissolved 10 mM ammonium acetate in methanol and subjected to mass spectrometry.

4.2.6.6 Lipid extraction from NRK Golgi membranes for DAG quantification

Preparation of Golgi membranes from NRK cells and ilimaquinone (IQ) treatment was performed by Dr. Josse van Galen (Research Group: Prof. Dr. Vivek Malhotra, Centre for Genomic Regulation, Barcelona, Spain). Briefly, ~10-100 µg Golgi membranes were incubated for 1 h in 25 µM IQ in DMSO or DMSO (control) in 50 mM Tris pH 7.4, 150 mM KCl, 2 mM DTT, 30 mM $MgCl_2$, 1 mg/ml BSA, 250 mM sucrose and protease inhibitors. Golgi membranes were pelleted and resuspended in Tris buffered saline

followed by a two-step lipid extraction in the presence of 20 pmol DAG 17:0/17:0 as described in chapter 4.2.6.8. Dried lipids were dissolved in 10 mM ammonium acetate in methanol and DAG quantification was performed in neutral lipid extracts.

4.2.6.7 Lipid extraction from primary human T cells

T cell lysates were either immediately processed or snap frozen and stored at -80℃ until further processing. The storage time was restricted to a maximum of 2-3 weeks to minimize sample degradation. Prior to lipid extraction, TCA lysates were precipitated (13,800 x g, 2 min at 4℃) and pellets washed two times with 1 ml cold 5% TCA/ 1 mM EDTA. After centrifugation (13,800 x g, 2 min at 4℃), the supernatant was discarded and lipids were extracted from the pellet by a two-step extraction in Eppendorf tubes (similar as described in chapter 4.2.6.4). Prior neutral extraction, 15 pmol DAG 17:0/17:0 and 250 pmol PC mix was spiked to the pellet and lipids were extracted with 750 µl chloroform/methanol (1:2, v/v) by incubating 10 min at RT and vortexing every 3 min for 30 sec. After centrifugation (13,800 x g, 2 min at 4℃), the supernatant was carefully removed from the pellet and transferred to a new tube. The supernatant was subjected to a second extraction after the addition of 250 µl chloroform and 450 µl water. Phase separation was induced by centrifugation (6,500 x g, 2 min at 4℃) and the lower phase was transferred to a new tube. Dried lipids were dissolved in 10 mM ammonium acetate in methanol and subjected to mass spectrometry.

Prior acidic extraction of PIPs, 15 pmol PI(4)P 37:4 and 160 pmol PI(4,5)P_2 37:4 was spiked to the remaining pellet (which was kept on ice all the time). The pellet was resuspended in 375 µl chloroform/methanol/37% HCl (40:80:1, v/v/v), incubated at RT for 15 min and vortexed every 5 min for 30 sec. After transferring the tube to ice, 125 µl cold chloroform and 225 µl cold 0.1 M HCl were added followed by 1 min vortexing. Phase separation was induced by centrifugation (6,500 x g, 2 min at 4℃). The lower organic phase was immediately transferred to a new tube and kept on ice until further processing. For mass spectrometric analysis, an aliquot (10 µl) of the organic phase was diluted 1:2 with 50 mM ammonium acetate in chloroform/methanol (1:1, v/v).

4.2.6.8 Lipid extraction from Golgi membranes and COPI vesicles

Golgi membranes and COPI vesicles were subjected to a modified two-step extraction procedure based on Ejsing *et al* (Ejsing et al., 2009). Golgi input (2-4 µg protein) and vesicle fractions (-/+ GTPγS) were extracted in Eppendorf tubes in the presence of 125-150 pmol PC mix, 125 pmol SM mix, 75 pmol PE mix, 75 pmol PS mix, 100-150 pmol

PI 32:0, 10 pmol ceramide mix, 150 pmol D_6-cholesterol, 150 pmol pl-PE mix, 15 pmol LPC 17:1 and 15-25 pmol LPE 17:1. To determine experimental-dependent response factors for cholesterol quantification, 100 pmol, 200 pmol and 400 pmol cholesterol were processed together with the samples. A blank extraction (only lipid standards) was included to correct for background derived ion signals.

Neutral extraction was performed by adding 990 µl chloroform/methanol (17:1, v/v) and 200 µl water - x µl sample followed by 30 min shaking at 1,400 rpm and 20℃. Phase separation was induced by centrifugation (6,500 x g, 2 min at 4℃) and the lower organic phase was transferred to a new tube. Before drying, an aliquot (150 µl) of the chloroform phase was transferred to a new tube for cholesterol acetylation according to Liebisch *et al* (Liebisch et al., 2006). Briefly, dried lipids were incubated for 1 h in 50 µl acetylchloride/ chloroform (1:5, v/v) followed by drying. For acidic extraction, the remaining aqueous phase (~200 µl) was adjusted to 0.1 M HCl by adding 10 µl 2 M HCl followed by the addition of 375 µl chloroform/methanol/37% HCl (40:80:1, v/v/v) and 125 µl chloroform. After vortexing for 1 min a phase separation was induced and the lower organic phase transferred to a new tube and dried.

For mass spectrometric analysis, neutral and acidic extracts were dissolved in 10 mM ammonium acetate in methanol. PC, SM, LPC, PE, pl-PE, ceramide and cholesterol analysis was performed in neutral extracts. PS and PI were analyzed in acidic extracts and LPE was analyzed in neutral and acidic extracts. For SM analysis, neutral and acidic extracts (dissolved in 10 mM ammonium acetate in methanol) were pooled and subjected to mild alkaline hydrolysis. Briefly, after solvent evaporation, 4 ml 12.5% ammonia in methanol was added followed by incubation for 2.5 h at 50℃. The ammonia/methanol mixture was evaporated and lipids dissolved in 10 mM ammonium acetate in methanol followed by mass spectrometric analysis.

4.2.7 Mass spectrometry

4.2.7.1 Quattro II

Quantification of PC, SM, PE, pl-PE, PI, PS, LPC, LPE, ceramide, PG, PIP and PIP_2 and qualitative analysis of PGP was performed in positive ion mode with the Quattro II operated by the Mass Lynx software. 10 µl of lipid sample was loaded into a nanoflow probe tip that was subsequently mounted into a nano-ESI source (Z spray). Argon was used as collision gas at a nominal pressure of 2.5 x 10^{-3} millibar. The cone voltage was set to 30 V (50 V for PC analysis). The quadrupoles Q1 and Q3 were operated at unit

resolution. Detection of PC and SM was achieved by precursor ion scanning for the fragment ion m/z 184 (CE: 32 eV). LPC and ceramide were measured by precursor ion scanning for the fragment ion m/z 184 (CE: 20 eV) and m/z 264 (CE: 30 eV), respectively. (L)PE, PI, PIP, PIP_2, PS, PG and PGP measurements were carried out by scanning for neutral losses of 141 Da (CE: 20 eV), 277 Da (CE: 30 eV), 357 Da (CE: 30 eV), 437 Da (CE: 35 eV), 185 Da (CE: 20 eV), 189 Da (CE: 20 eV) and 269 Da (CE: 25 eV), respectively. Detection of pl-PE was achieved by scanning for plasmalogen-specific precursor ions (Zemski Berry and Murphy, 2004), m/z 364 at 20 eV (16:0p), m/z 390 at 18 eV (18:1p) and m/z 392 at 20 eV (18:0p). 20-50 MCA spectra were acquired for every scan. For data processing, spectra were smoothed (Savitzky Golay, peak width: 0.85 Da, number of smoothes: 4) and background subtracted (polynomial order: 1, below curve %: 10, tolerance: 0.01 and flatten edges). The spectrum peak list was exported and processed with a self programmed tool for correction of isotopic overlap and mass-dependent intensity differences. The data was transferred to Excel for final lipid quantification.

4.2.7.2 QStar Elite and QTrap 5500

Quantification of DAG, PIP, PIP_2, PGP and cholesterol in positive ion mode and quantification of CL in negative ion mode was performed with the QStar Elite operated by the Analyst 2.0 Software. Quantification of PIP and PIP_2 was also achieved with the AB Sciex QTrap 5500 operated by the Analyst 1.5.1 Software. Before infusion, lipid extracts (in Eppendorf tubes) were subjected to centrifugation (13,800 x g, 5 min at 4℃) to remove debris. 20 µl of lipid samples were loaded into 96-well plates and sealed with sealing tape. Lipid infusion and ionization was achieved with the Triversa Nanomate operated with the ChipSoft Software under the following settings: sample infusion volume: 10 µl, volume of air to aspirate after sample: 1 µl, air gap before chip: enabled, aspiration delay: 0 sec, pre-piercing: with mandrel, spray sensing: enabled, cooling temperature: 12℃, gas pressure: 0.5 psi. Following ionization mode and solvent-dependent settings were used:

	Positive ion mode		**Negative ion mode**
Infusion solvent	25 mM ammonium acetate in chloroform/ methanol/(H_2O)	10 mM ammonium acetate in methanol	5 mM ammonium acetate + 0.05% piperidine in methanol
Vent headspace	No	Yes	Yes
Pre-wetting	2x	1x	1x
Voltage (kV)	1.3-1.6	1.3-1.6	-1.1

Mass spectrometric analysis was performed under the following, instrument-dependent settings:

	QStar Elite	QTrap 5500
Curtain Gas	10	10
CAD Gas	2	5
Operating pressure (torr)	2.5×10^{-5}	1.6×10^{-5}
Interface heater temperature IHT (℃)	40	40
Declustering potential (DP)	40	100
Focusing potential (FP)	200	-
Declustering potential 2 (DP2)	10	-
Entrance potential (EP)	-	7
Collision cell exit potential (CXP)	-	19
Detector (CEM)	2500	2100
Quadrupole resolution	Unit (Q1)	Unit (Q1 and Q3)

4.2.7.3 Acquisition methods - QStar Elite

4.2.7.3.1 Product ion analysis of CL species

CL species (all combinations of fatty acids 16:0, 16:1, 16:2, 18:0, 18:1 and 18:2, see Table 1) were analyzed by product ion analysis of singly-charged ions $[M-H]^-$ at a CE of -85 eV. The TOF mass analyzer was set to m/z 200-350 to monitor fatty acid fragment ions of the corresponding CL precursors. Trapping of ions in Q2 (peak enhancement) was applied to a mass of m/z 275. Data acquisition was done in the continuum mode for 40 min, 80 cycles were acquired at a cycle time of 30 sec. For quantification, the peak areas of CL-derived fatty acid fragments were extracted from the respective product ion spectra through the “Extract Fragments” script. Isotope correction was done manually. Values were corrected for response factors of standards.

4.2.7.3.2 Product ion analysis of PGP species

Quantification of PGP was achieved by product ion analysis of PGP species as identified in lipid extracts of Δgep4 mitochondria (Figure 23 B). As a PGP standard is commercially not available, PGP quantification was performed using the PG standard mix, assuming that PG and PGP show the same mass spectrometric response behavior. Product ion analyses were conducted at a CE of 25 eV. The TOF mass analyzer was set to m/z 450-750 to monitor fragments derived from neutral losses of 189 Da (PG) and 269 Da (PGP) of the corresponding PG and PGP precursors. Trapping of ions in Q2 (peak enhancement) was applied to a mass of m/z 600. Data acquisition was done in the continuum mode for 19 min, 60 cycles were acquired at a cycle time of 19 sec. Quantification of the parent molecules was done as described for CL.

4.2.7.3.3 Product ion analysis of PIP and PIP_2 species

Quantification of brain PIPs in positive ion mode was done by product ion analysis of PIP and PIP_2 precursors (Table 4) conducted at CEs of 25 eV for PIP and 35 eV for PIP_2, respectively. The TOF mass analyzer was set to m/z 500-700 to monitor neutral loss derived fragments. Trapping of ions in Q2 (peak enhancement) was applied to a mass of m/z 600. Data acquisition was done in the continuum mode for 32 min, 100 cycles were acquired at a cycle time of 19 sec. Quantification of the parent molecules was done as described for CL.

4.2.7.3.4 Product ion analysis of D_6-cholesterol and cholesterol

Quantification of cholesterol was achieved in positive ion mode by product ion analysis of cholesterol acetate (m/z 446.4) and D_6-cholesterol acetate (m/z 452.4) at a CE of 12 eV similar as described (Ejsing, 2006). The TOF mass analyzer was set to m/z 350-400 to monitor neutral loss (77 Da = $C_2H_7NO_2$) derived fragments at m/z 369.36 (cholesterol) and m/z 375.39 (D_6-cholesterol). Trapping of ions in Q2 (peak enhancement) was applied to a mass of m/z 375. Data acquisition was done in the continuum mode for 5 min, 150 cycles were acquired at a cycle time of 2 sec. Quantification of the parent molecules was done as described for CL.

4.2.7.3.5 DAG MPIS

MPIS of 18 DAG-specific MAG-H_2O fragments (Table 2) was performed at a CE of 25 eV. 44 MCA spectra for every precursor ion scan were acquired. The TOF mass range was set to m/z 250-400. Trapping of ions in Q2 (peak enhancement) was applied to m/z 327.3. Q1-scanning was done in the profile mode with a step size of 0.2 Da. MPIS spectra were evaluated with the Lipid Profiler software (V1.0.99, Applied Biosystems) under the following settings: smoothing: enabled, deisotoping: enabled, PIS mass tolerance: 0.3 Da. Peak intensities where exported as “corrected areas” and evaluated in Excel.

4.2.7.4 Acquisition methods - QTrap 5500

4.2.7.4.1 Neutral loss scanning and MRM - PIP and PIP_2

Quantification of PIP and PIP_2 was achieved by scanning for neutral losses of 357 Da and 437 Da at CEs of 25 eV and 35 eV, respectively. Neutral loss scans were performed in the profile mode (step size 0.1 Da) at a scan rate of 200 Da/s. For every scan mode 100-500 MCA spectra were accumulated. For quantification, the peak intensities (cps) were

extracted from the spectra and further evaluated in Excel or by self-programmed software tools.

Quantification of PIP 38:4 and PIP_2 38:4 in primary human T cells was also done by multiple reaction monitoring (MRM). Following Q1-Q3 transitions were monitored for PIP species: m/z 970.5 → m/z 613.4 (PI(4)P 37:4) and m/z 984.6 → m/z 627.6 (PIP 38:4) at a CE of 25 eV. For PIP_2 species: m/z 1050.5 → m/z 613.5 ($PI(4,5)P_2$ 37:4) and m/z 1064.5 → m/z 627.5 (PIP_2 38:4) at a CE of 35 eV. The dwell time was set to 100 msec. 100-200 cycles were acquired for PIP transitions and 720 cycles were acquired for PIP_2 transitions.

5 References

Acharya,U., McCaffery,J.M., Jacobs,R., and Malhotra,V. (1995). Reconstitution of vesiculated Golgi membranes into stacks of cisternae: requirement of NSF in stack formation. J. Cell Biol. *129*, 577-589.

An,X., Guo,X., Wu,Y., and Mohandas,N. (2004). Phosphatidylserine binding sites in red cell spectrin. Blood Cells Mol. Dis. *32*, 430-432.

Anderl, F. Identifizierung und Charakterisierung von Interaktionen der kleinen GTPase Arf1 während der COPI Vesikel-Biogenese. 2-1-2008.
Ref Type: Thesis/Dissertation

Antonsson,B. (1997). Phosphatidylinositol synthase from mammalian tissues. Biochim. Biophys. Acta *1348*, 179-186.

Ardail,D., Privat,J.P., Egret-Charlier,M., Levrat,C., Lerme,F., and Louisot,P. (1990). Mitochondrial contact sites. Lipid composition and dynamics. J. Biol. Chem. *265*, 18797-18802.

Askari,A., Xie,Z.J., Wang,Y.H., Periyasamy,S., and Huang,W.H. (1991). A second messenger role for monoacylglycerols is suggested by their activating effects on the sodium pump. Biochim. Biophys. Acta *1069*, 127-130.

Asp,L., Kartberg,F., Fernandez-Rodriguez,J., Smedh,M., Elsner,M., Laporte,F., Barcena,M., Jansen,K.A., Valentijn,J.A., Koster,A.J., Bergeron,J.J., and Nilsson,T. (2009). Early stages of Golgi vesicle and tubule formation require diacylglycerol. Mol. Biol. Cell *20*, 780-790.

Athenstaedt,K. and Daum,G. (1999). Phosphatidic acid, a key intermediate in lipid metabolism. Eur. J. Biochem. *266*, 1-16.

Back,J.W., Sanz,M.A., De,J.L., De Koning,L.J., Nijtmans,L.G., De Koster,C.G., Grivell,L.A., Van Der,S.H., and Muijsers,A.O. (2002). A structure for the yeast prohibitin complex: Structure prediction and evidence from chemical crosslinking and mass spectrometry. Protein Sci. *11*, 2471-2478.

Bankaitis,V.A. (2009). The Cirque du Soleil of Golgi membrane dynamics. J. Cell Biol. *186*, 169-171.

Bannykh,S.I. and Balch,W.E. (1997). Membrane dynamics at the endoplasmic reticulum-Golgi interface. J. Cell Biol. *138*, 1-4.

Barenholz,Y. and Thompson,T.E. (1999). Sphingomyelin: biophysical aspects. Chem. Phys. Lipids *102*, 29-34.

Beck,R., Rawet,M., Wieland,F.T., and Cassel,D. (2009). The COPI system: molecular mechanisms and function. FEBS Lett. *583*, 2701-2709.

Beranek,A., Rechberger,G., Knauer,H., Wolinski,H., Kohlwein,S.D., and Leber,R. (2009). Identification of a cardiolipin-specific phospholipase encoded by the gene CLD1 (YGR110W) in yeast. J. Biol. Chem. *284*, 11572-11578.

Bielawska,A., Perry,D.K., and Hannun,Y.A. (2001). Determination of ceramides and diglycerides by the diglyceride kinase assay. Anal. Biochem. *298*, 141-150.

Billah,M.M. and Anthes,J.C. (1990). The regulation and cellular functions of phosphatidylcholine hydrolysis. Biochem. J. *269*, 281-291.

Bird,I.M. (1994). Analysis of cellular phosphoinositides and phosphoinositols by extraction and simple analytical procedures. Methods Mol. Biol. *27*, 227-248.

Blero,D., Payrastre,B., Schurmans,S., and Erneux,C. (2007). Phosphoinositide phosphatases in a network of signalling reactions. Pflugers Arch. *455*, 31-44.

BLIGH,E.G. and DYER,W.J. (1959). A rapid method of total lipid extraction and purification. Can. J. Biochem. Physiol *37*, 911-917.

Bloch,K. (1965). The biological synthesis of cholesterol. Science *150*, 19-28.

Bolender,N., Sickmann,A., Wagner,R., Meisinger,C., and Pfanner,N. (2008). Multiple pathways for sorting mitochondrial precursor proteins. EMBO Rep. *9*, 42-49.

Bonfanti,L., Mironov,A.A., Jr., Martinez-Menarguez,J.A., Martella,O., Fusella,A., Baldassarre,M., Buccione,R., Geuze,H.J., Mironov,A.A., and Luini,A. (1998). Procollagen traverses the Golgi stack without leaving the lumen of cisternae: evidence for cisternal maturation. Cell *95*, 993-1003.

Brosche,T. and Platt,D. (1998). The biological significance of plasmalogens in defense against oxidative damage. Exp. Gerontol. *33*, 363-369.

Brugger,B., Erben,G., Sandhoff,R., Wieland,F.T., and Lehmann,W.D. (1997). Quantitative analysis of biological membrane lipids at the low picomole level by nano-electrospray ionization tandem mass spectrometry. Proc. Natl. Acad. Sci. U. S. A *94*, 2339-2344.

Brugger,B., Glass,B., Haberkant,P., Leibrecht,I., Wieland,F.T., and Krausslich,H.G. (2006). The HIV lipidome: a raft with an unusual composition. Proc. Natl. Acad. Sci. U. S. A *103*, 2641-2646.

Brugger,B., Graham,C., Leibrecht,I., Mombelli,E., Jen,A., Wieland,F., and Morris,R. (2004). The membrane domains occupied by glycosylphosphatidylinositol-anchored prion protein and Thy-1 differ in lipid composition. J. Biol. Chem. *279*, 7530-7536.

Brugger,B., Sandhoff,R., Wegehingel,S., Gorgas,K., Malsam,J., Helms,J.B., Lehmann,W.D., Nickel,W., and Wieland,F.T. (2000). Evidence for segregation of sphingomyelin and cholesterol during formation of COPI-coated vesicles. J. Cell Biol. *151*, 507-518.

Callender,H.L., Forrester,J.S., Ivanova,P., Preininger,A., Milne,S., and Brown,H.A. (2007). Quantification of Diacylglycerol Species from Cellular Extracts by Electrospray Ionization Mass Spectrometry Using a Linear Regression Algorithm
1. Anal. Chem. *79*, 263-272.

Carrasco,S. and Merida,I. (2004). Diacylglycerol-dependent binding recruits PKCtheta and RasGRP1 C1 domains to specific subcellular localizations in living T lymphocytes. Mol. Biol. Cell *15*, 2932-2942.

Carrasco,S. and Merida,I. (2007). Diacylglycerol, when simplicity becomes complex. Trends Biochem. Sci. *32*, 27-36.

Casaubon,R.L. and Snapper,M.L. (2001). S-adenosylmethionine reverses ilimaquinone's vesiculation of the Golgi apparatus: a fluorescence study on the cellular interactions of ilimaquinone. Bioorg. Med. Chem. Lett. *11*, 133-136.

Chang,S.C., Heacock,P.N., Clancey,C.J., and Dowhan,W. (1998a). The PEL1 gene (renamed PGS1) encodes the phosphatidylglycero-phosphate synthase of Saccharomyces cerevisiae. J. Biol. Chem. *273*, 9829-9836.

Chang,S.C., Heacock,P.N., Mileykovskaya,E., Voelker,D.R., and Dowhan,W. (1998b). Isolation and characterization of the gene (CLS1) encoding cardiolipin synthase in Saccharomyces cerevisiae. J. Biol. Chem. *273*, 14933-14941.

Collet,J.F., Stroobant,V., Pirard,M., Delpierre,G., and Van,S.E. (1998). A new class of phosphotransferases phosphorylated on an aspartate residue in an amino-terminal DXDX(T/V) motif. J. Biol. Chem. *273*, 14107-14112.

Contreras,F.X., Sanchez-Magraner,L., Alonso,A., and Goni,F.M. (2010). Transbilayer (flip-flop) lipid motion and lipid scrambling in membranes. FEBS Lett. *584*, 1779-1786.

Contreras,F.X., Villar,A.V., Alonso,A., and Goni,F.M. (2009). Ceramide-induced transbilayer (flip-flop) lipid movement in membranes. Methods Mol. Biol. *462*, 155-165.

Cooke,F.T. (2009). Measurement of polyphosphoinositides in cultured mammalian cells. Methods Mol. Biol. *462*, 43-58.

Cui,Z., Vance,J.E., Chen,M.H., Voelker,D.R., and Vance,D.E. (1993). Cloning and expression of a novel phosphatidylethanolamine N-methyltransferase. A specific biochemical and cytological marker for a unique membrane fraction in rat liver. J. Biol. Chem. *268*, 16655-16663.

Cullis,P.R. and de Kruijff,B. (1978). The polymorphic phase behaviour of phosphatidylethanolamines of natural and synthetic origin. A 31P NMR study. Biochim. Biophys. Acta *513*, 31-42.

Cullis,P.R. and de Kruijff,B. (1979). Lipid polymorphism and the functional roles of lipids in biological membranes. Biochim. Biophys. Acta *559*, 399-420.

Daum,G. and Vance,J.E. (1997). Import of lipids into mitochondria. Prog. Lipid Res. *36*, 103-130.

Dawson,R.M. and Eichberg,J. (1965). Diphosphoinositide and triphosphoinositide in animal tissues. Extraction, estimation and changes post mortem. Biochem. J. *96*, 634-643.

De Matteis,M.A., Di,C.A., and Godi,A. (2005). The role of the phosphoinositides at the Golgi complex. Biochim. Biophys. Acta *1744*, 396-405.

Devaux,P.F. and Morris,R. (2004). Transmembrane asymmetry and lateral domains in biological membranes. Traffic. *5*, 241-246.

Devaux,P.F., Zachowski,A., Morrot,G., Cribier,S., Fellmann,P., Geldwerth,D., Bitbol,M., and Herve,P. (1990). Control of the transmembrane phospholipid distribution in eukaryotic cells by aminophospholipid translocase. Biotechnol. Appl. Biochem. *12*, 517-522.

Di Paolo,G. and De Camilli,P. (2006). Phosphoinositides in cell regulation and membrane dynamics. Nature *443*, 651-657.

Dowhan,W. (1997). Molecular basis for membrane phospholipid diversity: why are there so many lipids? Annu. Rev. Biochem. *66*, 199-232.

Downes,C.P., Gray,A., and Lucocq,J.M. (2005). Probing phosphoinositide functions in signaling and membrane trafficking. Trends Cell Biol. *15*, 259-268.

Drecktrah,D., Chambers,K., Racoosin,E.L., Cluett,E.B., Gucwa,A., Jackson,B., and Brown,W.J. (2003). Inhibition of a Golgi complex lysophospholipid acyltransferase induces membrane tubule formation and retrograde trafficking. Mol. Biol. Cell *14*, 3459-3469.

Ejsing, C. S. Molecular characterization of the lipidome by mass spectrometry. 10-16-2006. Ref Type: Thesis/Dissertation

Ejsing,C.S., Duchoslav,E., Sampaio,J., Simons,K., Bonner,R., Thiele,C., Ekroos,K., and Shevchenko,A. (2006). Automated identification and quantification of glycerophospholipid molecular species by multiple precursor ion scanning. Anal. Chem. *78*, 6202-6214.

Ejsing,C.S., Sampaio,J.L., Surendranath,V., Duchoslav,E., Ekroos,K., Klemm,R.W., Simons,K., and Shevchenko,A. (2009). Global analysis of the yeast lipidome by quantitative shotgun mass spectrometry. Proc. Natl. Acad. Sci. U. S. A *106*, 2136-2141.

Ekroos,K., Chernushevich,I.V., Simons,K., and Shevchenko,A. (2002). Quantitative profiling of phospholipids by multiple precursor ion scanning on a hybrid quadrupole time-of-flight mass spectrometer. Anal. Chem. *74*, 941-949.

Ernst,A.M., Contreras,F.X., Brugger,B., and Wieland,F. (2010). Determinants of specificity at the protein-lipid interface in membranes. FEBS Lett. *584*, 1713-1720.

Fadok,V.A., Bratton,D.L., Frasch,S.C., Warner,M.L., and Henson,P.M. (1998). The role of phosphatidylserine in recognition of apoptotic cells by phagocytes. Cell Death. Differ. *5*, 551-562.

Fagone,P. and Jackowski,S. (2009). Membrane phospholipid synthesis and endoplasmic reticulum function. J. Lipid Res. *50 Suppl*, S311-S316.

Fahy,E., Subramaniam,S., Brown,H.A., Glass,C.K., Merrill,A.H., Jr., Murphy,R.C., Raetz,C.R., Russell,D.W., Seyama,Y., Shaw,W., Shimizu,T., Spener,F., van,M.G., VanNieuwenhze,M.S., White,S.H., Witztum,J.L., and Dennis,E.A. (2005). A comprehensive classification system for lipids. J. Lipid Res. *46*, 839-861.

Falardeau,P., Robillard,M., and Hui,R. (1993). Quantification of diacylglycerols by capillary gas chromatography-negative ion chemical ionization-mass spectrometry 25. Anal. Biochem. *208*, 311-316.

Fernandez-Ulibarri,I., Vilella,M., Lazaro-Dieguez,F., Sarri,E., Martinez,S.E., Jimenez,N., Claro,E., Merida,I., Burger,K.N., and Egea,G. (2007). Diacylglycerol Is Required for the Formation of COPI Vesicles in the Golgi-to-ER Transport Pathway. Mol. Biol. Cell.

Feske,S. (2007). Calcium signalling in lymphocyte activation and disease. Nat. Rev. Immunol. *7*, 690-702.

Fleischer,B., Zambrano,F., and Fleischer,S. (1974). Biochemical characterization of the golgi complex of mammalian cells. J. Supramol. Struct. *2*, 737-750.

FOLCH,J., LEES,M., and SLOANE STANLEY,G.H. (1957). A simple method for the isolation and purification of total lipides from animal tissues. J. Biol. Chem. *226*, 497-509.

Fuller,N. and Rand,R.P. (2001). The influence of lysolipids on the spontaneous curvature and bending elasticity of phospholipid membranes. Biophys. J. *81*, 243-254.

Garrett,T.A., Kordestani,R., and Raetz,C.R. (2007). Quantification of cardiolipin by liquid chromatography-electrospray ionization mass spectrometry. Methods Enzymol. *433*, 213-230.

Gaynor,E.C., Graham,T.R., and Emr,S.D. (1998). COPI in ER/Golgi and intra-Golgi transport: do yeast COPI mutants point the way? Biochim. Biophys. Acta *1404*, 33-51.

Gebert,N., Joshi,A.S., Kutik,S., Becker,T., McKenzie,M., Guan,X.L., Mooga,V.P., Stroud,D.A., Kulkarni,G., Wenk,M.R., Rehling,P., Meisinger,C., Ryan,M.T., Wiedemann,N., Greenberg,M.L., and Pfanner,N. (2009). Mitochondrial cardiolipin involved in outer-membrane protein biogenesis: implications for Barth syndrome. Curr. Biol. *19*, 2133-2139.

Gibellini,F. and Smith,T.K. (2010). The Kennedy pathway--De novo synthesis of phosphatidylethanolamine and phosphatidylcholine. IUBMB. Life *62*, 414-428.

Gkantiragas,I., Brugger,B., Stuven,E., Kaloyanova,D., Li,X.Y., Lohr,K., Lottspeich,F., Wieland,F.T., and Helms,J.B. (2001). Sphingomyelin-enriched microdomains at the Golgi complex. Mol. Biol. Cell *12*, 1819-1833.

Glick,B.S., Elston,T., and Oster,G. (1997). A cisternal maturation mechanism can explain the asymmetry of the Golgi stack. FEBS Lett. *414*, 177-181.

Gohil,V.M. and Greenberg,M.L. (2009). Mitochondrial membrane biogenesis: phospholipids and proteins go hand in hand. J. Cell Biol. *184*, 469-472.

Gohil,V.M., Thompson,M.N., and Greenberg,M.L. (2005). Synthetic lethal interaction of the mitochondrial phosphatidylethanolamine and cardiolipin biosynthetic pathways in Saccharomyces cerevisiae. J. Biol. Chem. *280*, 35410-35416.

Goni,F.M. and Alonso,A. (1999). Structure and functional properties of diacylglycerols in membranes. Prog. Lipid Res. *38*, 1-48.

Goni,F.M. and Alonso,A. (2002). Sphingomyelinases: enzymology and membrane activity. FEBS Lett. *531*, 38-46.

Gray,A., Olsson,H., Batty,I.H., Priganica,L., and Peter,D.C. (2003). Nonradioactive methods for the assay of phosphoinositide 3-kinases and phosphoinositide phosphatases and selective detection of signaling lipids in cell and tissue extracts. Anal. Biochem. *313*, 234-245.

Gu,Z., Valianpour,F., Chen,S., Vaz,F.M., Hakkaart,G.A., Wanders,R.J., and Greenberg,M.L. (2004). Aberrant cardiolipin metabolism in the yeast taz1 mutant: a model for Barth syndrome. Mol. Microbiol. *51*, 149-158.

Guizzunti,G., Brady,T.P., Fischer,D., Malhotra,V., and Theodorakis,E.A. (2010). Chemical biology studies on norrisolide. Bioorg. Med. Chem. *18*, 2115-2122.

Haimovitz-Friedman,A., Kolesnick,R.N., and Fuks,Z. (1997). Ceramide signaling in apoptosis. Br. Med. Bull. *53*, 539-553.

Halling,K.K., Ramstedt,B., Nystrom,J.H., Slotte,J.P., and Nyholm,T.K. (2008). Cholesterol interactions with fluid-phase phospholipids: effect on the lateral organization of the bilayer. Biophys. J. *95*, 3861-3871.

Hama,H., Takemoto,J.Y., and DeWald,D.B. (2000). Analysis of phosphoinositides in protein trafficking. Methods *20*, 465-473.

Hama,H., Torabinejad,J., Prestwich,G.D., and DeWald,D.B. (2004). Measurement and immunofluorescence of cellular phosphoinositides. Methods Mol. Biol. *284*, 243-258.

Han,X. and Gross,R.W. (1994). Electrospray ionization mass spectroscopic analysis of human erythrocyte plasma membrane phospholipids. Proc. Natl. Acad. Sci. U. S. A *91*, 10635-10639.

Han,X. and Gross,R.W. (2005). Shotgun lipidomics: electrospray ionization mass spectrometric analysis and quantitation of cellular lipidomes directly from crude extracts of biological samples. Mass Spectrom. Rev. *24*, 367-412.

Han,X., Yang,J., Yang,K., Zhao,Z., Abendschein,D.R., and Gross,R.W. (2007). Alterations in myocardial cardiolipin content and composition occur at the very earliest stages of diabetes: a shotgun lipidomics study. Biochemistry *46*, 6417-6428.

Han,X., Yang,K., Yang,J., Cheng,H., and Gross,R.W. (2006). Shotgun lipidomics of cardiolipin molecular species in lipid extracts of biological samples. J. Lipid Res. *47*, 864-879.

Hanada,K. (2010). Intracellular trafficking of ceramide by ceramide transfer protein. Proc. Jpn. Acad. Ser. B Phys. Biol. Sci. *86*, 426-437.

Hanada,K., Kumagai,K., Tomishige,N., and Kawano,M. (2007). CERT and intracellular trafficking of ceramide. Biochim. Biophys. Acta *1771*, 644-653.

Hanada,K., Kumagai,K., Tomishige,N., and Yamaji,T. (2009). CERT-mediated trafficking of ceramide. Biochim. Biophys. Acta *1791*, 684-691.

Hanahan,D.J. (1986). Platelet activating factor: a biologically active phosphoglyceride. Annu. Rev. Biochem. *55*, 483-509.

Harder,T. and Sangani,D. (2009). Plasma membrane rafts engaged in T cell signalling: new developments in an old concept. Cell Commun. Signal. *7*, 21.

Hauff,K.D. and Hatch,G.M. (2006). Cardiolipin metabolism and Barth Syndrome. Prog. Lipid Res. *45*, 91-101.

Hax,W.M. and van Kessel,W.S. (1977). High-performance liquid chromatographic separation and photometric detection of phospholipids. J. Chromatogr. *142*, 735-741.

Hayashi,T., Rizzuto,R., Hajnoczky,G., and Su,T.P. (2009). MAM: more than just a housekeeper. Trends Cell Biol. *19*, 81-88.

Hegewald,H. (1996). One-dimensional thin-layer chromatography of all known D-3 and D-4 isomers of phosphoinositides. Anal. Biochem. *242*, 152-155.

Hein,L.K., Duplock,S., Hopwood,J.J., and Fuller,M. (2008). Lipid composition of microdomains is altered in a cell model of Gaucher disease. J. Lipid Res. *49*, 1725-1734.

Henneberry,A.L., Wright,M.M., and McMaster,C.R. (2002). The major sites of cellular phospholipid synthesis and molecular determinants of Fatty Acid and lipid head group specificity. Mol. Biol. Cell *13*, 3148-3161.

Hess,K.A., Morre,D.J., and Merritt,W.D. (1979). Lipoprotein secretion by rat liver Golgi apparatus. Lipoprotein particles and lipase activity. Cytobiologie. *18*, 431-449.

Holthuis,J.C. and Levine,T.P. (2005). Lipid traffic: floppy drives and a superhighway. Nat. Rev. Mol. Cell Biol. *6*, 209-220.

Horibata,Y. and Hirabayashi,Y. (2007). Identification and characterization of human ethanolaminephosphotransferase1. J. Lipid Res. *48*, 503-508.

Hsu,F.F. and Turk,J. (2000). Characterization of phosphatidylinositol, phosphatidylinositol-4-phosphate, and phosphatidylinositol-4,5-bisphosphate by electrospray ionization tandem mass spectrometry: a mechanistic study. J. Am. Soc. Mass Spectrom. *11*, 986-999.

Hsu,F.F., Turk,J., Rhoades,E.R., Russell,D.G., Shi,Y., and Groisman,E.A. (2005). Structural characterization of cardiolipin by tandem quadrupole and multiple-stage quadrupole ion-trap mass spectrometry with electrospray ionization. J. Am. Soc. Mass Spectrom. *16*, 491-504.

Hubbard,W.C., Hundley,T.R., Oriente,A., and MacGlashan,D.W., Jr. (1996). Quantitation of 1-stearoyl-2-arachidonoyl-sn-3-glycerol in human basophils via gas chromatography-negative ion chemical ionization mass spectrometry. Anal. Biochem. *236*, 309-321.

Hui,N., Nakamura,N., Slusarewicz,P., and Warren,G. (1998). Purification of Rat Liver Golgi Stacks. In Cell Biology: A Laboratory Handbook, pp. 46-55.

Ikonen,E. and Simons,K. (1998). Protein and lipid sorting from the trans-Golgi network to the plasma membrane in polarized cells. Semin. Cell Dev. Biol. *9*, 503-509.

Jackowski,S., Xu,X.X., and Rock,C.O. (1997). Phosphatidylcholine signaling in response to CSF-1. Mol. Reprod. Dev. *46*, 24-30.

Jamora,C., Takizawa,P.A., Zaarour,R.F., Denesvre,C., Faulkner,D.J., and Malhotra,V. (1997). Regulation of Golgi structure through heterotrimeric G proteins. Cell *91*, 617-626.

Jia,L., Dienhart,M.K., and Stuart,R.A. (2007). Oxa1 directly interacts with Atp9 and mediates its assembly into the mitochondrial F1Fo-ATP synthase complex. Mol. Biol. Cell *18*, 1897-1908.

Jiang,F., Rizavi,H.S., and Greenberg,M.L. (1997). Cardiolipin is not essential for the growth of Saccharomyces cerevisiae on fermentable or non-fermentable carbon sources. Mol. Microbiol. *26*, 481-491.

Karlsson,K.A. (1970). Sphingolipid long chain bases. Lipids *5*, 878-891.

Kawai,F., Shoda,M., Harashima,R., Sadaie,Y., Hara,H., and Matsumoto,K. (2004). Cardiolipin domains in Bacillus subtilis marburg membranes. J. Bacteriol. *186*, 1475-1483.

Kearns,B.G., McGee,T.P., Mayinger,P., Gedvilaite,A., Phillips,S.E., Kagiwada,S., and Bankaitis,V.A. (1997). Essential role for diacylglycerol in protein transport from the yeast Golgi complex. Nature *387*, 101-105.

Keenan,T.W. and Morre,D.J. (1970). Phospholipid class and fatty acid composition of golgi apparatus isolated from rat liver and comparison with other cell fractions. Biochemistry *9*, 19-25.

Kerwin,J.L., Tuininga,A.R., and Ericsson,L.H. (1994). Identification of molecular species of glycerophospholipids and sphingomyelin using electrospray mass spectrometry. J. Lipid Res. *35*, 1102-1114.

Kiebish,M.A., Han,X., Cheng,H., Chuang,J.H., and Seyfried,T.N. (2008). Cardiolipin and electron transport chain abnormalities in mouse brain tumor mitochondria: lipidomic evidence supporting the Warburg theory of cancer. J. Lipid Res. *49*, 2545-2556.

Klemm,R.W., Ejsing,C.S., Surma,M.A., Kaiser,H.J., Gerl,M.J., Sampaio,J.L., de,R.Q., Ferguson,C., Proszynski,T.J., Shevchenko,A., and Simons,K. (2009). Segregation of sphingolipids and sterols during formation of secretory vesicles at the trans-Golgi network. J. Cell Biol. *185*, 601-612.

Kocsis,M.G. and Weselake,R.J. (1996). Phosphatidate phosphatases of mammals, yeast, and higher plants. Lipids *31*, 785-802.

Kohlwein,S.D., Kuchler,K., Sperka-Gottlieb,C., Henry,S.A., and Paltauf,F. (1988). Identification of mitochondrial and microsomal phosphatidylserine synthase in Saccharomyces cerevisiae as the gene product of the CHO1 structural gene. J. Bacteriol. *170*, 3778-3781.

Koivusalo,M., Haimi,P., Heikinheimo,L., Kostiainen,R., and Somerharju,P. (2001). Quantitative determination of phospholipid compositions by ESI-MS: effects of acyl chain length, unsaturation, and lipid concentration on instrument response. J. Lipid Res. *42*, 663-672.

Ktistakis,N.T., Brown,H.A., Sternweis,P.C., and Roth,M.G. (1995). Phospholipase D is present on Golgi-enriched membranes and its activation by ADP ribosylation factor is sensitive to brefeldin A. Proc. Natl. Acad. Sci. U. S. A *92*, 4952-4956.

Ktistakis,N.T., Brown,H.A., Waters,M.G., Sternweis,P.C., and Roth,M.G. (1996). Evidence that phospholipase D mediates ADP ribosylation factor-dependent formation of Golgi coated vesicles. J. Cell Biol. *134*, 295-306.

Kuchler,K., Daum,G., and Paltauf,F. (1986). Subcellular and submitochondrial localization of phospholipid-synthesizing enzymes in Saccharomyces cerevisiae. J. Bacteriol. *165*, 901-910.

Langhorst,M.F., Reuter,A., and Stuermer,C.A. (2005). Scaffolding microdomains and beyond: the function of reggie/flotillin proteins. Cell Mol. Life Sci. *62*, 2228-2240.

Lanoix,J., Ouwendijk,J., Stark,A., Szafer,E., Cassel,D., Dejgaard,K., Weiss,M., and Nilsson,T. (2001). Sorting of Golgi resident proteins into different subpopulations of COPI vesicles: a role for ArfGAP1. J. Cell Biol. *155*, 1199-1212.

Lev,S. (2010). Non-vesicular lipid transport by lipid-transfer proteins and beyond. Nat. Rev. Mol. Cell Biol.

Levine,T. and Loewen,C. (2006). Inter-organelle membrane contact sites: through a glass, darkly. Curr. Opin. Cell Biol. *18*, 371-378.

Li,G., Chen,S., Thompson,M.N., and Greenberg,M.L. (2007a). New insights into the regulation of cardiolipin biosynthesis in yeast: implications for Barth syndrome. Biochim. Biophys. Acta *1771*, 432-441.

Li,Y.L., Su,X., Stahl,P.D., and Gross,M.L. (2007b). Quantification of diacylglycerol molecular species in biological samples by electrospray ionization mass spectrometry after one-step derivatization. Anal. Chem. *79*, 1569-1574.

Liebisch,G., Binder,M., Schifferer,R., Langmann,T., Schulz,B., and Schmitz,G. (2006). High throughput quantification of cholesterol and cholesteryl ester by electrospray ionization tandem mass spectrometry (ESI-MS/MS)
1. Biochim. Biophys. Acta *1761*, 121-128.

Lingwood,D., Kaiser,H.J., Levental,I., and Simons,K. (2009). Lipid rafts as functional heterogeneity in cell membranes. Biochem. Soc. Trans. *37*, 955-960.

Lingwood,D. and Simons,K. (2010). Lipid rafts as a membrane-organizing principle. Science *327*, 46-50.

Litvak,V., Dahan,N., Ramachandran,S., Sabanay,H., and Lev,S. (2005). Maintenance of the diacylglycerol level in the Golgi apparatus by the Nir2 protein is critical for Golgi secretory function. Nat. Cell Biol. *7*, 225-234.

Malhotra,A., Xu,Y., Ren,M., and Schlame,M. (2009). Formation of molecular species of mitochondrial cardiolipin. 1. A novel transacylation mechanism to shuttle fatty acids between sn-1 and sn-2 positions of multiple phospholipid species. Biochim. Biophys. Acta *1791*, 314-320.

Mallo,G.V., Espina,M., Smith,A.C., Terebiznik,M.R., Aleman,A., Finlay,B.B., Rameh,L.E., Grinstein,S., and Brumell,J.H. (2008). SopB promotes phosphatidylinositol 3-phosphate formation on Salmonella vacuoles by recruiting Rab5 and Vps34. J. Cell Biol. *182*, 741-752.

Malsam,J., Satoh,A., Pelletier,L., and Warren,G. (2005). Golgin tethers define subpopulations of COPI vesicles. Science *307*, 1095-1098.

Manneville,J.B., Casella,J.F., Ambroggio,E., Gounon,P., Bertherat,J., Bassereau,P., Cartaud,J., Antonny,B., and Goud,B. (2008). COPI coat assembly occurs on liquid-disordered domains and the associated membrane deformations are limited by membrane tension. Proc. Natl. Acad. Sci. U. S. A *105*, 16946-16951.

Matsumoto,K., Kusaka,J., Nishibori,A., and Hara,H. (2006). Lipid domains in bacterial membranes. Mol. Microbiol. *61*, 1110-1117.

Matsuura-Tokita,K., Takeuchi,M., Ichihara,A., Mikuriya,K., and Nakano,A. (2006). Live imaging of yeast Golgi cisternal maturation. Nature *441*, 1007-1010.

McKenzie,M., Lazarou,M., Thorburn,D.R., and Ryan,M.T. (2006). Mitochondrial respiratory chain supercomplexes are destabilized in Barth Syndrome patients. J. Mol. Biol. *361*, 462-469.

McMillin,J.B. and Dowhan,W. (2002). Cardiolipin and apoptosis. Biochim. Biophys. Acta *1585*, 97-107.

Merkwirth,C., Dargazanli,S., Tatsuta,T., Geimer,S., Lower,B., Wunderlich,F.T., von Kleist-Retzow,J.C., Waisman,A., Westermann,B., and Langer,T. (2008). Prohibitins control cell

proliferation and apoptosis by regulating OPA1-dependent cristae morphogenesis in mitochondria. Genes Dev. *22*, 476-488.

Merkwirth,C. and Langer,T. (2009b). Prohibitin function within mitochondria: essential roles for cell proliferation and cristae morphogenesis. Biochim. Biophys. Acta *1793*, 27-32.

Merkwirth,C. and Langer,T. (2009a). Prohibitin function within mitochondria: essential roles for cell proliferation and cristae morphogenesis. Biochim. Biophys. Acta *1793*, 27-32.

Merz,S., Hammermeister,M., Altmann,K., Durr,M., and Westermann,B. (2007). Molecular machinery of mitochondrial dynamics in yeast. Biol. Chem. *388*, 917-926.

Michell,R.H., Hawthorne,J.N., Coleman,R., and Karnovsky,M.L. (1970). Extraction of polyphosphoinositides with neutral and acidified solvents. A comparison of guinea-pig brain and liver, and measurements of rat liver inositol compounds which are resistant to extraction. Biochim. Biophys. Acta *210*, 86-91.

Milne,S.B., Ivanova,P.T., DeCamp,D., Hsueh,R.C., and Brown,H.A. (2005). A targeted mass spectrometric analysis of phosphatidylinositol phosphate species. J. Lipid Res. *46*, 1796-1802.

Mironov,A.A., Weidman,P., and Luini,A. (1997). Variations on the intracellular transport theme: maturing cisternae and trafficking tubules. J. Cell Biol. *138*, 481-484.

Moelleken,J., Malsam,J., Betts,M.J., Movafeghi,A., Reckmann,I., Meissner,I., Hellwig,A., Russell,R.B., Sollner,T., Brugger,B., and Wieland,F.T. (2007). Differential localization of coatomer complex isoforms within the Golgi apparatus. Proc. Natl. Acad. Sci. U. S. A *104*, 4425-4430.

Mombelli,E., Morris,R., Taylor,W., and Fraternali,F. (2003). Hydrogen-bonding propensities of sphingomyelin in solution and in a bilayer assembly: a molecular dynamics study. Biophys. J. *84*, 1507-1517.

Monaco,M.E., Cassai,N.D., and Sidhu,G.S. (2006). Subcellular localization of phosphatidylinositol synthesis. Biochem. Biophys. Res. Commun. *348*, 1200-1204.

Mor,A., Campi,G., Du,G., Zheng,Y., Foster,D.A., Dustin,M.L., and Philips,M.R. (2007). The lymphocyte function-associated antigen-1 receptor costimulates plasma membrane Ras via phospholipase D2. Nat. Cell Biol. *9*, 713-719.

Mor,A. and Philips,M.R. (2006). Compartmentalized Ras/MAPK signaling. Annu. Rev. Immunol. *24*, 771-800.

Mu,H. and Hoy,C.E. (2000). Application of atmospheric pressure chemical ionization liquid chromatography-mass spectrometry in identification of lymph triacylglycerols. J. Chromatogr. B Biomed. Sci. Appl. *748*, 425-437.

Murphy,R.C., James,P.F., McAnoy,A.M., Krank,J., Duchoslav,E., and Barkley,R.M. (2007). Detection of the abundance of diacylglycerol and triacylglycerol molecular species in cells using neutral loss mass spectrometry. Anal. Biochem. *366*, 59-70.

Nagan,N. and Zoeller,R.A. (2001). Plasmalogens: biosynthesis and functions. Prog. Lipid Res. *40*, 199-229.

Newkirk,J.D. and Waite,M. (1973). Phospholipid hydrolysis by phospholipase A 1 and A 2 in plasma membranes and microsomes of rat liver. Biochim. Biophys. Acta *298*, 562-576.

Newton,A.C. (1995). Protein kinase C: structure, function, and regulation. J. Biol. Chem. *270*, 28495-28498.

Nickel,W., Brugger,B., and Wieland,F.T. (1998a). Protein and lipid sorting between the endoplasmic reticulum and the Golgi complex. Semin. Cell Dev. Biol. *9*, 493-501.

Nickel,W., Malsam,J., Gorgas,K., Ravazzola,M., Jenne,N., Helms,J.B., and Wieland,F.T. (1998b). Uptake by COPI-coated vesicles of both anterograde and retrograde cargo is inhibited by GTPgammaS in vitro. J. Cell Sci. *111 (Pt 20)*, 3081-3090.

Nickel,W. and Wieland,F.T. (1998). Biosynthetic protein transport through the early secretory pathway. Histochem. Cell Biol. *109*, 477-486.

Nishibori,A., Kusaka,J., Hara,H., Umeda,M., and Matsumoto,K. (2005). Phosphatidylethanolamine domains and localization of phospholipid synthases in Bacillus subtilis membranes. J. Bacteriol. *187*, 2163-2174.

Norton,W.T., Abe,T., Poduslo,S.E., and DeVries,G.H. (1975). The lipid composition of isolated brain cells and axons. J. Neurosci. Res. *1*, 57-75.

Oberle,N., Eberhardt,N., Falk,C.S., Krammer,P.H., and Suri-Payer,E. (2007). Rapid suppression of cytokine transcription in human CD4+CD25 T cells by CD4+Foxp3+ regulatory T cells: independence of IL-2 consumption, TGF-beta, and various inhibitors of TCR signaling. J. Immunol. *179*, 3578-3587.

Ohvo-Rekila,H., Ramstedt,B., Leppimaki,P., and Slotte,J.P. (2002). Cholesterol interactions with phospholipids in membranes. Prog. Lipid Res. *41*, 66-97.

Op den Kamp,J.A. (1979). Lipid asymmetry in membranes. Annu. Rev. Biochem. *48*, 47-71.

Orci,L., Ravazzola,M., Volchuk,A., Engel,T., Gmachl,M., Amherdt,M., Perrelet,A., Sollner,T.H., and Rothman,J.E. (2000). Anterograde flow of cargo across the golgi stack potentially mediated via bidirectional "percolating" COPI vesicles. Proc. Natl. Acad. Sci. U. S. A *97*, 10400-10405.

Orci,L., Stamnes,M., Ravazzola,M., Amherdt,M., Perrelet,A., Sollner,T.H., and Rothman,J.E. (1997). Bidirectional transport by distinct populations of COPI-coated vesicles. Cell *90*, 335-349.

Osman, C. Characterization of the genetic interactome of prohibitins in S. cerevisiae. 6-17-2009. Ref Type: Thesis/Dissertation

Osman,C., Haag,M., Potting,C., Rodenfels,J., Dip,P.V., Wieland,F.T., Brugger,B., Westermann,B., and Langer,T. (2009). The genetic interactome of prohibitins: coordinated control of cardiolipin and phosphatidylethanolamine by conserved regulators in mitochondria. J. Cell Biol. *184*, 583-596.

Osman,C., Haag,M., Wieland,F.T., Brugger,B., and Langer,T. (2010). A mitochondrial phosphatase required for cardiolipin biosynthesis: the PGP phosphatase Gep4. EMBO J. *29*, 1976-1987.

Osman,C., Wilmes,C., Tatsuta,T., and Langer,T. (2007). Prohibitins interact genetically with Atp23, a novel processing peptidase and chaperone for the F1Fo-ATP synthase. Mol. Biol. Cell *18*, 627-635.

Ostrander,D.B., Sparagna,G.C., Amoscato,A.A., McMillin,J.B., and Dowhan,W. (2001). Decreased cardiolipin synthesis corresponds with cytochrome c release in palmitate-induced cardiomyocyte apoptosis. J. Biol. Chem. *276*, 38061-38067.

Ozcan,N., Ejsing,C.S., Shevchenko,A., Lipski,A., Morbach,S., and Kramer,R. (2007). Osmolality, temperature, and membrane lipid composition modulate the activity of betaine transporter BetP in Corynebacterium glutamicum. J. Bacteriol. *189*, 7485-7496.

Patterson,G.H., Hirschberg,K., Polishchuk,R.S., Gerlich,D., Phair,R.D., and Lippincott-Schwartz,J. (2008). Transport through the Golgi apparatus by rapid partitioning within a two-phase membrane system. Cell *133*, 1055-1067.

Pettitt,T.R., Dove,S.K., Lubben,A., Calaminus,S.D., and Wakelam,M.J. (2006). Analysis of intact phosphoinositides in biological samples
1. J. Lipid Res. *47*, 1588-1596.

Pfeiffer,K., Gohil,V., Stuart,R.A., Hunte,C., Brandt,U., Greenberg,M.L., and Schagger,H. (2003). Cardiolipin stabilizes respiratory chain supercomplexes. J. Biol. Chem. *278*, 52873-52880.

Potting,C., Wilmes,C., Engmann,T., Osman,C., and Langer,T. (2010). Regulation of mitochondrial phospholipids by Ups1/PRELI-like proteins depends on proteolysis and Mdm35. EMBO J. *29*, 2888-2898.

Radeke,H.S., Digits,C.A., Casaubon,R.L., and Snapper,M.L. (1999). Interactions of (-)-ilimaquinone with methylation enzymes: implications for vesicular-mediated secretion. Chem. Biol. *6*, 639-647.

Ramstedt,B. and Slotte,J.P. (1999). Interaction of cholesterol with sphingomyelins and acyl-chain-matched phosphatidylcholines: a comparative study of the effect of the chain length. Biophys. J. *76*, 908-915.

Ramstedt,B. and Slotte,J.P. (2006). Sphingolipids and the formation of sterol-enriched ordered membrane domains. Biochim. Biophys. Acta *1758*, 1945-1956.

Riebeling,C., Morris,A.J., and Shields,D. (2009). Phospholipase D in the Golgi apparatus. Biochim. Biophys. Acta *1791*, 876-880.

Rojo,J.M., Bello,R., and Portoles,P. (2008). T-cell receptor. Adv. Exp. Med. Biol. *640*, 1-11.

Rosati,O., Albrizio,S., Montesano,D., Riccieri,R., Cossignani,L., Curini,M., Simonetti,M.S., Rastrelli,L., and Damiani,P. (2007). HPLC separation and NMR structural elucidation of sn-1,2-, 2,3-, and 1,3-diacylglycerols from olive oil as naphthylethylurethane derivatives. J. Agric. Food Chem. *55*, 191-196.

Roth,J. and Berger,E.G. (1982). Immunocytochemical localization of galactosyltransferase in HeLa cells: codistribution with thiamine pyrophosphatase in trans-Golgi cisternae. J. Cell Biol. *93*, 223-229.

Rouser,G., Fkeischer,S., and Yamamoto,A. (1970). Two dimensional then layer chromatographic separation of polar lipids and determination of phospholipids by phosphorus analysis of spots. Lipids *5*, 494-496.

Sadeghlar,F., Sandhoff,K., and van Echten-Deckert,G. (2000). Cell type specific localization of sphingomyelin biosynthesis. FEBS Lett. *478*, 9-12.

Sasaki,T., Takasuga,S., Sasaki,J., Kofuji,S., Eguchi,S., Yamazaki,M., and Suzuki,A. (2009). Mammalian phosphoinositide kinases and phosphatases. Prog. Lipid Res. *48*, 307-343.

Schlame,M. (2008). Thematic Review Series: Glycerolipids. Cardiolipin synthesis for the assembly of bacterial and mitochondrial membranes
1. J. Lipid Res. *49*, 1607-1620.

Schlame,M., Brody,S., and Hostetler,K.Y. (1993). Mitochondrial cardiolipin in diverse eukaryotes. Comparison of biosynthetic reactions and molecular acyl species. Eur. J. Biochem. *212*, 727-735.

Schlame,M. and Otten,D. (1991). Analysis of cardiolipin molecular species by high-performance liquid chromatography of its derivative 1,3-bisphosphatidyl-2-benzoyl-sn-glycerol dimethyl ester. Anal. Biochem. *195*, 290-295.

Schlame,M., Ren,M., Xu,Y., Greenberg,M.L., and Haller,I. (2005). Molecular symmetry in mitochondrial cardiolipins
9. Chem. Phys. Lipids *138*, 38-49.

Schlame,M., Rua,D., and Greenberg,M.L. (2000). The biosynthesis and functional role of cardiolipin. Prog. Lipid Res. *39*, 257-288.

Schneiter,R., Brugger,B., Sandhoff,R., Zellnig,G., Leber,A., Lampl,M., Athenstaedt,K., Hrastnik,C., Eder,S., Daum,G., Paltauf,F., Wieland,F.T., and Kohlwein,S.D. (1999). Electrospray ionization tandem mass spectrometry (ESI-MS/MS) analysis of the lipid molecular species composition of yeast subcellular membranes reveals acyl chain-based sorting/remodeling of distinct molecular species en route to the plasma membrane. J. Cell Biol. *146*, 741-754.

Schwudke,D., Hannich,J.T., Surendranath,V., Grimard,V., Moehring,T., Burton,L., Kurzchalia,T., and Shevchenko,A. (2007a). Top-down lipidomic screens by multivariate analysis of high-resolution survey mass spectra. Anal. Chem. *79*, 4083-4093.

Schwudke,D., Liebisch,G., Herzog,R., Schmitz,G., and Shevchenko,A. (2007b). Shotgun lipidomics by tandem mass spectrometry under data-dependent acquisition control. Methods Enzymol. *433*, 175-191.

Schwudke,D., Oegema,J., Burton,L., Entchev,E., Hannich,J.T., Ejsing,C.S., Kurzchalia,T., and Shevchenko,A. (2006). Lipid profiling by multiple precursor and neutral loss scanning driven by the data-dependent acquisition. Anal. Chem. *78*, 585-595.

Siddhanta,A. and Shields,D. (1998). Secretory vesicle budding from the trans-Golgi network is mediated by phosphatidic acid levels. J. Biol. Chem. *273*, 17995-17998.

Simons,K. and van,M.G. (1988). Lipid sorting in epithelial cells. Biochemistry *27*, 6197-6202.

Skipski,V.P., Peterson,R.F., and Barclay,M. (1964). Quantitative analysis of phospholipids by thin-layer chromatography. Biochem. J. *90*, 374-378.

Smets,L.A., Van,R.H., and Salomons,G.S. (1999). Signalling steps in apoptosis by ether lipids. Apoptosis. *4*, 419-427.

Smirnova,E., Goldberg,E.B., Makarova,K.S., Lin,L., Brown,W.J., and Jackson,C.L. (2006). ATGL has a key role in lipid droplet/adiposome degradation in mammalian cells. EMBO Rep. *7*, 106-113.

Smith-Garvin,J.E., Koretzky,G.A., and Jordan,M.S. (2009). T cell activation. Annu. Rev. Immunol. *27*, 591-619.

Sonoda,H., Okada,T., Jahangeer,S., and Nakamura,S. (2007). Requirement of phospholipase D for ilimaquinone-induced Golgi membrane fragmentation. J. Biol. Chem. *282*, 34085-34092.

Sparagna,G.C., Johnson,C.A., McCune,S.A., Moore,R.L., and Murphy,R.C. (2005). Quantitation of cardiolipin molecular species in spontaneously hypertensive heart failure rats using electrospray ionization mass spectrometry. J. Lipid Res. *46*, 1196-1204.

Sprong,H., van der Sluijs,P., and van Meer,G. (2001). How proteins move lipids and lipids move proteins. Nat. Rev. Mol. Cell Biol. *2*, 504-513.

Stahlman,M., Ejsing,C.S., Tarasov,K., Perman,J., Boren,J., and Ekroos,K. (2009). High-throughput shotgun lipidomics by quadrupole time-of-flight mass spectrometry. J. Chromatogr. B Analyt. Technol. Biomed. Life Sci. *877*, 2664-2672.

Stone,S.J. and Vance,J.E. (2000). Phosphatidylserine synthase-1 and -2 are localized to mitochondria-associated membranes. J. Biol. Chem. *275*, 34534-34540.

Stremmel,W. and Debuch,H. (1979). The lipids of the Golgi apparatus subfractions from rat liver. Biochim. Biophys. Acta *573*, 301-307.

Tafesse,F.G., Huitema,K., Hermansson,M., van der,P.S., van den,D.J., Uphoff,A., Somerharju,P., and Holthuis,J.C. (2007). Both sphingomyelin synthases SMS1 and SMS2 are required for sphingomyelin homeostasis and growth in human HeLa cells. J. Biol. Chem. *282*, 17537-17547.

Takizawa,P.A., Yucel,J.K., Veit,B., Faulkner,D.J., Deerinck,T., Soto,G., Ellisman,M., and Malhotra,V. (1993). Complete vesiculation of Golgi membranes and inhibition of protein transport by a novel sea sponge metabolite, ilimaquinone. Cell *73*, 1079-1090.

Tamura,Y., Endo,T., Iijima,M., and Sesaki,H. (2009). Ups1p and Ups2p antagonistically regulate cardiolipin metabolism in mitochondria. J. Cell Biol. *185*, 1029-1045.

Tan,M., Hao,F., Xu,X., Chisolm,G.M., and Cui,M.Z. (2009). Lysophosphatidylcholine activates a novel PKD2-mediated signaling pathway that controls monocyte migration. Arterioscler. Thromb. Vasc. Biol. *29*, 1376-1382.

Tatsuta,T., Model,K., and Langer,T. (2005). Formation of membrane-bound ring complexes by prohibitins in mitochondria. Mol. Biol. Cell *16*, 248-259.

Taylor,T.C., Kanstein,M., Weidman,P., and Melancon,P. (1994). Cytosolic ARFs are required for vesicle formation but not for cell-free intra-Golgi transport: evidence for coated vesicle-independent transport. Mol. Biol. Cell *5*, 237-252.

Thai,T.P., Rodemer,C., Jauch,A., Hunziker,A., Moser,A., Gorgas,K., and Just,W.W. (2001). Impaired membrane traffic in defective ether lipid biosynthesis. Hum. Mol. Genet. *10*, 127-136.

Toker,A. (2005). The biology and biochemistry of diacylglycerol signalling. Meeting on molecular advances in diacylglycerol signalling
1. EMBO Rep. *6*, 310-314.

Tolias,K.F. and Cantley,L.C. (1999). Pathways for phosphoinositide synthesis. Chem. Phys. Lipids *98*, 69-77.

Ullman,M.D. and Radin,N.S. (1974). The enzymatic formation of sphingomyelin from ceramide and lecithin in mouse liver. J. Biol. Chem. *249*, 1506-1512.

Urbani,L. and Simoni,R.D. (1990). Cholesterol and vesicular stomatitis virus G protein take separate routes from the endoplasmic reticulum to the plasma membrane. J. Biol. Chem. *265*, 1919-1923.

Valianpour,F., Mitsakos,V., Schlemmer,D., Towbin,J.A., Taylor,J.M., Ekert,P.G., Thorburn,D.R., Munnich,A., Wanders,R.J., Barth,P.G., and Vaz,F.M. (2005). Monolysocardiolipins accumulate in Barth syndrome but do not lead to enhanced apoptosis. J. Lipid Res. *46*, 1182-1195.

Valianpour,F., Wanders,R.J., Barth,P.G., Overmars,H., and van Gennip,A.H. (2002). Quantitative and compositional study of cardiolipin in platelets by electrospray ionization mass spectrometry: application for the identification of Barth syndrome patients. Clin. Chem. *48*, 1390-1397.

van Blitterswijk,W.J., van der Luit,A.H., Veldman,R.J., Verheij,M., and Borst,J. (2003). Ceramide: second messenger or modulator of membrane structure and dynamics? Biochem. J. *369*, 199-211.

van den Brink-van der Laan, Killian,J.A., and de Kruijff,B. (2004). Nonbilayer lipids affect peripheral and integral membrane proteins via changes in the lateral pressure profile. Biochim. Biophys. Acta *1666*, 275-288.

van Meer,G. (1989). Lipid traffic in animal cells. Annu. Rev. Cell Biol. *5*, 247-275.

van Meer,G. (1998). Lipids of the Golgi membrane. Trends Cell Biol. *8*, 29-33.

van Meer,G. (2005). Cellular lipidomics. EMBO J. *24*, 3159-3165.

van Meer,G. and Simons,K. (1988). Lipid polarity and sorting in epithelial cells. J. Cell Biochem. *36*, 51-58.

van Meer,G., Stelzer,E.H., Wijnaendts-van-Resandt,R.W., and Simons,K. (1987). Sorting of sphingolipids in epithelial (Madin-Darby canine kidney) cells. J. Cell Biol. *105*, 1623-1635.

van Meer,G., Voelker,D.R., and Feigenson,G.W. (2008). Membrane lipids: where they are and how they behave. Nat. Rev. Mol. Cell Biol. *9*, 112-124.

Vance,D.E., Walkey,C.J., and Cui,Z. (1997). Phosphatidylethanolamine N-methyltransferase from liver. Biochim. Biophys. Acta *1348*, 142-150.

Vance,J.E. (2008). Phosphatidylserine and phosphatidylethanolamine in mammalian cells: two metabolically related aminophospholipids. J. Lipid Res. *49*, 1377-1387.

Vance,J.E. and Steenbergen,R. (2005). Metabolism and functions of phosphatidylserine. Prog. Lipid Res. *44*, 207-234.

Vasilenko,I., de Kruijff,B., and Verkleij,A.J. (1982). Polymorphic phase behaviour of cardiolipin from bovine heart and from Bacillus subtilis as detected by 31P-NMR and freeze-fracture techniques. Effects of Ca2+, Mg2+, Ba2+ and temperature. Biochim. Biophys. Acta *684*, 282-286.

Veiga,M.P., Arrondo,J.L., Goni,F.M., Alonso,A., and Marsh,D. (2001). Interaction of cholesterol with sphingomyelin in mixed membranes containing phosphatidylcholine, studied by spin-label ESR and IR spectroscopies. A possible stabilization of gel-phase sphingolipid domains by cholesterol. Biochemistry *40*, 2614-2622.

Veit,B., Yucel,J.K., and Malhotra,V. (1993). Microtubule independent vesiculation of Golgi membranes and the reassembly of vesicles into Golgi stacks. J. Cell Biol. *122*, 1197-1206.

Verkleij,A.J., Leunissen-Bijvelt,J., de Kruijff,B., Hope,M., and Cullis,P.R. (1984). Non-bilayer structures in membrane fusion. Ciba Found. Symp. *103*, 45-59.

Vickers,J.D. (1995). Extraction of polyphosphoinositides from platelets: comparison of a two-step procedure with a common single-step extraction procedure. Anal. Biochem. *224*, 449-451.

Voelker,D.R. (1997). Phosphatidylserine decarboxylase. Biochim. Biophys. Acta *1348*, 236-244.

Voelker,D.R. and Kennedy,E.P. (1982). Cellular and enzymic synthesis of sphingomyelin. Biochemistry *21*, 2753-2759.

Volchuk,A., Amherdt,M., Ravazzola,M., Brugger,B., Rivera,V.M., Clackson,T., Perrelet,A., Sollner,T.H., Rothman,J.E., and Orci,L. (2000). Megavesicles implicated in the rapid transport of intracisternal aggregates across the Golgi stack. Cell *102*, 335-348.

Wang,E. and Merrill,A.H., Jr. (2000). Ceramide synthase. Methods Enzymol. *311*, 15-21.

Wegmann,D., Hess,P., Baier,C., Wieland,F.T., and Reinhard,C. (2004). Novel isotypic gamma/zeta subunits reveal three coatomer complexes in mammals. Mol. Cell Biol. *24*, 1070-1080.

Wenk,M.R. (2007). Greys method for phosphatidylinositol phosphate extraction. In A Manual for Biochemistry Protocols, World Scientific Publishing Company), pp. 42-43.

Wenk,M.R., Lucast,L., Di,P.G., Romanelli,A.J., Suchy,S.F., Nussbaum,R.L., Cline,G.W., Shulman,G.I., McMurray,W., and De,C.P. (2003). Phosphoinositide profiling in complex lipid mixtures using electrospray ionization mass spectrometry. Nat. Biotechnol. *21*, 813-817.

Xu,Y., Kelley,R.I., Blanck,T.J., and Schlame,M. (2003). Remodeling of cardiolipin by phospholipid transacylation. J. Biol. Chem. *278*, 51380-51385.

Xu,Y., Malhotra,A., Ren,M., and Schlame,M. (2006). The enzymatic function of tafazzin. J. Biol. Chem. *281*, 39217-39224.

Yunghans,W.N., Keenan,T.W., and Morre,D.J. (1970). Isolation of golgi apparatus from rat liver. 3. Lipid and protein composition. Exp. Mol. Pathol. *12*, 36-45.

Zambrano,F., Fleischer,S., and Fleischer,B. (1975). Lipid composition of the Golgi apparatus of rat kidney and liver in comparison with other subcellular organelles. Biochim. Biophys. Acta *380*, 357-369.

Zaru,R., Berrie,C.P., Iurisci,C., Corda,D., and Valitutti,S. (2001). CD28 co-stimulates TCR/CD3-induced phosphoinositide turnover in human T lymphocytes. Eur. J. Immunol. *31*, 2438-2447.

Zemski Berry,K.A. and Murphy,R.C. (2004). Electrospray ionization tandem mass spectrometry of glycerophosphoethanolamine plasmalogen phospholipids. J. Am. Soc. Mass Spectrom. *15*, 1499-1508.

Zhao,W., Rog,T., Gurtovenko,A.A., Vattulainen,I., and Karttunen,M. (2008). Role of phosphatidylglycerols in the stability of bacterial membranes. Biochimie *90*, 930-938.

Zhong,Q., Gohil,V.M., Ma,L., and Greenberg,M.L. (2004). Absence of cardiolipin results in temperature sensitivity, respiratory defects, and mitochondrial DNA instability independent of pet56. J. Biol. Chem. *279*, 32294-32300.

I herewith declare that I have produced this thesis without the prohibited assistance of third parties and without making use of aids other than those specified. Notions taken over directly or indirectly from other sources have been identified as such. This paper has not previously been presented in identical or similar form to any other German or foreign examination board. The thesis work was conducted from November 2006 – November 2010 under the supervision of Prof. Dr. Felix Wieland and PD. Dr. Britta Brügger at the Heidelberg University Biochemistry Center (BZH).

Heidelberg, November 2010 Mathias Haag

6 Acknowledgments

I am very grateful to my supervisors Prof. Dr. Felix Wieland and PD. Dr. Britta Brügger who gave me the great opportunity to accomplish my PhD work in their lab. I want to express my gratitude, especially to Britta Brügger for offering me fascinating projects in the field of mass spectrometry and lipidomics, for her supervision and inspiring discussions. Britta opened a fascinating and challenging field of analytical biochemistry to me.

I would like to thank Prof. Dr. Felix Wieland, PD. Dr. Britta Brügger, PD. Dr. Matthias Mayer and PD. Dr. Hans-Michael Müller for agreeing to form my thesis committee.

I want to thank all members of the Wieland lab who provided a pleasant, friendly and productive working atmosphere. In particular, I would like to thank Dr. Vincent Popoff, Dr. Xabier Contreras, Dr. Alexander Brodde, Andreas Max Ernst and Timo Sachsenheimer for stimulating discussions and for supporting me in the lab. My thanks go to Dr. Frank Anderl, Dr. Oliver Schmidt and Dr. Per Haberkant for their support at the beginning of my work. I thank Iris Leibrecht, Gabi Weiß and Ingrid Meißner for their excellent technical assistance.

I am obliged to Dr. Andrej Shevchenko from the Max Planck Institute of Molecular Cell Biology and Genetics in Dresden and his group members Julio Sampaio, Dr. Dominik Schwudke and Dr. Christer Ejsing for their expertise advice on automated quadrupole time-of-flight mass spectrometry and data processing.

I thank Prof. Dr. Thomas Langer and Dr. Christof Osman (Institute for Genetics, University of Cologne) for the excellent collaboration work on mitochondrial lipids. My thanks go to Prof. Dr. Vivek Malhotra and Dr. Josse Van Galen (Centre for Genomic Regulation, Barcelona, Spain) for collaborative studies on the Golgi complex. For the collaboration work on primary human T cells I thank Prof. Dr. Peter H. Krammer and Angelika Schmidt (DKFZ, Heidelberg).

Furthermore, but most importantly, I am indebted to Claudia, to my parents Thekla and Walter Haag, to my brother Christoph Haag and to my friends for their continuous support throughout the thesis.